University of Alberta

A Comparative Study of CO_2 Adsorption on Intact and Crushed Coal

by

Ali Sabir ©

A thesis submitted to the Faculty of Graduate Studies and Research in partial fulfillment of the requirements for the degree of Master of Science

in

Geoenvironmental Engineering

Department of Civil and Environmental Engineering

Edmonton, Alberta
Spring 2004

Library and Archives Canada

Published Heritage Branch

395 Wellington Street
Ottawa ON K1A 0N4
Canada

Bibliothèque et Archives Canada

Direction du Patrimoine de l'édition

395, rue Wellington
Ottawa ON K1A 0N4
Canada

Your file Votre référence
ISBN: 0-612-96545-7
Our file Notre référence
ISBN: 0-612-96545-7

The author has granted a non-exclusive license allowing the Library and Archives Canada to reproduce, loan, distribute or sell copies of this thesis in microform, paper or electronic formats.

L'auteur a accordé une licence non exclusive permettant à la Bibliothèque et Archives Canada de reproduire, prêter, distribuer ou vendre des copies de cette thèse sous la forme de microfiche/film, de reproduction sur papier ou sur format électronique.

The author retains ownership of the copyright in this thesis. Neither the thesis nor substantial extracts from it may be printed or otherwise reproduced without the author's permission.

L'auteur conserve la propriété du droit d'auteur qui protège cette thèse. Ni la thèse ni des extraits substantiels de celle-ci ne doivent être imprimés ou aturement reproduits sans son autorisation.

In compliance with the Canadian Privacy Act some supporting forms may have been removed from this thesis.

Conformément à la loi canadienne sur la protection de la vie privée, quelques formulaires secondaires ont été enlevés de cette thèse.

While these forms may be included in the document page count, their removal does not represent any loss of content from the thesis.

Bien que ces formulaires aient inclus dans la pagination, il n'y aura aucun contenu manquant.

Canada

Abstract

Production of CO_2 from fossil fuel combustion is a significant environmental concern. At present, major challenge has been set to reduce CO_2 emissions below and equal to emission levels in 1990. One of the geological storage options being studied to assist in reducing CO_2 emissions is the sequestration of CO_2 in unmineable coal deposits. One of the technical issues associated with this storage technique is the lack of knowledge regarding adsorption characteristics of coalbed methane reservoirs. Kinematics of CO_2 adsorption on in situ coal seams cannot be captured using crushed coal which is traditionally studied. The current research compares the CO_2 adsorption behavior of crushed and intact coal specimens. Tests were carried out using a modified triaxial testing apparatus under an isotropic effective stress of 3.75MPa to simulate field conditions. Diffusion from the samples was minimized by putting them in copper membranes. Comparison of moisture content determined before and after the test validated the efficiency of the sealing mechanism. A different technique of constant pressure was used in this study as compared to constant volume approach in previous studies.

Comparison of results with the previous studies shows that the adsorption of CO_2 on intact coal varied from that of crushed coal especially at lower CO_2 equilibrium pressures and exhibits attenuated adsorption kinetics in comparison to crushed coal specimen.

Dedicated to my Family

Acknowledgements

First of all I am thankful to Allah Almighty for giving me the strength to complete this work. Secondly I am thankful to my parents especially to my mother due to whom I am here and it is she who always made me work hard and my brothers who were always encouraging me to do my utmost best.

Dr. Chalaturnyk and Dr. Donahue without whose guidance I would never have been able to carry out any of the work done here. I must thank them for giving me some of their valuable time and their constant input in the work and advices. I do not have the words to thank them enough for their guidance.

Big thanks go to Gerry, Steve and Christine for answering all of my questions and giving me their time and constant input in the experimental part of the work. Ken, just I can't thank him enough for the untiring work he did alongside me. Big thanks go to Dr. Steve Talman for answering my constant questions and giving helpful advice whenever I asked him for it.

Friends, well I think very big thanks goes to Tarek, Gurpreet and Soe Moe who understood me perfectly and always were there for helping me out in every aspect of my work. Last but not the least, Khuram, who went through my thesis with me as I corrected and gave valuable input every time I asked for it.

I really enjoyed my last two years with all these guys.

Thank you everyone for making my time memorable

Table of Contents

Description	Page #
Chapter 1: Introduction	**1**
1.1 Introduction	1
1.2 Objectives	8
1.3 Scope	8
1.4 Outline of the Thesis	9
Chapter 2: Literature Review	**11**
2.1 General	11
2.2 Coal	11
2.3 Descriptive Terminology for Coal	12
2.3.1 Grade	12
2.3.2 Rank	12
2.3.3 Lithotypes	12
2.3.4 Macerals	13
2.3.5 Coalification Process	17
2.3.6 Moisture Content	20
2.3.6.1 Moisture Content as indication of Oxidation	21
2.3.7 Porosity	23
2.3.8 Mineral Constituents	26
2.3.9 Density	26
2.4 Properties of CO_2	28

Description	Page #
2.5 Adsorption	31
2.5.1 Adsorption Forces	33
2.5.2 Physical Adsorption	34
2.5.2.1 Calculation of Surface Area	35
2.5.2.2 Calculation of Total Pore Volume	35
2.5.3 Chemical Adsorption	36
2.5.4 Distinction between Physical and Chemical Adsorption	36
2.6 Adsorption Isotherms	38
2.7 Effect of Water on Adsorption	41
2.8 Adsorption/Desorption Process	43
2.9 Carbon Dioxide Adsorption	48
2.10 Oxidation of Coal	49
2.11 Nature of Oxygen in Coal	50
2.12 Process of Oxidation	50
2.13 Structural Changes during Oxidation (Weathering)	51
2.14 Effect of Oxidation on Adsorption	51
2.15 Summary	53
Chapter 3: Sampling	**54**
3.1 Introduction	54
3.2 Field sampling	54
3.3 Freeze Sampling	56
3.3.1 Freezing Cell and Data Acquisition System	57

Description	Page #
3.3.2 Sample Placement into the Freezing Cell	60
3.3.3 Assembling the Freezing Cell	60
3.3.4 Freezing of the Sample	61
3.3.5 Advantages	67
3.3.6 Disadvantages	67
3.4 Alternate method of Sampling	68
3.5 Summary for Intact Specimen Preparation	74
3.6 Sample Preparation for Crushed Coal	75
3.7 Summary	79
Chapter 4: Experimental Setup	**81**
4.1 Introduction	81
4.2 Guiding principles	81
4.3 Temperature Limits and Control	83
4.4 Pressure Limits and Control	85
4.5 Cell Fluid	85
4.6 Membranes	88
4.7 Sealing Mechanisms	89
4.8 Plumbing	91
4.9 Data acquisition system	91
4.10 Calibration of Electronic Monitoring Devices	92
4.11 Experimental Procedure for Intact Sample	92
4.12 Experimental Procedure for Crushed Sample	106

Description	Page #
4.13 Summary	111
Chapter 5: Results and Discussion	**113**
5.1 Introduction	113
5.2 Physical Properties of Samples	113
5.3 Temperature Variation	115
5.4 Gas Compressibility Factor	116
5.5 Crushed Coal Adsorption Isotherms	119
5.6 Leakage Integrity Test	125
5.7 Test Results for Intact Coal Sample	128
5.8 Discussion of the results for Intact and Crushed Sample	136
5.8.1 Effective Confining Stress	137
5.8.2 Oxidation of the Sample	137
5.8.3 Moisture Content	138
5.8.4 Structure of Coal	139
Chapter 6: Conclusions and Recommendations	**142**
6.1 Introduction	142
6.2 Conclusion	142
6.2.1 Coal Sampling Techniques	142
6.2.2 Adsorption Test Results	143
6.2 Practical Application of Research	143
6.3 Recommendations	145
6.3.1 Experimental Procedure	145

Description	Page #
6.3.2 Scale Effects	145
6.3.3 Risk Assessment	145
References	**146**
APPENDIX A – Graphs between Total Gas inflow and time for Crushed Sample 1 for each pressure increment	**158**
APPENDIX B – Graphs between Total Gas inflow and time for Crushed Sample 2 for each pressure increment	**162**
APPENDIX C – Graphs between Total Gas inflow and time for Leakage Integrity Test for each pressure increment	**166**
APPENDIX D – Graphs between Total Gas inflow and time for Intact Sample 1 for each pressure increment	**170**
APPENDIX E – Graphs between Total Gas inflow and time for Intact Sample 2 for each pressure increment	**174**
APPENDIX F – Calculation of Moisture Content for Crushed Coal Samples	**178**
APPENDIX G – Glossary of Coal Terms	**182**
APPENDIX H – One Dimensional Freezing of the Sample	**188**

List of Tables

Description	Page #
Table 2.1: Table indicates the difference in rank parameter with increase in rank	13
Table 2.2: Major stages in Coalification Process	19
Table 2.3: Major Changes occurring in Coal during Transition from Peat to Lignite	20
Table 2.4: Physical Properties of CO_2	31
Table 4.1: Moisture Content Calculation for Crushed Sample	108
Table 5.1: Physical Properties of Intact Sample #1 (IS1)	114
Table 5.2: Physical Properties of Intact Sample #2 (IS2)	115
Table 5.3: Relationship of Compressibility Factor against Pressure	118
Table 5.4: Gas Adsorption Test Data for Crushed Specimen (CS1 and CS2)	121
Table 5.5: Gas Behavior at STP for Different Pressures for Crushed Samples	121
Table 5.6: Gas Behavior at STP for Different Pressures for Crushed Samples (daf Basis)	123
Table 5.7: Test Data for Leakage Integrity Test	125
Table 5.8: Time and Total Gas in for Different Pressures for Intact Samples	128
Table 5.9: Gas Behavior at STP for Different Pressures for Intact Samples	130
Table 5.10: Gas Behavior at STP for Different Pressures for Intact Samples (daf Basis)	133
Table 5.11: Specimen Properties for Various other studies	135
Table 5.12: Specimen Properties for Coal used in this Study	135
Table F.1: Calculations for the Residual Moisture Content for Crushed Sample 2	180
Table F.2: Calculations for the Air dry Loss	180

Description	Page #
Table F.3: Calculations for the Residual Moisture Content	181
Table F.4: Calculations for the Air dry Loss	181
Table F.5: Moisture Content for both Crushed samples	182

List of Figures

Description	Page #
Figure 1.1: 1000 Years of Global CO_2 and Temperature Change	4
Figure 1.2: Various Different Methods for Sequestration of CO_2	6
Figure 2.1: Figure depicting Cleats and Micropores	25
Figure 2.2: Different Basis of Proximate Analysis	27
Figure 2.3: Representations of three Different Displacement Volumes of Coal	27
Figure 2.4: CO_2 Phase Diagram	29
Figure 2.5: The 5 types of Adsorption Isotherms	40
Figure 2.6: Sorption of Different Pure gases on San Juan Basin Fruitland Coal	47
Figure 3.1: Location of Mine	55
Figure 3.2: Coal Seam Geology	56
Figure 3.3: Freezing Cell	58
Figure 3.4: Bottom Portion of the Cell	59
Figure 3.5: Graph between Temperature Gradient and Time in Cell	62
Figure 3.6: Freezing Cell: Bottom Drainage Platen	64
Figure 3.7: Freezing Cell: Porous Stone at Base of the Cell	64
Figure 3.8: Coal Sample and RTDs in the Freezing Cell	65
Figure 3.9: Freezing Cell: Top Porous Stone placed on Top of the Coal Sample	65
Figure 3.10: Weight placed on Coal Sample for Confinement	66
Figure 3.11: Installation of LVTD to Monitor Vertical Displacement during Freezing	66
Figure 3.12: Frozen Coal Sample	67

Description	Page #
Figure 3.13: Coring Machine and Core Barrel	69
Figure 3.14: Coal Specimen obtained using the Coring Device	70
Figure 3.15 Core in Acrylic Tube	71
Figure 3.16: Sample ready for Sawing	72
Figure 3.17: Sample being Sawed	72
Figure 3.18: Sample ready for Machining	73
Figure 3.19: Sample being Machined 73	
Figure 3.20: Prepared Sample	74
Figure 3.21: Hand Crushed Sample	76
Figure 3.22: Crushing Machine used	77
Figure 3.23: Sample after being Crushed using the Crushing Machine	77
Figure 3.24: Sample being passed through Sieve	78
Figure 3.25: Sample to be used in the Testing (passing sieve #60)	78
Figure 4.1: Applicability of Testing Framework in Field Conditions	83
Figure 4.2: Valve Placement on the Pump	95
Figure 4.3: Spacer for the Bottom Pedestal	97
Figure 4.4.: Spacer with the Porous Stone	97
Figure 4.5: Sample Placed on the Bottom Pedestal with Porous Stone	98
Figure 4.6: Sample in the Copper Tube	98
Figure 4.7: Top Porous Stone placed on the Sample	99
Figure 4.8: Top Pedestal	99

Description	Page #
Figure 4.9: Swedgelok fitting with O-Ring at the bottom	100
Figure 4.10: Fitting Placed on the Top Pedestal	100
Figure 4.11: Sample with Porous Stone and Copper Tube placed on the Top Pedestal	101
Figure 4.12: Copper Spacer and O-rings Placed and are Ready to be Tightened	101
Figure 4.13: Swedgelok fitting being Tightened	102
Figure 4.14: Top Portion being Tightened and ready for Placement	102
Figure 4.15: Bottom Portion ready for Placement of Sample	103
Figure 4.16: Swedgelok Fitting for Bottom Portion ready for Placement	103
Figure 4.17: Bottom Portion being Placed	104
Figure 4.18: Bottom Portion being Tightened in place	104
Figure 4.19: Top Ports being connected for Gas Input	105
Figure 4.20: Testing Cell ready for Placing into the Water Bath	105
Figure 4.21: Porous Stone after Opening	108
Figure 4.22: Copper Membrane Dismembered due to High Cell Pressure	109
Figure 4.23: Dismemberment of the Tubing	109
Figure 4.24: Sample inside the Copper Membrane after the Cell is Opened	110
Figure 4.25: Sample is Lumped due to Excessive Cell Pressure	110
Figure 5.1: Temperature Variation with Pressure for Intact and Crushed Sample Tests	116
Figure 5.2: Graph between Compressibility Factor and Pressure at 50°C	117
Figure 5.3: Step by Step Procedure of Calculating the Final Adsorbed Volume of the Gas	120
Figure 5.4: Crushed Specimen Adsorption Curves at STP Conditions (non daf Basis)	122

Description	Page #
Figure 5.5: Crushed Specimen Adsorption Curves at STP Conditions (daf Basis)	124
Figure 5.6: Relationship between Gas inflow at STP and Cumulative time for Pressure Increment of 1000 kPa to 2000 kPa	126
Figure 5.7: Graph showing Theoretical Curve and Experimental Data	127
Figure 5.8: Intact Specimen Adsorption Curves (at test conditions)	131
Figure 5.9: Intact Specimen Adsorption Curves at STP Conditions (non daf Basis)	132
Figure 5.10: Intact Specimen Adsorption Curves at STP Conditions (daf Basis)	133
Figure 5.11: Graph showing the Relationship between Results from this Study and Previous Studies	134
Figure 6.1: Difference in Langmuir Capacity and Experimental Capacity of Intact Coal	144
Figure A.1: Relationship between Total Gas inflow and Time for Pressure increment of 125kPa to 150kPa	159
Figure A.2: Relationship between Total Gas inflow and Time for Pressure increment of 150kPa to 250kPa	159
Figure A.3: Relationship between Total Gas inflow and Time for Pressure increment of 250kPa to 500kPa	160
Figure A.4: Relationship between Total Gas inflow and Time for Pressure increment of 500kPa to 1000kPa	160
Figure A.5: Relationship between Total Gas inflow and Time for Pressure increment of 1000kPa to 2000kPa	161
Figure A.6: Relationship between Total Gas inflow and Time for Pressure increment of 2000kPa to 4000kPa	161
Figure B.1: Relationship between Total Gas inflow and Time for Pressure increment of 125kPa to 150kPa	163
Figure B.2: Relationship between Total Gas inflow and Time for Pressure increment of 150kPa to 250kPa	163
Figure B.3: Relationship between Total Gas inflow and Time for Pressure increment of 250kPa to 500kPa	164
Figure B.4: Relationship between Total Gas inflow and Time for Pressure increment of 500kPa to 1000kPa	164

Description	Page #
Figure B.5: Relationship between Total Gas inflow and Time for Pressure increment of 1000kPa to 2000kPa	165
Figure B.6: Relationship between Total Gas inflow and Time for Pressure increment of 2000kPa to 4000kPa	165
Figure C.1: Relationship between Total Gas inflow and Time for Pressure increment of 125kPa to 150kPa	167
Figure C.2: Relationship between Total Gas inflow and Time for Pressure increment of 150kPa to 250kPa	167
Figure C.3: Relationship between Total Gas inflow and Time for Pressure increment of 250kPa to 500kPa	168
Figure C.4: Relationship between Total Gas inflow and Time for Pressure increment of 500kPa to 1000kPa	168
Figure C.5: Relationship between Total Gas inflow and Time for Pressure increment of 1000kPa to 2000kPa	169
Figure C.6: Relationship between Total Gas inflow and Time for Pressure increment of 2000kPa to 4000kPa	169
Figure D.1: Relationship between Total Gas inflow and Time for Pressure increment of 125kPa to 150kPa	171
Figure D.2: Relationship between Total Gas inflow and Time for Pressure increment of 250kPa to 500kPa	171
Figure D.3: Relationship between Total Gas inflow and Time for Pressure increment of 500kPa to 1000kPa	172
Figure D.4: Relationship between Total Gas inflow and Time for Pressure increment of 1000kPa to 2000kPa	172
Figure D.5: Relationship between Total Gas inflow and Time for Pressure increment of 2000kPa to 4000kPa	173
Figure E.1: Relationship between Total Gas inflow and Time for Pressure increment of 125kPa to 150kPa	175
Figure E.2: Relationship between Total Gas inflow and Time for Pressure increment of 150kPa to 250kPa	175
Figure E.3: Relationship between Total Gas inflow and Time for Pressure increment of 250kPa to 500kPa	176
Figure E.4: Relationship between Total Gas inflow and Time for Pressure increment of 500kPa to 1000kPa	176

Description	Page #
Figure E.5: Relationship between Total Gas inflow and Time for Pressure increment of 1000kPa to 2000kPa	177
Figure E.6: Relationship between Total Gas inflow and Time for Pressure increment of 2000kPa to 4000kPa	177
Figure H.1: Graph between Room Temperature and Time over the Length of Test	188
Figure H.2: Relationship between Temperature in Water Bath and Time	189
Figure H.3: Graph Showing relationship between Displacement and time	190
Figure H.4: Graph between Freezing Front and time over the length of Test (Sample 1)	191
Figure H.5: Graph between Freezing Front and Time over the length of Test (Sample 2)	191

Chapter 1: Introduction

1.1 Introduction

Global warming refers to an expected increase in the global average temperature due to the anthropogenic emissions of greenhouse gases (Ladd, 1998). Subsequent change in precipitation distribution and intensity, and a rise of the global sea level due to melting glaciers will result in higher average yearly temperatures. The greenhouse effect is a natural process that helps maintain the earth's temperature. The sun's rays enter the atmosphere and warm the earth. Carbon dioxide, methane, nitrous oxide, ozone, other trace gases and water vapor in the atmosphere trap some of the heat energy radiated back from the earth. This raises the temperature of the atmosphere and is called the greenhouse effect. Human activity has increased the levels of greenhouse gases in the atmosphere in several ways:

- by producing and using fossil fuels;
- by releasing chemicals outside of the energy sector into the atmosphere; and
- by destroying forests and other vegetation that absorb carbon dioxide.

Carbon dioxide (CO_2), the most important human-made greenhouse gas, is released primarily by the burning of fossil fuels like coal, oil, and natural gas as well as deforestation. Its concentration has risen by nearly 30% over its value in pre-industrial times (Francis, 1998). Other important greenhouse gases are methane (CH_4) and nitrous oxide (NO_2), both primarily emitted through agricultural activities. Finally, hydro-fluorocarbons (HFCs), per-fluorocarbons (PFCs), sulphur hexafluoride (SF_6) and ozone (O_3) also contribute to the greenhouse gas problem. Slowly, the international community

became aware of the risks and in 1979 at the First World Climate Conference recognised that climate change was a major problem.

While the pace and magnitude of future climate change is still uncertain, there is widespread agreement among scientists and government officials on the key aspects of global warming. This consensus led to negotiation and signing of the United Nations Framework Convention on Climate Change at the Earth Summit held at Rio de Janeiro in 1992. The treaty embodied a voluntary commitment by industrial countries to return their emissions to 1990 levels by year 2000. The treaty was further strengthened in 1997 by addition of the Kyoto Protocol.

There is a worldwide consensus among climate scientists that global average temperature will rise over the next 100 years if the release of greenhouse gases from human activity continues to grow at the same rate as it is now (Hansen et al., 1998). According to the assessments done by the U.S. National Academy of Sciences and the United Nations' Intergovernmental Panel on Climate Change (IPCC), Earth could experience the fastest warming in the history of civilisation during the 21st century. According to the IPCC Summary Report, Earth may warm by 1 to 3.5°C by the end of the next century, i.e. warmer than at any time since the evolution of humans. Such a rise in global temperature would be associated with significant climate change. During the last ice age – when a thick ice sheet covered much of Europe and North America – the average temperature was only about 5°C colder than now. The expected global warming could have serious, potentially devastating effects on society and ecosystems e.g. harming the animal husbandry, disruption of food chain and lack of wood and biofuel production. Global warming may increase frequencies of flooding, erosion, droughts and hurricanes. It is

argued that the global net emissions must be reduced to 30-40 % of the present emissions within 50 years from now in order to avoid significant changes on the climate (IPCC).

The change predicted by the Intergovernmental Panel on Climate Change is larger than anything that has occurred in the past 160,000 years. Even a change of 1°C in long-term average temperature can have major impacts on species survival, forest cover, permafrost levels, sea ice and the availability of fresh water.

Humans are used to temperature changes of 10°C within a day and changes of up to 50°C within a year. There are also differences in the yearly average from year to year. Nevertheless, there is a big difference between these ordinary fluctuations and changes in temperatures averaged over longer periods. Figure 1.1 from the United States global research program on the Climate Change show the variation of temperature, CO_2 concentration and Carbon emission during the past 1000 years.

Energy producers and consumers are responsible for nearly two-thirds of Alberta's contribution to global warming and climate change, almost entirely from the burning of fossil fuels (Gunter et al., 1998). For example, the operation of a home furnace contributes to global warming (natural gas), as does the driving of a car (gasoline) and the operation of industrial boilers (natural gas, fuel oil, coal).

Greenhouse gas emissions are typically measured in terms of carbon dioxide equivalence. This means that the impact on global warming of other greenhouse gases are expressed in terms of how much carbon dioxide would produce the same effect.

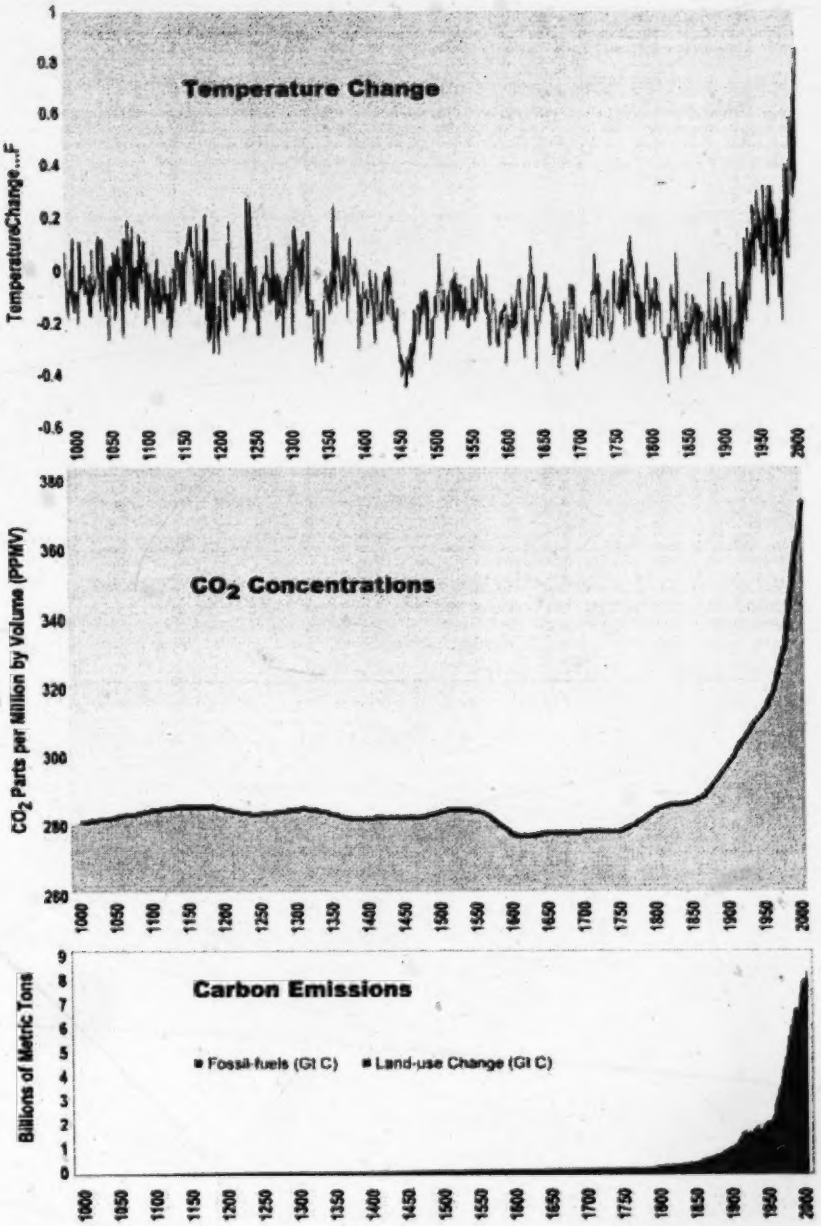

Figure 1.1: 1000 Years of Global CO_2 and Temperature Change (US Global research Program, 2003)

Carbon dioxide from fossil fuel combustion cannot practically be removed from the smokestack or tail pipe (Bruce, 1998). Ninety-four per cent of the carbon dioxide emitted through human activity is from burning of fossil fuels. Carbon dioxide is unique among fossil fuel combustion products. It must be produced in order to release energy from fossil fuels and it is produced in amounts several hundred times greater than other combustion products.

No technology can prevent the production of carbon dioxide in the combustion process. Technologies to control "end of pipe" emissions have not yet been demonstrated commercially and appear to be prohibitively expensive. Carbon dioxide emissions from fossil fuels can only be reduced by using less fossil fuel energy or by substituting oil or natural gas for coal or substituting natural gas for oil. Therefore, to reduce the CO_2 concentration in atmosphere we have to come up with a procedure that is relatively safe and economical. Geological Storage is one such method, which has been developed over the past two decades, and its reliability is being studied worldwide. Figure 1.2 depicts various procedures for the sequestration of CO_2 into underground reservoirs.

Injection into the ocean at different depths (shallow, intermediate or deep release) is feasible mainly for near shoreline power plants. Brewer et al., (1999) recommended CO_2 release at intermediate ocean depths. However, the economic penalty for removal, recovery and disposal is severe. Shore pumping stations and long pipelines would be required. There are also some concerns of the unknown ecological effects and permanence of shallow and deep ocean disposal of CO_2. The proposal of terrestrial burial by injection under pressure into abandoned and depleted oil or gas wells or solution-mined salt domes has been studied by Frederick and Steinberg (1981). CO_2 pumped into

these wells must be maintained under pressure, and remain sealed. There is a big risk if these wells release the stored gas suddenly due to unexpected tectonic movements.

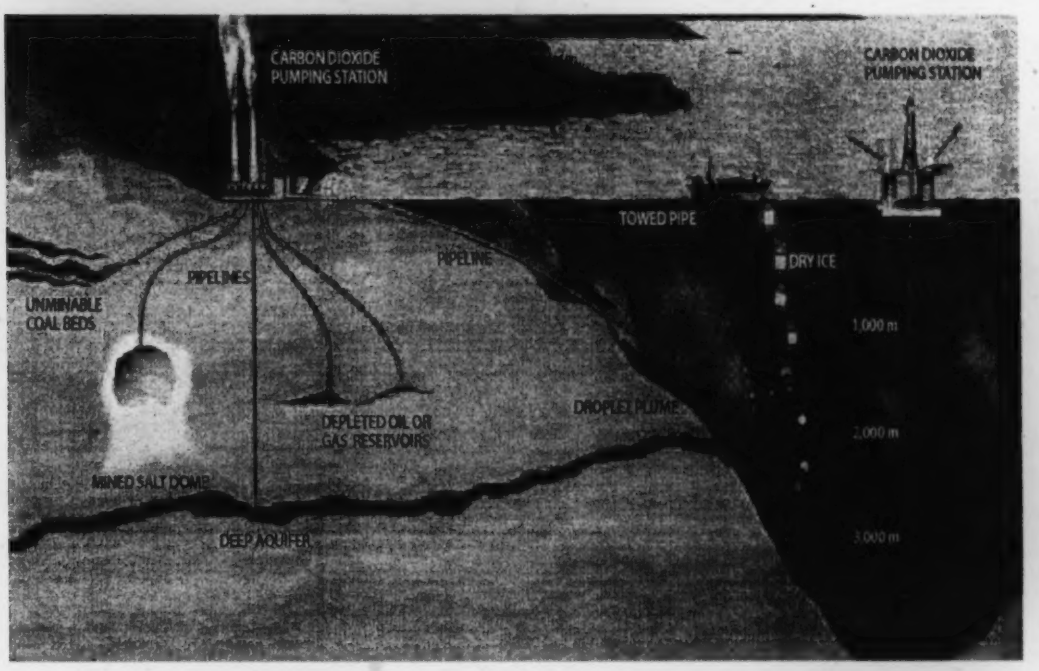

Figure 1.2: Various Different Methods for Sequestration of CO_2 (Herzog et al., 2000)

Storage by trees and plants appears feasible. A 1000 MW coal-burning plant requires on the average about 1000 Km2 of forest land to photosynthesize the effluent CO2. There appears to be little benefit of locating this area adjacent to the plant. There is, however, some concern about other environmental side effects due to a change in the Earth's albedo caused by extensive forestation.

Conversion of CO_2 into useful marketable products is extremely limited compared to the large quantities of CO_2 being produced from various sources. Some of these products

include methanol, formaldehyde, methane and other organic compounds are widely used commercially. These products, however, eventually return CO_2 into the atmosphere.

Extraterrestrial disposal is considered impractical because of the large payload to be lifted clear of the earth (816 Mgh^{-1} of CO_2 for a 1000 MW plant). The large fuel to payload ratio in conventional fueled rockets would generate much more CO_2 in the atmosphere than it would dispose (Perkins et al., 1996).

The injection of carbon dioxide (CO_2) in unmineable, deep coalbeds is probably the most attractive option of all underground CO_2 storage possibilities as the CO_2 is stored and at the same time, the recovery of coalbed methane (CBM) is enhanced (Gunter et al., 1997). Gunter et al., (1997), studied injecting CO_2 in aquifers and the experiments and modelling indicated that geochemical trapping reactions of CO_2 are slow – at least in the order of tens of hundreds of years. The capacity of these traps is large, in order of million of metric tons. On the other hand, this method of CO_2 disposal is expensive, of the order of $50/tonne if flue gas separation costs are included (Gunter et al., 1997).

A synergy is needed between the production of the fossil fuels and the disposal of their gaseous emissions created during the energy conversion process. One such synergy is the use of CO_2 for enhanced oil recovery, which is done regularly and considered a mature technology (Bailey and McDonald, 1993). In contrast, production of coalbed methane (CBM) by enhanced recovery techniques utilizing injection of CO_2 is still in the research stage.

1.2 Objectives

The objectives of this thesis are based on the need to better understand the geomechanical phenomena associated with CO_2 injection into coalbed methane reservoirs. The geomechanical and geochemical response of a coalbed methane reservoir will be influenced to a greater extent by the cleat or fracture system than by the intact matrix. While this is true, the intact matrix response must still be characterized in order to fully understand the reservoir response to CO_2 injection and CH_4 production.

Utilizing experimental methods, the kinematics of CO_2 adsorption on intact coal and crushed coal specimens have been examined. Based on the comparison of these two test programs, the objective is to quantify the relative difference in adsorption behavior on intact specimens rather than crushed coal specimens. As well, a secondary objective was to assess the ability to use constant pressure adsorption tests procedures rather than the conventional constant volume methodology for adsorption tests.

1.3 Scope

The complication of the CO_2 sequestration processes combined with CH_4 desorption creates an equally multifaceted geomechanical response in coal. Consequently, for the research conducted in this thesis, the scope was restricted to the following condition:

- Coal specimens would be obtained from surface coalmine deposits. While it would have been ideal to test insitu specimens, the requirement to produce a series of coal specimens with properties as similar as possible was paramount in enabling the comparison of test results for two different test methodologies; therefore different sampling techniques were tested;

- Assess the suitability of one dimensional freezing technique for preparing specimens of highly fractured coal; and
- Comparison of the adsorption capacities of intact and crushed coal specimens under effective stress conditions.

1.4 Outline of the Thesis

Chapter 1 provides an introduction to the global issues surrounding greenhouse gases. The environmental and political background, in particular, is discussed and concluded with summarizing the technical challenges faced in meeting its greenhouse gas reduction targets. The scope and outline for the research is presented.

Chapter 2 is a technical review of the structure and flow behavior of coal and other coal properties as well as gases in coal and their properties. The process of adsorption and desorption are reviewed. A discussion on the weathering (oxidation) of coal is also included in this chapter.

Chapter 3 describes coal sampling in detail and discusses the options that were available during the sampling process and the one adopted as well as discussion regarding the freezing mechanism of the coal sampling is discussed in detail.

Chapter 4 explains the experimental procedure of adsorption tests. It describes the set up procedure and the application of isotropic stresses on the coal samples.

Chapter 5 presents the experimental results of the adsorption tests on the intact as well as crushed samples. The adsorption behavior of the gas onto the coal sample is discussed and explained under various gas pressures and factors influencing it are discussed in detail.

Chapter 6 summarizes the findings in the thesis and provides conclusions on the geomechanical behavior of the coalbed formation under different isotropic stress conditions and different gas pressures. Topics of further research are identified and discussed.

Chapter 2: Literature Review

2.1 General

This chapter provides a technical overview of coal formation and the different physical and mechanical properties of coal. It also introduces selected aspects and concepts of CO_2 disposal and the properties of CO_2.

2.2 Coal

Coal is an abundant mineral with an estimated worldwide recoverable volume of about 9.8×10^5 million Tons (International Energy Annual 2001). It is structured heterogeneously by organic and inorganic constituents and has a resistant chemical structure, grown and preserved over millions of years. Coal refers to a metamorphic rock comprised of at least 50% by weight (70% by volume) of carbonaceous material (Schopf, 1956). An inorganic (mineral matter) content of 30% in coal is considered to be the boundary between pure coal and impure coal (Mukhopadhyay et al., 1993).

The material undergoes a process of progressive change called coalification. The transformation of plant material into coal takes place in two stages, biochemical degradation and physio-chemical degradation. Biochemical degradation involves chemical decomposition of botanical matter assisted by organisms. Coal is very resistant to decomposition and can be attacked by strong reactants and/or severe conditions only (van Heek, 2000). Although coal has traditionally been regarded as a "solid" fuel, recent studies by Derbyshire et al., (1991) have shown that coal is also found in fluid phase.

Coal generally consists of pores and solid particles. This is called the *two component model* but it has been pointed out by Herod et al., (1991), that this is overly simplistic since the molecular fraction within coal is compositionally very complex.

2.3 Descriptive Terminology for Coal

Coal can be systematically described and classified according to following compositional criteria: grade, rank, lithotype, maceral, coalification process, moisture content, porosity, mineral constituents and density.

2.3.1 Grade

Grade represents the relative proportion of organic to that of inorganic constituents in the coal sample: the higher the coal grade, the lower the inorganic constituents. Higher grade coals are preferred as a fuel source for coal fired or combustion related industries.

2.3.2 Rank

The rank of a coal refers to the degree of coalification endured by the organic matter. It is estimated by measuring the moisture content, specific energy, reflectance of vitrinite or volatile matter, which are known as rank parameters. Table 2.1 provides details on the classification of different rank stages.

2.3.3 Lithotypes

Coal is often banded, reflecting a change in material composition and conditions in the mine. These bands are termed lithotypes and there are several systems of classification according to rank and preference.

The classification of coal lithotypes is given in Table 2.1 (from Diessel 1992). The properties of lustre (brightness), type of fracture, proportion of banding and mineral matter content are used to distinguish the coal lithotype. Each individual band must be greater than 5mm in width to be distinguishable.

Table 2.1: Table Indicates the Difference in Rank Parameter with Increase in Rank (modified from Diessel, 1992).

Rank Stages	% Carbon (daf*)	%Volatile matter (daf*)	Specific Energy (gross in MJ/kg)	% in situ moisture	% vitrinite reflectance	
					random	max
wood	50	>65	-	-	-	-
peat	60	>60	14.7	75	0.20	0.20
brown coal	71	52	23	30	0.40	0.42
sub-bituminous	80	40	33.5	5	0.60	0.63
high volatile bituminous coal	86	31	35.6	3	0.97	1.03
medium volatile bituminous coal	90	22	36	<1	1.47	1.58
low volatile bituminous coal	91	14	36.4	1	1.85	1.97
semi-anthracite	92	8	36	1	2.65	2.83
anthracite	95	2	35.2	2	6.55	7

** daf: dry ash free basis*

The terms vitrain, clarain, durain and fusain were developed in the classification scheme of Stopes (Meyers, 1982), which has been extended and applied to a wider range of coals. In practice during logging of core or a coal face, an estimate is made of the percentage of coal brightness; this is useful as a guide to the composition of the coal and technological application. The brightness log may also be used in determining roof and floor limits of mining.

2.3.4 Macerals

The smallest microscopically recognisable entities in coal are called macerals; they are analogous to minerals in rocks. However, they differ from each other since minerals have a homogeneous chemistry and an orderly internal structure, while coal macerals consist of a mixture of compounds. The chemical and physical properties of macerals vary with coal rank. Coal macerals are distinguished by:

- Optical characteristics: Appearance of macerals under the microscope. Dark coloured macerals indicate high carbon content while lighter coloured maceral contents implies low carbon content.
- Relief of the polished surface: The quality of the polished surface is of importance for both the microprobe and for reflected light microscopy. Contacts between hard and soft minerals are important locations for minute components of prime significance, which are not visible if the surface has high relief.
- Morphology: The form and structure of the coal. This has an influence on all the properties of the coal like adsorption, permeability and strength.
- Reflectance and fluorescence: The amount of light is reflected back from the specimen. When more light is reflected this means that the specimen can be designated as bright coal and have different behaviour as compared to dull coal. Fluorescence can help to reveal the normally hidden internal structures of the macerals under microscope and their chemical and physical properties during analysis.

Macerals characteristics differ because they represent different parts of the original plant material and micro organisms that contributed to the peat. The mode of preservation, that is, whether or not the organic fragments were oxidised before being preserved, is also considered in the classification of macerals. The three maceral groups are vitrinite, inertinite and liptinite. These groups are all further subdivided into maceral subgroups.

The vitrinite group is relatively enriched in hydrogen compared with the other two groups, inertinites have greater carbon content and vitrinites have intermediate carbon content. As rank increases the differences in the chemistry between the groups

diminishes. The vitrinite group generally represents the woody plant material e.g. stems, trunks, roots and branches of the trees while liptinite includes more resistant parts of a plant like spores, cuticles and resins and inertinite is material that has been oxidised prior to coalification. Vitrinite and inertinite are subdivided into maceral subgroups depending on size and the degree of gelification. Three prefixes are used to divide the macerals into maceral subgroups. Telo- and detro- differentiate between the size of the individual particles and gelo- means the material has been gelified. Vitrinite in bituminous coal is dark to light grey in colour, depending on the rank. Telo-vitrinite represents intact fragments of plant matter although the original plant cell structure may be visible in this maceral subgroup. Detro-vitrinite results from smaller fragments (must be >20 μm in greatest dimension) that often form a groundmass for other macerals. Gelified material produced before or during coalification becomes gelovitrinite which is relatively uncommon.

The inertinite maceral group originates from the same material as the vitrinite group however the oxidation endured before coalification changes its optical properties and chemistry. It is much lighter coloured (varying from light grey, to white, to yellow) in comparison with vitrinite. Cell structure is visible in telo-inertinites that are subdivided according to the degree of oxidation. These macerals may exhibit a high degree of relief. The oxidation may have occurred at any time before peat preservation. Forest fires that oxidise wood can occur during peat accumulation. Burnt leaves and wood (charcoal) result in the formation of the maceral fusinite. Since it has high carbon content to start with the composition of this maceral does not vary with rank. Plant material may have

already started to gelify and break down before oxidation, this oxidised gel can form the maceral inertinite.

The final maceral group is liptinite; these macerals include the parts of plants, which because of their chemistry are more resistant to physical and chemical degradation. Quantitatively this maceral group is usually much less common, than the other two maceral groups. Above approximately 1.25% mean random vitrinite reflectance, liptinite is indistinguishable from vitrinite. Spores, cuticles (found on the surface of leaves and stems), waxes and resin are included in this group, as is alginite, which is the remains of algae, and rarer substances that may only be detected using fluorescence microscopy. In general this group has a grey to brownish appearance with distinctive morphology and is highly fluorescent when irradiated with short wave (ultra violet or blue) light.

Using a microscope individual species of plants and micro-organisms that contributed to the peat deposit has been identified, by studying the type of spores and pollen, plant tissue or fungal spores. This can then be used to correlate some seams or seam splits, gain a rough estimate of the age of the deposit or provide some insight into the environment of deposition. Knowledge of the environment of deposition may be useful to predict changes in coal quality.

The quantity of each maceral group varies both between and within coal seams. Technologically vitrinite is usually the most desirable maceral group, since it contains more hydrogen and oxygen, but these elements decrease with increasing rank.

Macerals differ in their specific gravity and this can be used to separate the coal from the mineral matter in crushed samples and also to separate out some inertinite. Liptinite

macerals are the lightest group followed by vitrinite then inertinite. Fusinite the most carbon rich inertinite has a specific gravity greater than 1.5.

2.3.5 Coalification Process

Coalification begins at the sediment surface and continues throughout the burial history, encompassing a diverse set of physical, chemical, and biological processes. Although a distinction is commonly drawn between chemical and physical changes during coalification (Levine, 1993), the two are so closely related that it is impossible to assess them independently in practice.

The nature of coalification changes significantly at different stages of coalification (Levine, 1993). In tropical environments, this process may be faster, since the warm moist conditions are ideal for the organisms that assist in this process, such as bacteria and fungi. However, plant growth is also more rapid and so the increased rate of decomposition may be balanced by plant growth. In tropical conditions high rates of evaporation need to be coupled with high precipitation to maintain plant growth and peat accumulation. While in cooler climates the growth rate of vegetation may be cyclic in nature and slower since the seasonal variation in conditions is greater. The conditions are less ideal for fungi and bacteria so the slower growth rate is matched by a slower rate of biochemical degradation.

Humification affects the soft content of the plant cells before the cell walls, which consist of cellulose, hemicellulose and lignin although it is the most resistant compound. Humification begins with the oxidation of plant matter and attack by aerobic organisms such as fungi, insects and aerobic bacteria. Hydrocarbons are extracted from the tissue

and the material left behind is relatively rich in oxygen and carbon. Semifusinite, an inertinite maceral may be formed in this manner.

Various humic substances are formed at this time, which are acidic in nature. If this continues the plant material will be completely degraded into carbon dioxide and water. When the degraded plant material is buried below the ground water table aerobic organisms and oxidation can no longer attack the material. Anaerobic bacteria may still decompose the plant matter until it reaches a depth or conditions unsuitable for these organisms. Aerobic bacteria utilise the oxygen in the plant matter so all molecules may be attacked even the more resistant compounds. However the softer tissue may be more rapidly affected. Biochemical coalification ends at the rank of sub-bituminous coal, when humic substances have polymerised. Physico-chemical coalification that follows is caused by conditions of burial.

The overburden (which is deposited), heat flow (generated from the earth's crust and tectonic movement) and pressure, change the chemistry and structure of the organic material. The same conditions are applied to all the macerals. By the application of this overburden, water is squeezed out and pore size is reduced as pressure increases and oxygen and hydrogen are released during thermal cracking. Water and carbon dioxide are the first products released.

Although coalification is a complex process but in spite of its major complexities, it can be viewed in simplified fashion as five successive, but overlapping, stages (Table 2.2): (1) Peatification, (2) Dehydration, (3) Bituminization, (4) De-bituminization, and (5) Graphitization (Levine, 1993). Each stage involves a combination of physico-chemical processes, and there are no sharp divisions between the stages. Rather, as coalification

advances, the indicated process becomes predominant in roughly the sequence listed although multiple processes may act simultaneously.

Table 2.2: Major Stages in Coalification Process (Levine, 1993)

#	Coalification Stage	Approximate ASTM Rank Ranges	Predominant Processes(s)	Predominant Physio-Chemical Changes
1	peatification	peat	maceration, humification, gelification, fermentation, concentration of resistant substances	formation of humic substances, increased aromaticity
2	dehydration	lignite through subbituminous	dehydration, compaction, loss of O-bearing group, expulsion of -COOH, CO_2 & H_2O	decreased moisture contents and O/C ratio, increased heating value, cleat growth
3	bituminization	upper bituminous A through high volatile A bituminous	generation and entrapment of hydrocarbons, depolymerization of matrix, increased hydrogen bonding	increased vitrinite Ro, increased fluorescence, increased extract yields, decrease in density and sorbate accessibility, increased strength
4	debituminization	uppermost high volatile A through low volatile bituminous	cracking, expulsion of low molecular weight hydrocarbons, especially methane	decreased fluorescence, decreased molecular weight of extract, decreased H/C ratio, decreased strength, cleat growth
5	graphitization	semi-anthracite to anthracite to meta-anthracite	coalescence and ordering of pre-graphitic aromatic lamellae, loss of hydrogen and nitrogen	decrease in H/C ratio, stronger XRD peaks, increased sorbate accessibility, anisotropy, strength and ring condensation, cleat healing

Peats are organic-rich sedimentary beds possessing in-ground moisture contents greater than 75% wt and/or burial depths less than 100m (Suggate, 1990). Peats consist of a wide variety of organic materials, admixed with variable amounts of inorganic minerals and water, which form loosely to moderately well compacted mass.

The transition from peat to lignite entails a number of significant physical changes to the coal (Table 2.3). Many of these changes relate to the progressive loss of water from the

coal structure. This represents the most important compositional change occurring in coals of this rank range.

Table 2.3: Major Changes Occurring in Coal During Transition from Peat to Lignite (modified from Levine 1993)

Darkening of colour, hardening, and increasing lustourness
Decrease in porosity and moisture content
Decrease in oxygen content and volatile matter yield
Increase in carbon content and heating value
Degeneration and selective preservation of plant polymers
Increase in aromicity of huminites and liptinites
Increase in reflectance of huminites
Decrease in primary fluorescence

The bituminous coal rank series, encompassing the range from high-volatile-A, involves a significant rearrangement of the molecular composition and structure of the coal. The entire complex process can be entrapment, and subsequent destruction of petroleum and asphaltic materials. Virtually all properties of the coal are directly or indirectly influenced by this process.

Whereas coalification in the bituminous rank centers on changes to the molecular component, coalification at anthracite and meta-anthracite stage is principally related to the structural rearrangement of the matrix component.

2.3.6 Moisture Content

Moisture content of near surface peat is over 75%. By the time the transition is reached between sub-bituminous A and high-volatile C bituminous coal, moisture content has diminished to around 20%. Water loss continues through upper high-volatile-A bituminous coal, dropping to less than 1-2% in some cases.

Four types of moisture in coal are usually considered. These, as reported by Levine (1993), are as follows:

- Adherent or free moisture – retained in coal in a free state on the surface, cracks or cavities. It is not connected to the structure of coal and has normal vapour pressure.
- Inherent or bed moisture – physically adsorbed in the micropores and capillaries of the coal structure and possess subnormal pressure
- Chemically bound moisture or water of decomposition – organically associated within the molecular structure of the coal. During coalification, this moisture is released.
- Water of hydration – associated with the inorganic constituents of coal such as clay minerals and gypsum. During coalification they release the water of hydration.

2.3.6.1 Moisture Content as indication of Oxidation

The moisture content of the coal depends on its rank and composition; it decreases progressively with rank from over 75 to 90% in peat to 30-50% in lignite to 7-10% in high volatile bituminous, to 1-5% in low volatile bituminous coal (Mukhopadhyay 1993). Moisture has been found to be an indicator of oxidation in naturally weathered bituminous coals. Fredericks et al., (1983) examined core samples of near surface seams in New South Wales, Australia. A typical analysis of the coal was 85% carbon (dry mineral matter free basis - dmmf) and 22.3% ash (dry basis). Oxidation was visually obvious over the top 2.45 m with no apparent oxidation below that point and the moisture content increased with degree of oxidation from 3.4% to 10.8%. This progressive change

in air-dried moisture content prompted the suggestion that moisture content could be a quick and easy method of indicating the level of oxidation. This work was in accordance with that of Teo et al., (1982), who examined naturally outcropping British Columbia coal. They found that the moisture on an air-dried basis increased with oxidation from 1.4% to 15.6%. This absorbed water affected the 1600 cm^{-1} band in the infrared spectrum. The band increased markedly with degree of oxidation/moisture content. Ingram and Rimstidt (1984) found that in the most severely weathered zone of an exposed coal seam in Virginia the moisture content was higher than in the less weathered zones. Banerjee and Bhattacharyya (1988) found that outcropping coal in the Indian Jharia coalfield exhibited similar behaviour. Ingram and Rimstidt (1984) attribute the increase in moisture content to an increase in surface area caused by the physical effects of weathering and an increase in hydrophilic functional groups that are able to chemisorb water. These arise from chemical weathering. This is consistent with findings, based on brown coal, that water molecules can be attached to polar oxygen sites in coal.

Yokokawa et al., (1989) agree with this interpretation. Their measurements of coal samples oxidised at 150°C for about one hour indicated that the pore walls were oxidised and the polarity of the surface was increased. The specific surface area (based on the CO_2 adsorption isotherm) increased for the oxidised samples.

Adsorption/desorption studies showed clear differences with rank. The lowest rank coals showed scarcely any difference in adsorption/desorption isotherms between the fresh and oxidised samples. However, as the rank increased differences emerged. It was suggested that the mechanism for the increase in moisture content changed with different coals. For

some, the development of pores of 2-3 nm could account for the increase, while for others, an increase in accessibility of the polar liquid may be more important.

Pandolfo et al., (1989) investigated the reactivity of maceral lithotypes towards aerial oxidation. The lithotypes came from Queensland Blair Athol coals. The oxidation was performed under a continuous flow of moist air at 100°C. It was found that fusain (81.2% inertinite) showed a dramatic increase in its ability to absorb water vapour as oxidation progressed. Vitrain, on the other hand, showed little change.

2.3.7 Porosity

Porosity is more difficult to define in the case of coal, which constitutes integral part of the coal structure. It is considered that coal has a dual-porosity system comprised of micropores and macropores (Harpalani and Chen, 1993). Whereas conventional rock pores are micrometers to millimetres (10^{-6} to 10^{-3} m) in dimension, typical "pores" in coal are orders of magnitude smaller. The micropores have a diameter of 0.5 to 2 nm and exist throughout the coal matrix (Harpalani and Chen, 1993). The macroporosity for a large part is inherited from the original plant structure.

Although the movement of the gas is not completely understood in the coal it is generally assumed that the macropores are generally responsible for the permeability of coal, whereas most of the gas is adsorbed in micropores, which is the major contribution to the surface area of the coal (Mavor, 1996).

Most of the previous studies attribute all or most of the permeability of coal to discrete fractures (Puri and Siedle, 1992). Coal fractures, or cleats, originate as a result of dehydration and associated shrinkage during coalification, or due to tectonic forces. Most coals have at least two regular fracture sets that are generally perpendicular to each other.

The dimensions of these fractures vary from few micrometers to tens of centimetres (Bustin, 1997). These two types of cleat (fracture) structure in coal are called the face cleat and the butt cleat and these are primary and secondary avenues respectively for fluid (gas and water) flow in coal (Figure 2.1). The two are commonly mutually orthogonal or nearly orthogonal and are essentially perpendicular or near perpendicular to bedding surfaces (Law and Rice, 1993). The face cleat is extensive, vertical and continuous throughout the seam. The butt cleat however is discontinuous, ending at an intersection with the face cleat, generally at a right angle but it is also vertical in some cases. Cleat spacing is known to be affected by the coal rank and bed thickness. It generally decreases as a function of decreasing layer thickness. It also decreases from the sub-bituminous to medium- and low-volatile bituminous coal rank through to anthracite. The aperture width of cleats under in situ conditions is another important attribute to the cleat geometry and permeability but it is quite difficult to obtain meaningful data under natural or replicated natural conditions. Estimates of cleat aperture under in situ confining pressures vary from 0.1 to 0.0001 mm (Harpalani and Chen, 1997). Finally cleats are often confined to coal layers with bulk densities between 1.2 and 1.75g/cm^3. The highest value corresponds to rock comprising 50% coal, with increasing mineral matter content, which is roughly equal to ash content (Law and Rice, 1993)

The micropores exist in the coal matrix between the seam cleats. The micropore system consists of the cleats, which are very uniformly distributed in coal, with spacing ranging from a fraction of an inch to several inches. The face cleat is laterally extensive, vertical and continuous throughout the seam, while the butt cleat in many cases is discontinuous.

The permeability of coal is due to the micropores present in the coal (Harpalani and Chen, 1993).

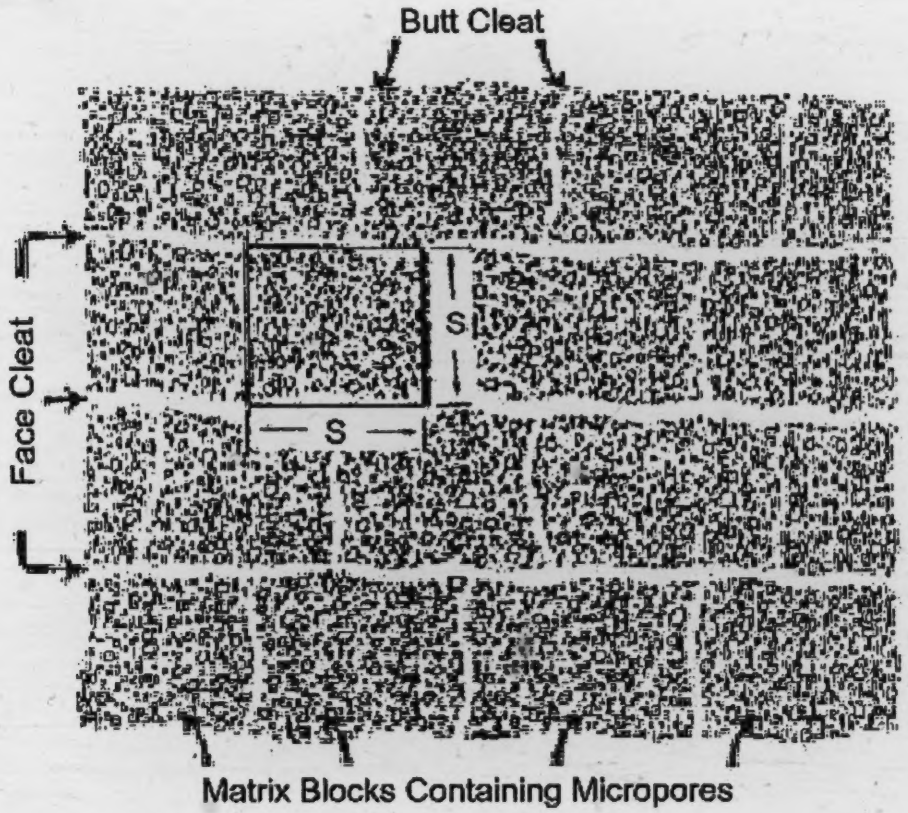

Figure 2.1: Figure Depicting Cleats and Micropores (adapted from Harpalani 1993)
S being the distance between the Face Cleats

Due to the phenomenon of activated diffusion, coupled with the "molecular sieve" character of coal, the dimensions of the coal micro-pores are on the same order of the magnitude as the sorbate molecules themselves (0.5nm) (Nandi and Walker, 1966). Mahajan (1991) have classified the coal pores into three size categories: micro-pore, meso-pores and macro-pores.

2.3.8 Mineral Constituents

In addition to the organic material coal also contains the inorganic material, called the mineral matter. The mineral matter can be found as finely distributed particles throughout the coal or as distinct non-coal inter-beds such as shale partings or splits. Most coal seams often contain both forms of the mineral material.

Clay minerals constitute about 60 to 80% of the total mineral in coal the most common being kaolinite and illite (Bustin et al., 1985). Clay minerals can occur in a finely dispersed form associated with macerals or in a finely dispersed form associated with macerals as tonsteins, clay bands or cleat and fracture fillings. Iron sulphides in coal include pyrite, marcasite and menikovite. Siderite is a major carbonate mineral in coal, generally occurring as cell infillings or as individual grains and is considered to be syngenetic. The most common non-clay mineral in the coal is quartz and it occurs in two forms as detrital grains and as euhedral grains. Other minerals include zircon, tourmaline, diopside, hornblende, mica, apatite, gypsum, microcline, and talc. (Mukhopadhyay et al., 1993).

2.3.9 Density

For the purpose of density, the coal can be defined in at least three distinct ways (Figure 2.3) (Levine, 1993):

(1) The volume of the organic structure of the coal, excluding "pores", (V_s),

(2) The "bulk" volume of the coal including all the pores (V_g), or

(3) The volume of fluids (f) displaced by the coal (V_f)

V_s and V_g are fixed for a specimen, but they are difficult to measure.

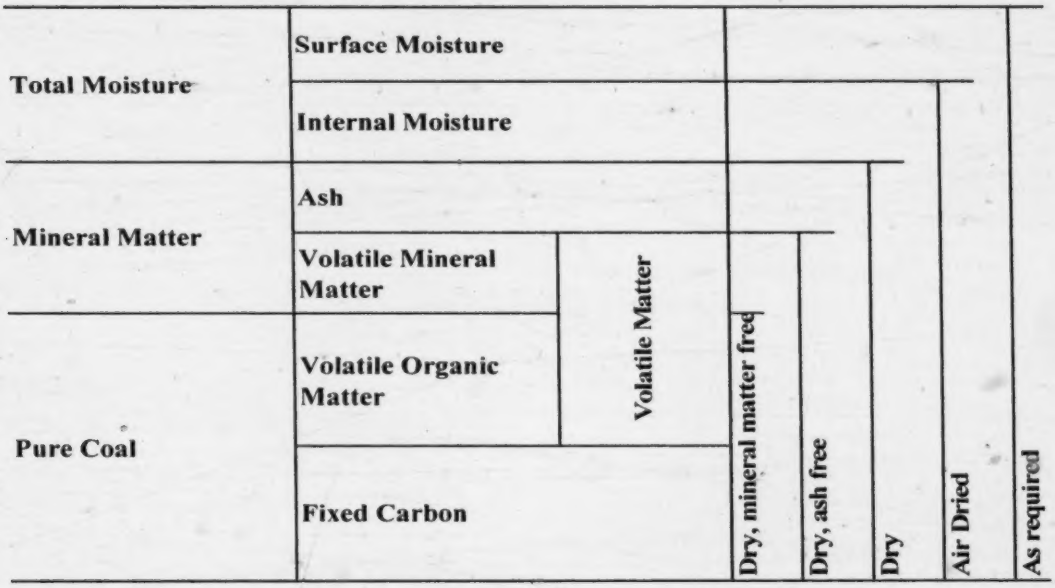

Figure 2.2: Different Basis of Proximate Analysis (after Ward, 1984).

The density of coal (vitrinite-rich, mineral matter-free) progressively decreases with increasing rank, reaching a minimum of around 1.3 at approximately 85% carbon, before increasing once again at high rank (van Krevelen, 1994).

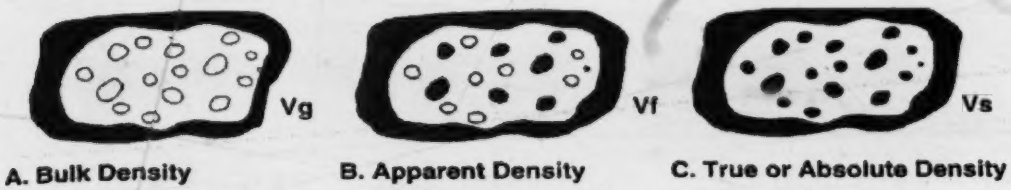

Figure 2.3: Representations of three different displacement volumes of coal (shown in white), measured in three different fluids. (A) Fluid does not penetrate the coal structure at all, providing an effective measure of "bulk density". The area in white is V_g. (B) Fluid penetrates the coal only partially, gaining access to some sites, but not to others (V_f). (C) Fluid fills every available pore, hence provides a measure of "true density". Area in white is V_s. (van Krevelen, 1994)

2.4 Properties of CO_2

The properties and behaviour of CO_2 vary in relation to the in situ conditions of the reservoir. Pressure and temperature conditions will determine whether the CO_2 is in gas, liquid or supercritical phase. Disposal into deep aquifers, where CO_2 is in a supercritical state, is desired due to the increased density of CO_2 in that phase, and therefore a more efficient use of the pore space. Understanding the variation in the properties of CO_2 with temperature and pressure is necessary to evaluate its transport mechanisms.

A nonpolar molecule, CO_2 is currently found in the atmosphere at concentrations of 360 ppmv (parts per million by volume) (Houghton, 1997), and is a known contributor to the natural greenhouse effect. Physical properties of CO_2 are summarized in Table 2.4, where the triple point represents the temperature and pressure at which all three phases (solid, liquid and gas) can coexist for CO_2.

The CO_2 phase diagram (Figure 2.4) illustrates its behaviour over a range of temperatures and pressures. As the gas approaches its critical point its properties, particularly density, begin to vary considerably with small change in pressure and temperature. The supercritical phase represents the region for which the critical pressure and temperature has been exceeded. Supercritical, by definition, refers to the point at which increasing pressure will not induce any changes in phase no matter how high the pressure is raised so long as the temperature is beyond its critical point (Felder and Rousseau, 1986). In other words, at supercritical pressures there is no distinct phase change occurring. Where the supercritical fluid is close to its normal liquid density fluid exhibits lower viscosity and higher diffusivity (Kyle, 1992).

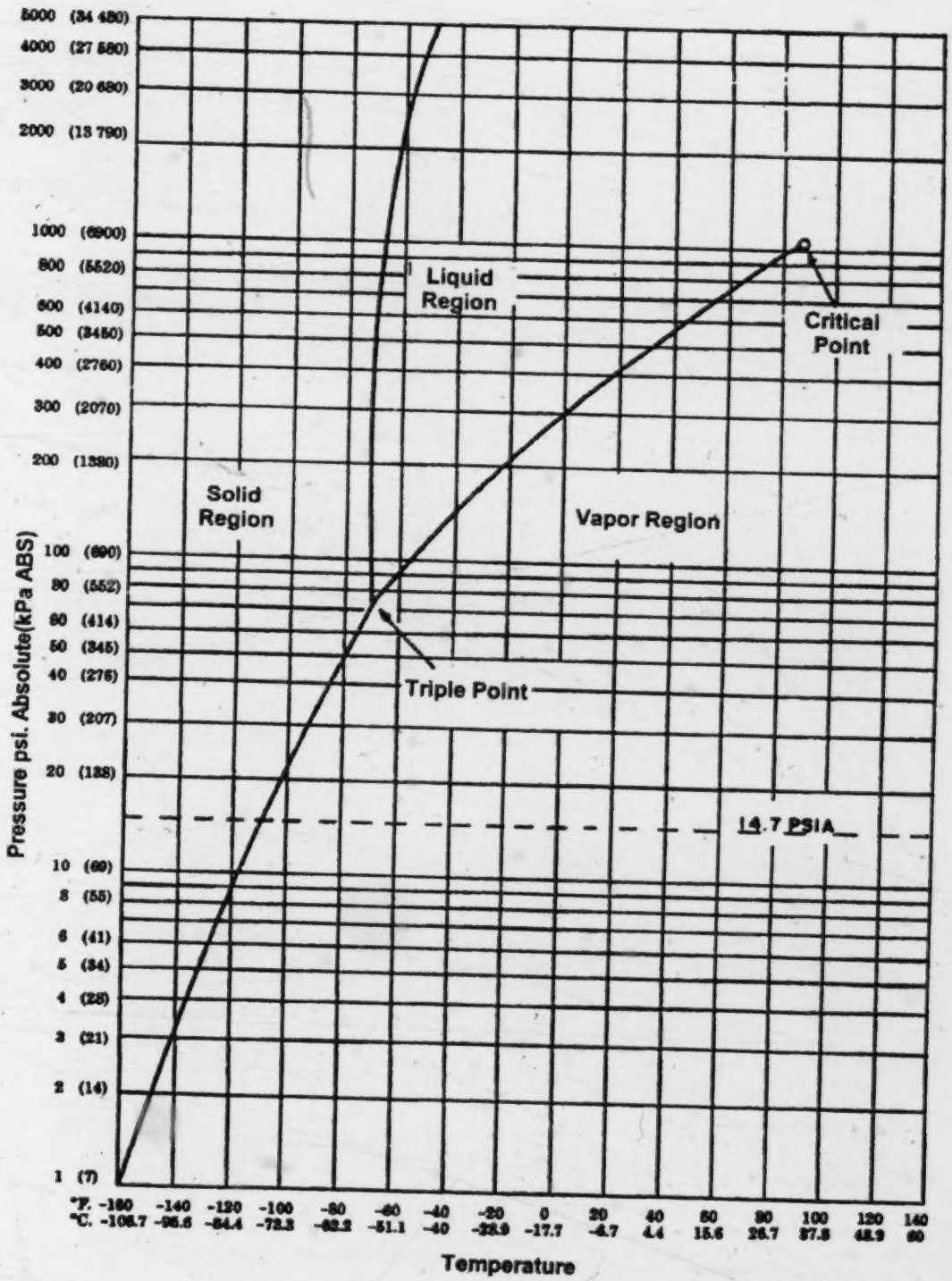

Figure 2.4: CO_2 Phase Diagram (Modified from the Handbook of Compressed Gases)

Supercritical properties of CO_2 significantly differ from the properties of gaseous and liquid CO_2. Its behaviour in geologic materials under varying pressures and temperatures is still widely unknown. In particular, its phase behaviour and reactive potential associated with CO_2 storage is not well understood, and continues to be investigated (White et al., 2001; Johnson et al., 2001).

Theoretically, dry supercritical CO_2 exhibits no surface tension (Lemmon et al., 2001), and therefore would move through any microporous material. However, the existence of naturally occurring CO_2 deposits, which have remained under supercritical conditions, sealing gas volumes in the order of billions of tonnes by cap rocks challenges the notion of CO_2 movement through these classes of materials, as a result of zero surface tension. (Stevens et al., 2000). Research is currently underway to investigate naturally occurring CO_2 deposits, and the nature of the cap rock, as an analogue to anthropogenic CO_2 storage (Pearce et al., 1996; Stevens et al., 2001).

Further complexities are introduced as its thermodynamic behaviour becomes increasingly complex as CO_2 interactions with water and brine also becomes a factor in geological storage (McPherson and Cole, 2000). Therefore, it is important to bear in mind the varying properties of CO_2 with temperature and pressure, particularly under supercritical conditions. In this thesis, the notation of CO_2 refers to the generic properties of CO_2, and not specific to its phase, unless otherwise noted.

Table 2.4: Physical Properties of CO_2 (modified from Fogg and Gerrard, 1991).

Molecular Mass	44.009 g/mol
Density (Solid)	97.5 lbs/ft^3 at -109°F / 1565kg/m^3 at -78°C
Density (Liquid)	63.7 lbs/ft^3 at 0°F / 1022kg/m^3 at -18°C
Density (Gas)	0.123 lbs/ft^3 at 32°F / 1.974kg/m^3 at 0°C
Melting Point	-69.9°F at 75.1 psia/ 56.6°C at 5.2 bar absolute (triple point)
Boiling Point	-109.3°F / -78.5°C (sublimates)
Sublimation Point at 101.3 kPa	194.4K
Triple Point	216.6K and 517.6 kPa
Critical Temperature	304.3K
Critical Pressure	7.39 MPa
Critical Volume	2.147 cm^3/g or 94.04 cm^3/mol

2.5 Adsorption

When a fluid (gas or liquid) comes in contact with a solid surface (adsorbent), fluid-solid intermolecular forces of attraction cause some of the fluid molecules (adsorbates) to be concentrated at the surface is a process generally referred to as Adsorption.

Some of the important definitions used are as follows:

Adsorbent: A material used for carrying out the adsorption process.

Adsorbate: It is the general term for the atomic or molecular species, which are adsorbed (or are capable of being adsorbed) onto the substrate.

Adsorption: The surface phenomenon by which the molecules of a bulk fluid phase are attracted by a solid surface in contact with the fluid.

Adsorption equilibrium: The thermodynamic property describing the extent of adsorption of a fluid species by a solid surface.

Adsorption kinetics: The measure of travel time of an adsorbate molecule from bulk fluid phase to the adsorption site.

Desorption: The process of removing the adsorbed molecules from the solid surface to the bulk fluid phase.

Heat of adsorption: The measure of thermal energy released during the exothermic adsorption process.

Adsorption processes may be classified as physical or chemical, depending on the nature of the forces involved. Physical adsorption, also termed van der Waals adsorption, is caused by molecular interaction forces; the formation of a physically adsorbed layer may be likened to the condensation of a vapour to form a liquid. Not only is the heat of physical adsorption of the same order of magnitude as that of liquefaction, but physically adsorbed layers, particularly those that are many molecular diameters thick, behave in many respects like liquids. Chemical adsorption, usually abbreviated to chemisorption, involves transfer of electrons between the solid (or adsorbent) and the gas (or adsorbate). The process essentially involves the formation of a chemical compound between the adsorbate and the outermost layer of adsorbent atoms.

The surface area of any body, in thermodynamic sense, is more reactive than the interior of the body, especially when the system is composed of tiny particles and the ratio of the surface area to volume is very large. Generally, when two immiscible phases are brought into contact, it is always found that the concentration of one phase is greater at the interface than in its bulk.

Usually adsorption is thermodynamically spontaneous process. Energy is released (exothermic) during the process. The reverse process by which the adsorbed molecules are removed from the surface to the bulk fluid phase is called desorption. Energy must be

supplied to the adsorbed phase (endothermic) for the desorption process. This energy can be in terms of temperature or pressure change.

2.5.1 Adsorption Forces

The forces giving rise to adsorption are no different from those involved in any other interatomic or intermolecular interaction phenomenon, but there are problems of special interest because the atoms of the solid are affected by the fact that they participate in the structure of the solid. According to Gregg (1967) the interactions between an atom or molecule and a solid surface are electromagnetic in origin, involving the electrons and nuclei of the system, the state of which is determined by quantum mechanics. When the equilibrium charge distribution is such that there is no transfer or sharing of electrons among the participating atoms and the individuality of the interacting species is thus maintained, the forces are said to be physical. Such forces are associated with physical or van der Waals adsorption. In principle then, the interaction between an atom or molecule and a solid surface can be found by determining the quantum mechanical state of the system of an atom or molecule and a solid, and then calculating the electromagnetic interactions (Flood, 1966). Since far simpler problems cannot be dealt with exactly, it is necessary to resort to various approximations.

The van der Waal's equation is a second order approximation of the equation of state of a gas that will work even when the density of the gas is not low and is given by equation 2.1:

$$[P + a(\frac{n}{V})^2](V - nb) = nRT \qquad 2.1$$

where P is the Pressure, a and b are the equation constant, V is the volume of the gas, n is the number of moles of the gas, R is the gas constant and T is the temperature.

The physical interaction between an atom or molecule and a solid surface is due to the attractive van der Waal's forces which may be defined simply as the forces which give rise to the constant ***a*** in van der Waal's equation, and the repulsive forces which arise when atoms come close enough together to allow interpenetration of the electron clouds. Attractive forces pertinent to physical adsorption may be divided into several categories. If the adsorbed atom or molecule possesses no permanent dipole or multipole moment, then the attractive interaction with the solid surface is due to non-polar dispersion forces only, unless the solid itself has an external electric field. If the adsorbed atom or molecule has multipole moments of its own, there will be additional interactions with the adsorbent due to:

- charge distributions induced in the adsorbent, and
- interactions of these moments with any permanent field of the solid.

Although it is undoubtedly artificial to separate the above interactions, it is convenient to do so, both for ease in conception and simplicity in computation. The following sections further discuss two types of adsorption processes.

2.5.2 Physical Adsorption

In the process of physical adsorption, adsorbates may freely move on the adsorbent surface. Repeated addition of adsorbate produces an adsorbate monolayer. Physical adsorption does not stop at monolayer formation but may, usually, advance into multilayer adsorption (although specific conditions are required for this) (Brunauer 1943). The weak electrostatic forces involved in physical adsorption include van der Waals forces and dipole interactions. These two also help in forming multilayers. It is usually associated with low heats of adsorption. Temperatures lower than room

temperatures are sufficient for these processes to take place. Physical adsorption is reversible, that is, there is an existence of adsorption-desorption equilibrium. Equilibrium is attained very rapidly (except when limited by mass transport rates in the gas phase or within a porous adsorbent).

2.5.2.1 Calculation of Surface Area

Based on the well-known Brunauer, Emmett and Teller (B.E.T.) (Brunauer et al., 1938) theory, of which Langmuir theory is a special case, one can estimate the number of molecules required to cover the adsorbent surface with a monolayer of adsorbed molecules, N_m. Multiplying N_m by the cross-sectional area of an adsorbate molecule yields the surface area of the sample.

When gas molecules are introduced into the system, the adsorbate molecules tend to form a thin layer that covers the entire adsorbent surface. Continuous addition of gas molecules beyond monolayer formation leads to the gradual stacking of multiple layers (or multi-layers) on top of each other. The formation of multi-layers occurs in parallel to capillary condensation. The latter process is adequately described by the Kelvin equation, which quantifies the proportionality between residual (or equilibrium) gas pressure and the size of capillaries capable of condensing gas within them (Young and Cromwell, 1962). With the use of computational methods, experimental curves (or isotherms) can be generated linking adsorbed gas volumes with relative saturation pressures at equilibrium, and convert them to cumulative or differential pore size distributions (Crank, 1975).

2.5.2.2 Calculation of Total Pore Volume

As the equilibrium adsorbate pressures approaches the saturation pressures, the pores become completely filled with adsorbate. By knowing the density of the adsorbate, one

can calculate the volume it occupies and, consequently, the total pore volume of the sample (Young and Cromwell, 1962). If at this stage one reverses the adsorption process by withdrawing known amount of gas from the system in steps, one can also generate desorption isotherms. Adsorption and desorption isotherms rarely overlay each other. The resulting hysteresis leads to isotherm shapes that can be mechanistically related to those expected from particular pore shapes.

2.5.3 Chemical Adsorption

Many gases react chemically with surfaces and form strong chemical bonds. In contrast to physical adsorption, chemical adsorption, or chemisorption as it is called, involves the formation of strong chemical bonds between adsorbate molecules and specific surface locations known as chemically active sites. Chemisorption is thus used primarily to count the number of surface active sites, which are likely to promote chemical and catalytic reactions.

2.5.4 Distinction between Physical and Chemical Adsorption

The distinction between physical adsorption and chemisorption is usually clear, but if doubt exists, a decision can be made on the basis of one or more of the following criteria:

- The heat of physical adsorption is of the same order of magnitude as the heat of liquefaction of the adsorbate and is rarely more than twice or three times as large, whereas the heat of chemisorption is of the same order as that of the corresponding bulk chemical reaction. In some cases, however, exceptionally low heats of chemisorption are found. In making such comparisons it should be noted that in both types of adsorption, because of surface heterogeneity and lateral interaction effects, the heat of adsorption may vary considerably with surface

coverage. This effect is particularly marked in chemisorption where the lateral interaction forces, being invariably repulsive, reinforce the effects of heterogeneity.

- Physical adsorption, like condensation, is a general phenomenon and will occur with any gas-solid system provided only that the conditions of temperature and pressure is suitable. On the other hand, chemisorption will take place only if the gas is capable of forming a chemical bond with the surface atoms of the adsorbent.
- A physically adsorbed layer may be removed by reducing the pressure, at the temperature at which adsorption took place, although the process may be slow on account of diffusion effects. The removal of a chemisorbed layer, however, often requires much more rugged conditions, especially on metal surfaces where very high temperatures or positive ion bombardment are needed. An exceptional case is the system oxygen on charcoal, in which the chemisorbed layer is so strongly held that even at high temperatures desorption yields not oxygen but a mixture of carbon monoxide and dioxide.
- Under suitable conditions of temperature and pressure, physically adsorbed layers, that are several molecular diameters thick, are frequently found. In contrast, chemisorption is complete once a monomolecular layer is built up, although physical adsorption may occur on top of the chemisorbed monolayer.
- Since physical adsorption is related to the process of liquefaction, it only occurs to an appreciable extent at pressures and temperatures close to those required for liquefaction. Thus if P is the equilibrium pressure of the adsorbed film and P_o is

the vapour pressure of the bulk liquid at the temperature of the experiment, it is generally found that below $P/P_o = 0.01$ no significant adsorption takes place. There are some exceptions, notably with adsorbents having very fine pores. On the other hand, chemisorption often proceeds at much lower pressures and much higher temperatures.

- Physical adsorption and chemisorption may sometimes be distinguished by their different rates of approach to equilibrium. Physical adsorption per se is instantaneous but, with highly porous or finely powdered adsorbents, diffusion of the gas into the adsorbent mass is often slow, particularly at low pressures. Chemisorption may be instantaneous but there are many systems where chemisorption involves activation energy. In both physical and chemical adsorption, the establishment of pseudo-equilibrium may hamper precise measurements. Thus the outer strata of adsorbent are more heavily covered with adsorbate than the centre of the solid mass; subsequent redistribution of the adsorbed film to give uniform coverage at all points in the solid mass is sometimes an extremely slow process. Clearly, the use of a rate criterion to distinguish physical from chemical adsorption is fraught with complications.

2.6 Adsorption Isotherms

Adsorption isotherms have been reported in the literature for a wide range of solids and fluids. Nevertheless the majority of these isotherms, which results from physical adsorption may for convenience be grouped into five classes, nowadays commonly referred to as the Brunauer, Emmett and Teller (BET) classification, as illustrated in

Figure 2.5. In fact many of the isotherms encountered in practice also show a further upward turn as the saturation vapour pressure is approached.

Type I is most often referred to as the Langmuir type and represents monolayer adsorption. Since chemisorption never exceeds a monolayer therefore isotherms for chemisorption are restricted to Type I.

Type II and Type III represent mono- as well as multilayer adsorption. Type III isotherms are characterized by their being convex to the pressure axis, that is, adsorption is co-operative in nature. The more molecules that are adsorbed already, the easier it is for further molecules to become adsorbed. Hence, Type III isotherms are expected for those systems which the differential heats of desorption are close to latent heat of evaporation, i.e., net heat of adsorption is not far from zero.

Type IV and Type V represent monolayer and multilayer adsorption plus capillary condensation. These isotherms are obtained in multilayer adsorption on highly porous adsorbents and the flattening of the isotherms at near saturation pressure that is attributed to capillary condensation phenomena.

Theoretically Type II and III are mostly valid for non-porous solids and sometimes for porous solids, while Type IV and V are valid only for porous materials.

The isotherms at the pressures in which we are more interested for the coal can be described very easily by using BET theory but it should be remembered that BET theory, can only be used at higher pressures and for low pressures it is not very suitable. In BET theory it is assumed that surface is energetically uniform i.e. all the adsorption sites are exactly equivalent. Brunauer (1943) suggested that the failure of BET equation to fit experimental data at low pressures is a consequence of this non-uniformity in the

assumptions for BET theory and they were unable to make quantitative allowance for this.

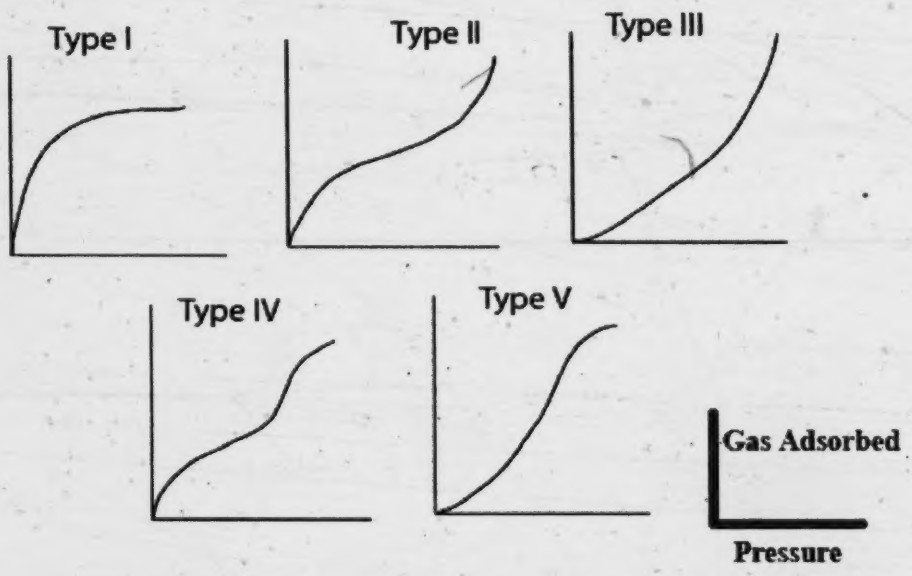

Figure 2.5: The 5 types of Adsorption Isotherms in the Classification of Brunauer, Deming, Deming and Teller (also called BET classification) (modified from Gregg, 1967)

A finite amount of time may be required for an adsorbate molecule to travel from the bulk fluid phase to the adsorption site in a microporous adsorbent and this rate process is generally referred to as adsorption kinetics (Brunaur, 1943). Adsorbate mass transfer resistance may be caused by (a) fluid film outside the adsorbent particle (for mixture adsorption), (b) anisotropic skin at the particle surface and (c) internal macro- and microporous diffusional resistances (pore and surface diffusion). The transport of an adsorbate can be severely affected by (a) the presence of other adsorbates in the pores and (b) local temperature changes caused by heat of adsorption/desorption (Gregg, 1967). Gas phase adsorption is generally faster than liquid phase adsorption. The overall mass

transfer coefficient for adsorption can be increased by reducing the length of diffusional path (adsorbent particle size).

The main feature that differentiates coalbed methane reservoirs from conventional methane gas reservoir is the manner in which the gas is stored in the reservoir. In conventional reservoirs gas exists in a free state in the pores of the reservoir rock and its behaviour can be described by the real gas law but in coal nearly all of the gas exists in a condensed form because of the physical sorption. Coal seams are usually under high pressure and the temperature in the seam is generally above the critical temperature of CO_2.

It is known from the previous discussion that the equilibrium between free gas and its sorbed phase is expressed in terms of a sorption isotherm. These sorption isotherms give sorbed gas content as a function of the free gas pressure at a constant temperature.

The Langmuir isotherm usually provides a reasonable description of sorption for the microporous sorbent like coal, where the gas molecule and the sorbent pore size are of comparable size. This is the case because the Langmuir isotherm approaches a saturation limit corresponding to filling of the micropores. The Langmuir constant also has a physical interpretation i.e. it is the initial slope of the isotherm at very low pressures, in Henry's law region hence it is also a measure of the isotherm curvature.

2.7 Effect of Water on Adsorption

Adsorption isotherms are often determined using pure gas and are inaccurate for predicting multi-component gas desorption columns. The composition of adsorbate gas significantly affects the total and single component adsorbed gas volume in coal systems. The presence of moisture in the coal matrix significantly changes the adsorption

equilibrium characteristics of mixed gases. Arri et al. (1992) showed that each component of gas does not adsorb independently, but competes for adsorption space. Experimental data presented by Arri et al., (1992) shows that CO_2 separation factors vary slightly between coal lithotypes, but the effects of variable coal composition and moisture upon selective adsorption are difficult to isolate. The moist coal adsorption isotherms have a greater uncertainty than the dry adsorption isotherms possibly due to slight variation in moisture content between replicate analyses (Arri et al., 1992). Model predictions indicate that the presence of moisture in coal decreases the selectivity for carbon dioxide. Water competes with gases for adsorption sites, and apparently occupies the higher energy sites that would otherwise be occupied by carbon dioxide if the coal were dry. Pure gas adsorption has been shown to be a function of water content and coal composition hence it is reasonable to anticipate that adsorption of a mixture of gases is also a function of these properties.

Dependence of adsorption on moisture content is very significant. Moisture has a much more significant effect in reducing methane sorption in high-oxygen coals (Crosdale et al., 1998). This is probably because the amount of adsorbed water is greater in these coals (at or above critical value), thereby causing more extensive blocking of the pore structure. Water present in excess of the adsorbed-water saturation capacity is probably quite mobile, or is located on the external surface of the coal; these have little or no effect on methane sorption.

Water molecules are strongly held by the coal structure, and removal of moisture during sample pre-treatment can collapse the interconnected pore network particularly for the coals of low rank. Ettinger et al., (1958) developed a simple analytical relation to correct

for moisture. Curl (1978) presents the results of a study that gives the correction as a plot of percent reduction in sorption capacity versus rank at different moisture contents varying from 0 to 10%. Joubert et al. (1973, 1974) found that the presence of the water reduced the sorption of the gas but only until critical moisture content was reached. At higher moisture contents, there was no further reduction of the methane sorption. Apparently, moisture in excess of the critical moisture content just coats the coal particles and does not affect the sorption process. In their research Joubert et al. (1973, 1974) also found that the critical moisture is also the equilibrium moisture. From the isotherms given by Joubert et al., (1973) it can be deduced that the monolayer area of each coal decreases with the increase in moisture content. Also there exists a certain percentage of moisture content that is called the critical value and above this value no further reduction in the methane sorption regardless of the amount of moisture in the coal occurs. Levine (1993) points out that the influence of moisture on gas sorption could change the trend to one of increasing gas content with rank, since low rank coals have high affinities for water. The trend of increasing sorption capacity with rank has become accepted.

It is clear from the literature review discussed above that water does block some of the sorption sites. Coal is commonly assumed to exist at its inherent or bed moisture at in situ conditions. As a result, sorption data should be measured at moisture content equal to or greater than the equilibrium moisture to be representative of the in situ conditions.

2.8 Adsorption/Desorption Process

A sorption isotherm represents equilibrium between the free and sorbed phases. In making sorption measurements, finely ground coal particles are commonly used so that equilibrium can be attained in practical amount of time. This is a process that typically

takes few hours to complete. If diffusion is still taking place it implies that the equilibrium has not been reached and thus the measured isotherm will be incorrect. This is particularly true at low pressures.

Desorption is fundamentally a result of reduction in gas pressure and causes shrinkage within the coal matrix, i.e. similar to compressive strains, there will be large compressive strains set up within the coal. It has been shown (Harpalani and Scraufnagel, 1990) that the coal matrix volume decrease with desorption as methane pressure decreased and that there is a linear relationship between the coal matrix volumetric strain and the quantity of gas released (Harpalani and Chen, 1993, Harpalani and Chen, 1997, Clarkson and Bustin, 1999, Clarkson and Bustin, 2001).

Firstly the diffusion distance depends upon the fracture spacing, which delineates the matrix block size of the coal. Secondly, gas flow volume through the fractures depends on fracture width, length, continuity and permeability. This model of gas transport through coal may best apply to predominantly vitrinite-rich coals in which fracture systems are open and not mineralized. However, complexities may arise due to secondary mineralization inhibiting gas flow and the presence of other macropore systems, especially phyteral porosity predominant in some inertinites, enhancing the gas flow.

Diffusion of gas through coal is usually described using a spherical unipore diffusion model. Sheared coals have usually very high diffusion rates, related to microstructural rather than petrographic controls. The process of CO_2 sorption on bituminous coal takes place in the micro-pore region of the macro-molecular elements of the coal substances and that it does not cause their permanent deformation. In other words, sorption on the bituminous coal is lattice sorption.

The method used to determine the adsorption capacity does not influence the amount of adsorbed CO_2 however there are differences in time needed to achieve the equilibrium state of sorption. Mechanism of CO_2 adsorption depends on both the microporous texture and the degree of activation of the carbon as well as the pore shape and the temperature of adsorption.

Gas storage by coals occurs predominantly by adsorption on the walls of the micropore network. At high vapour pressures, multilayer adsorption probably occurs after the micropores are filled, resulting in condensation to a bulk liquid; a process not uncommon in micropores are filled solids.

Process of coal saturation by gas is not governed by the micropore space being filled with gas but rather by structural changes in the coal substance, resulting in an increase of sorption space. The coal expands due to gas sorption. It has also been proposed (Joubert, 1974, Harpalani and Scraufnagel, 1990) that the coal may shrink as the gas is desorbed from the coal matrix, which not only shrinks the coal matrix but also reduce the effective horizontal stress, leading to the reduction of stress across the vertical and sub-vertical cleats further opening these and increasing the permeability.

The rank and type of coal may not be critical for controlling the factors related to gas sorption, rather both rank and type exert influence over the way pore structure develop. Bustin (1997) pointed out that there is little correlation between coal rank and adsorption capacity as these are obscured by various factors, although in particular basins there are general trends with rank and composition. Comparison of similar composition, but from different iso-rank suites, indicate however that the coals with highest adsorption capacity do not necessarily have the highest micropore capacity. In a paper by Ryan (1992) it is

assumed that the adsorbing capacity increases with the increase in coal rank. Within the iso-rank of the coals the adsorption capacity of coals increased with vitrinite content and decreases with inertinite and ash yield.

Comparison between the adsorption of different gases has been carried out by different researchers (Arri et al., 1992, Bustin, 1997, Bustin, 1998). Nitrogen is on an average, reportedly, 3 times less adsorbent than CO_2 while for CH_4 is half as adsorbing than CO_2, at the same temperature. Also nitrogen and carbon dioxide have similar molecular diameters and so the difference in their adsorption behaviour must be largely due to the polar nature of carbon dioxide, which allows it to adsorb on certain sites in place of water.

Arri et al. (1992) have studied the sorption of different pure component gases on coal and the results are shown in Figure 2.6. It can be seen that methane is sorbed more than nitrogen while carbon dioxide is sorbed more than methane. Patching (1970) reported the same behaviour. Gunther (1965) also noted the same trend but stated that the difference is less at high pressures. For common gases, the order of increasing sorption strength is hydrogen, nitrogen, methane, ethane and carbon dioxide. Multi-component gas sorption data show that different gas species are actually competing for the same sorption sites. The extended Langmuir isotherm has been shown to provide a reasonable description of multi-component gas sorption on coal (Gunther 1965).

As gas is physically adsorbed on the large internal surface of the coal, and is not chemisorbed or held in the type of solid solution as formed by compressed gases in rubbers and linear high polymers. Therefore when the gas pressure is reduced, the coal becomes less capable of holding the gas in adsorbed state. Gas molecules detach

themselves from the internal surfaces of the pores and hence the process of desorption is initiated.

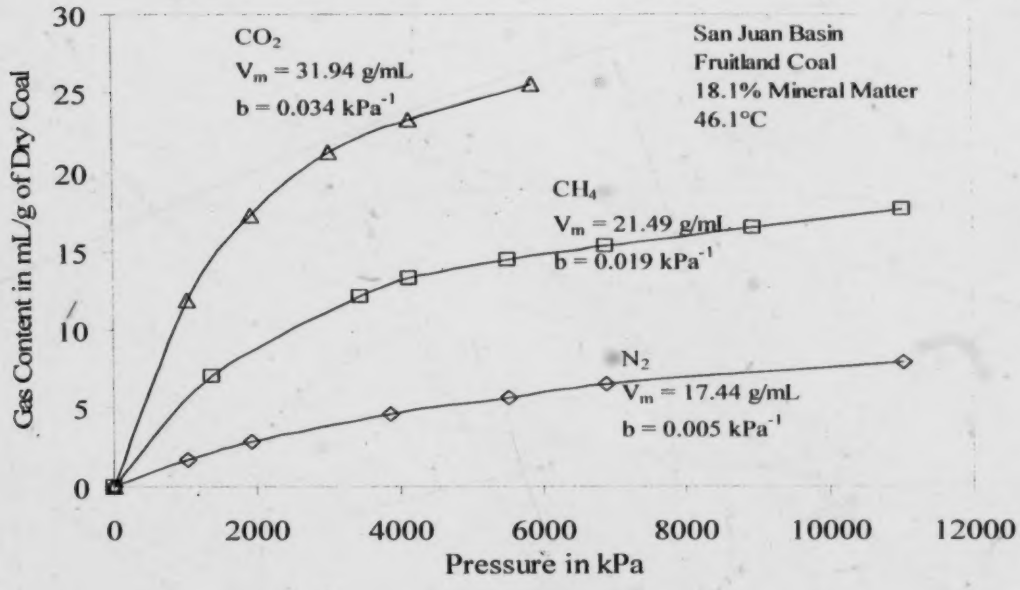

Figure 2.6: Sorption of Different Pure Gases on San Juan Basin Fruitland Coal (adapted from Arri et al., 1992)

The highest adsorbing coal may not have the highest vitrinite content. Lamberson and Bustin (1993) also found that although methane adsorption generally increased with the vitrinite content, the highest adsorbing coals did not have the highest vitrinite content, but only a mixture of vitrinite and inertinite

It has been shown by Moffet and Weale, (1955) that coal may have a greater adsorption capacity for the gas produced in-situ rather than the gas from an external source. Detail studies have been conducted by Ruppel et al., (1974) regarding the effect of oxidation at room temperature on crushed coal, but same cannot be said about the intact sample of the coal. During gas desorption, the temperature of the coal decreases if the process occurs

under conditions where heat exchange with the surroundings is difficult. This occurs under real conditions in coal beds in mines, mainly because of the large coal mass and the large amount of the gas evolved.

During outflow under quasi-adiabatic conditions (as approximately maintained during the experiments), the temperature decreased inside the coal samples and this decrease in temperature affected the adsorption capacity as reported by Arri et al., (1992). At high temperatures, gas is favoured in the "free state" rather than adsorbed state. The most important relative changes of both adsorption and of expansion for the coals under test are for gas pressures ranging from 1.0 to 2.0MPa (Arri et al., 1992).

2.9 Carbon Dioxide Adsorption

It has been suggested by Stacy and Jones (1986) that CO_2 does not affect the internal pore structure of the coal and therefore it is better for measuring the internal area by using CO_2 rather than any other gas. As CO_2 has polar bonds and a large quad-pole moment, specific chemical interactions between coal and carbon dioxide may make an important contribution to the adsorption process, and it may well vary significantly with the composition of the coal.

It has been reported by Faiz et al. (1992) that at 25°C essentially the entire pore volume of all the coals studied would be filled with CO_2 and the magnitude of adsorption increases with the increase in temperature. During these experiments by Faiz et al., (1992) the linear dependence of the temperature decrease in coal on the amount of gas desorbed, predicted theoretically for equilibrium conditions, has been confirmed experimentally for the non-isothermal desorption process which occurs under non-equilibrium conditions.

Some researchers have debated the relationship between the coal maceral and the gas adsorption. Faiz and Cook (1991), Faiz et al. (1992), and Crosdale and Beamish (1994) have argued that there is no relationship at all for Australian coal while Bartosiewicz and Hargraves (1985) have concluded that bright coals generally adsorb more gas than dull coals in the pressure range of 0 ~ 1MPa.

There are a number of factors that affect the extent to which coal can adsorb CO_2 or for that matter any gas. The nature of the coal will determine the maximum adsorption capacity under a given set of conditions, but the sequestration environment will determine an ultimate adsorption capacity. Parameters such as temperature, pressure, etc. define the sequestration environment and have a large influence on the properties and adsorption of CO_2.

According to some Clarkson et al., (1999) and Clarkson (2001) the bright coals have greater micropore capacity than the dull coals when measured using low-pressure CO_2 adsorption.

2.10 Oxidation of Coal

One of the fascinating problems of coal oxidation and weathering is the curious mixture of subtle and dramatic effects. That such a reaction, scarcely detectable by some chemical techniques, can lead to spontaneous combustion or severe degradation of coal properties, presents a considerable challenge to coal science.

In situ, coal exists in water-saturated seams with no oxygen present. Exposure to oxygen upon sampling of coal will initiate oxidization with possible detrimental effects on the properties of the coal. Loy et al. (1987) suggested that "the best option for dealing with oxidized coal is to avoid it"

It is a well established fact (Berkowitz, 1979, Beier 1983) that coal is generally extremely sensitive to oxidation such that exposure to even minute amounts of oxygen will alter the properties. Weathering involves aerial oxidation, mineral matter change in moisture content, particle size degradation. With the increase in the temperature the oxidation rate will also increases.

During weathering (oxidation at ambient temperature) an increase in weight, bound oxygen, hygroscopicity and solubility in alkaline matter can occur. In weathered coal, cleats are enlarged, vitrinite particles display irregular spider like microfractures while lower reflectance is seen along edges.

2.11 Nature of Oxygen in Coal

Oxygen, a combustible gas, as well as an oxidant is present in the coal in appreciable quantities. Oxygen is found in coal in following forms

(1) Hydroxyl;

(2) Carboxyl;

(3) Methoxyl;

(4) Carbonyl; and

(5) Unreactive Oxygen.

2.12 Process of Oxidation

Aerial oxidation of coal is not a single process but a complex phenomenon comprising of several simultaneous and interacting chemical processes resulting in erosive and structural alteration of coal. Initially oxygen is chemisorbed on the coal surface at readily available aromatic as well as non-aromatic sites. It is followed by formation of acidic functional group especially –COOH, =CO and –OH (phenolic). Also in the presence of

water, peroxide or hydro-peroxides are also formed and then these are further oxidized to ferrous thiocynate, titanous chloride and hydroquinone. With time, coal substance will deteriorate into alkali soluble humic acids and subsequently breaking into a number of smaller particles (Flood, 1966).

During the early stages of weathering, weight gain occurs but this is very difficult to measure. Also concentration of carbon and hydrogen are lowered.

It has been observed (Flood, 1966) that coal if stacked in piles catch fire if ventilation is not good enough and this phenomenon is also due to the oxidation of the coal pile.

2.13 Structural Changes during Oxidation (Weathering)

Structural changes caused by air oxidation offer several means for determining whether or to what extent a particular coal has been oxidized. Air oxidation of coal can degrade aromatic as well as non-aromatic structures. Slight oxidation can only be detected by recording infrared spectrum of coal and manifests itself in adsorption at $3300cm^{-1}$ (-OH stretching) and at $1700cm^{-1}$ (=CO Stretching) (Berkowitz, 1979). It has been studied that the oxidation in the outcrops or seams in contact with air can go from 10 to 15 meter depth. Hence to get a sample that is non-oxidized is a difficult process.

2.14 Effect of Oxidation on Adsorption

The presence of polar compounds may influence the extent of adsorption on the surface of oxidised coals. Al-Taweel et al., (1982) investigated the adsorption characteristics of coal as a means of determining the degree of surface oxidation. Two methods were reported; static adsorption of phenol from aqueous solutions and ultimate compactness of suspensions. Two samples of coal were oxidised in dry, pure oxygen at 110°C for times varying between 24 and 150 hours. Differences were found in the adsorption behaviour

of the oxidized samples but responses to the degree of oxidation were found to depend on the type of coal used.

Mikula et al., (1983) used the ΔP test, an empirical test that indicates the degree of fissuration of a coal by measuring the initial rate of desorption. They also measured the surface area of coal from an outcropping seam. They found that the surface area increased with the increase in sampling depth. Oxidised samples from near the surface showed the smallest surface areas. Laboratory oxidation at 100°C suggested that oxidation alone might not be responsible for the surface area changes; tectonic movements in the seam may have caused microfissuration. The relationship between microfissuration and oxidation was evaluated for both the natural and laboratory oxidised coals. The values decreased with increasing oxidation. Mikula et al., (1983) suggest that oxidation could cause the closing of fine pores and fissures that make up the microstructure of coal. Although contrary to what the petrographic evidence might lead one to expect, this is similar to the suggestion of Kaji et al., (1985). However, it would seem unlikely that tests based on porosity or surface area would be valid across a range of coals. Neill and Winans (1986, 1989) have studied the use of inverse gas chromatography (IGC). In this experiment coal acts as the stationary phase; the retention of known compounds is affected by the surface properties of the coal. Changes in the thermodynamics of retention result in discontinuities or changes in the slope of ln V_{ret} versus 1/T in the IGC graph.

Oxidation of the coal affects the IGC pattern. Normally, in fresh coals, a transition is observed which correlates with the onset of plasticity; this usually occurs 10°C to 15°C before the initial softening temperature. This transition was not observed in an oxidised

bituminous coal (100°C in air for 90 hours). Winans and Neill (1987) added details of a sample that had been exposed to sunlight at room temperature for four weeks.

2.15 Summary

Adsorption is a complex process and generally it is influenced by the porosity, pore size distribution, oxidation, and presence of minerals in the sample. Adsorption is also influenced by the diffusing gas molecule size and surface area available. In addition to these factors for coal, adsorption also depends on coalification method, moisture content, porosity, density and oxidation to name a few. For intact specimen, effect of these factors is enhanced and therefore in order to avoid most of these during the testing, the adsorption characteristics of coal have been traditionally studied using crushed coal samples. Although crushed coal samples reduce the overall testing time but kinematics of adsorption is not involved. As in crushed coals equilibrium is attained quite rapidly hence basic theories for isotherms can be applied easily

Handling of the sample is extremely important as any negligence in the sample handling will result in change in moisture content as well as lead to the oxidation of the sample.

Chapter 3: Sampling

3.1 Introduction

In order to execute the experimental program central to this thesis research, a field sampling program was undertaken. Ideally, in situ core samples from a coalbed methane reservoir would have been used but the realities of developing a coalbed methane reservoir precluded this option. All coal core samples taken from depth are almost always used for canister desorption tests, the primary method used to determine the amount of methane contained within the reservoir. Consequently, samples were obtained from a surface coal mine in Alberta. This chapter describes the sampling program to obtain coal samples for the experimental program.

3.2 Field sampling

Coal samples were collected in November 2002 from Luscar's Coal Valley open pit mine in West Central Alberta, as shown in Figure 3.1. The Luscar coals belong to the Tertiary age Val D'or seam of the Upper Coalsupr Formation, as shown in Figure 3.2.

Based on the experience of other researchers attempting to obtain high quality coal sample (Noonon, 1972, Kaiser, 1979, Al-Hawaree, 1999), it was decided that high quality, consistent samples of coal could only be obtained by collecting large, intact blocks of coal. The volume of these blocks would be approximately $0.3m^3$. High quality test specimens would be taken from the blocks using cutting and trimming equipment in the laboratory. All blocks were isolated with expanding foam and wrapped in plastic for transportation to the University of Alberta

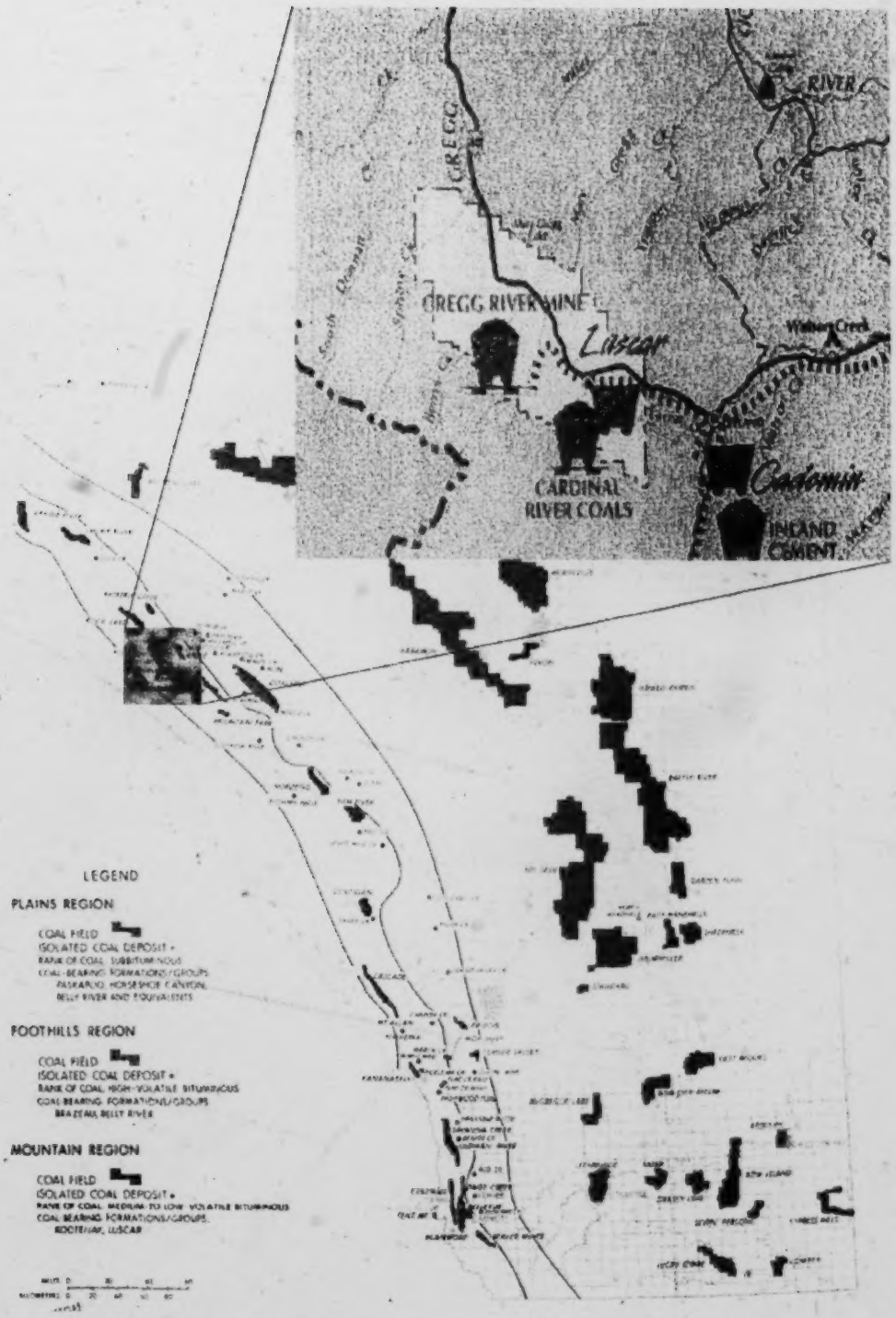

Figure 3.1: Location of Mine (modified from ESRB 1983)

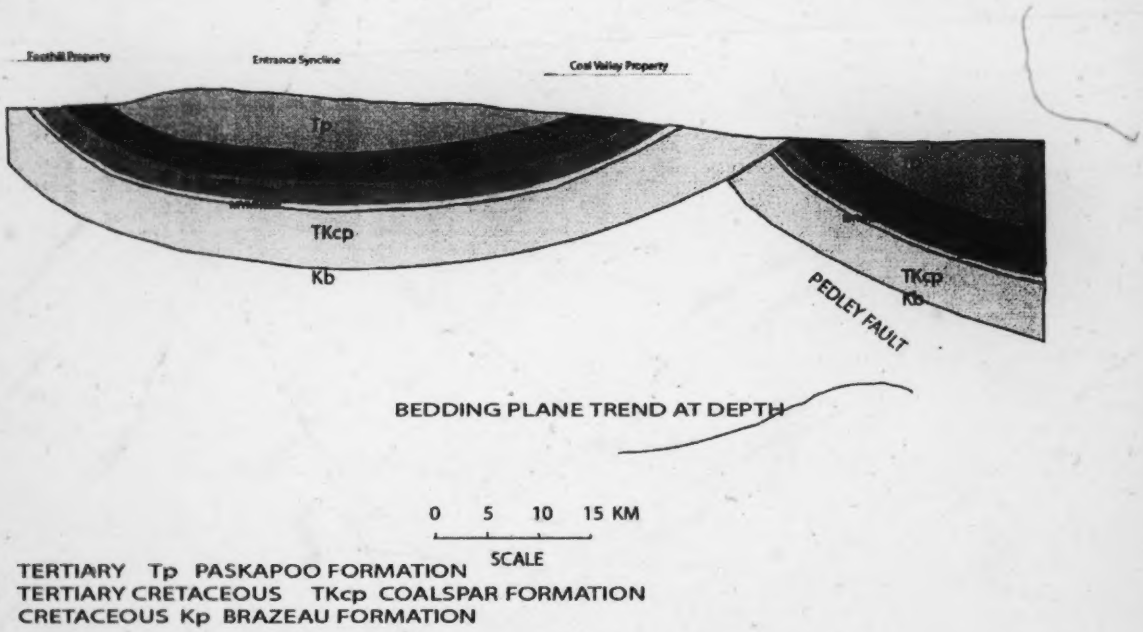

Figure 3.2: Coal Seam Geology (modified from Al-Hawaree, 1999)

Based on the previous experience of one dimensional freezing of sand samples at University of Alberta (Davila, 1992), it was decided to apply the same technique with some modifications for the coal samples.

3.3 Freeze Sampling

One of the objectives of this research is to investigate the use of freezing to prepare high quality specimens from fractured coal samples. As the samples were acquired with different methods and from different sources, a sampling technique was needed that prevented further opening of cracks and breakage of the samples during specimen preparation. For this reason, it was decided to get a coal core sample that was at least 9 cm in diameter, approximately one and half times the sample diameter required for the actual test. This also provided a sufficient diameter to allow easier coring.

The experimental apparatus utilized to conduct the uniaxial freezing test was the same apparatus originally used to study the properties of thawing permafrost (Konrad, 1980, Davila, 1992). The device (also called a freezing cell) was initially designed for controlled temperature conditions and one-dimensional freezing of a soil sample. The freezing cell is placed in a controlled temperature room maintained at temperature above the freezing point of water. Previous experiments carried out by Konrad (1980) and Davila (1992) on sand highlighted the importance of the combined effect of the use of the cold room with the freezing cell to help minimize the radial flow of heat into the soil specimen.

Although, the cold room is temperature controlled, defrost cycles are necessary to prevent ice build-up on the refrigeration system. The defrost cycle results in temperature fluctuations in the cold room environment which could be detrimental to the reproducibility of the test. These temperature fluctuations were attenuated by using an insulated cabinet. Nevertheless, in order to observe any significant fluctuations the room and cabinet temperatures were recorded continuously and shown in Appendix - H.

3.3.1 Freezing Cell and Data Acquisition System

The freezing cell is shown in Figure 3.3. Figure 3.4 shows the bottom cap in detail. The apparatus is the same as used by Hill (1977), Mageau (1978), Konrad (1980) and Divala (1992). The split cell is a 10 cm in diameter by 17 cm high Teflon lined cylinder. The outer jacket of the cell is made of thick walled PVC which prevents lateral strain during application of load and during freezing. The thermal conductivity of the PVC is very low, thereby reducing radial heat gain and resulting in primarily one-dimensional heat flow

through the sample. The freezing cell was placed on a table constructed to provide not only stiffness but a counterbalanced hanger-weight system as well.

The sealing of the sample in the freezing cell is achieved by means of O-rings placed in grooves in the wall of the top plate and at the wall of the pedestal in the bottom plate. The O-rings are effective up to a pressure of 103 kPa.

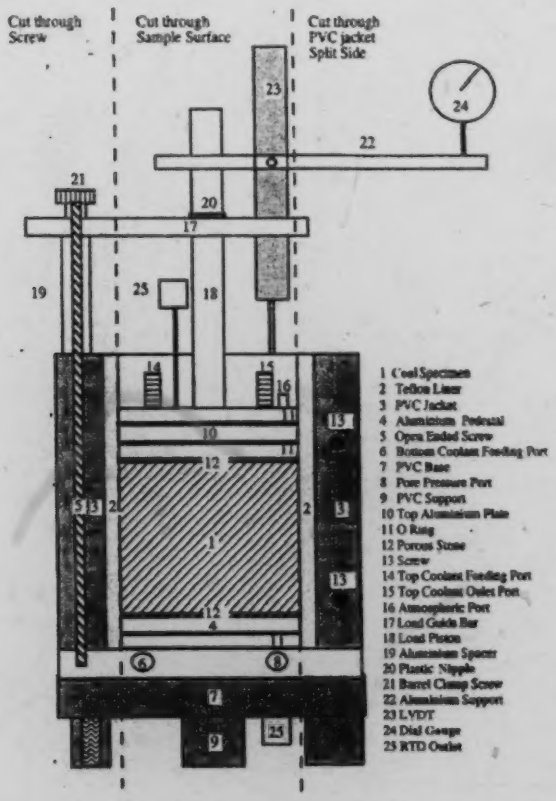

Figure 3.3: Freezing Cell (modified from Davila, 1992)

The thermal gradient is applied by circulating a coolant through the walls. Aluminum pieces are specifically designed for this purpose as the heat sinks of the system. The temperature of the coolant is controlled and maintained constant throughout the

experiment by separate HOTPACK 334 temperature bath. The temperature profile of the sample was recorded and logged with the help of resistance temperature devices (RTD) (Figure 3.5). These RTDs were placed in such a way that they were in contact with the sample for whole duration of the freezing of the sample.

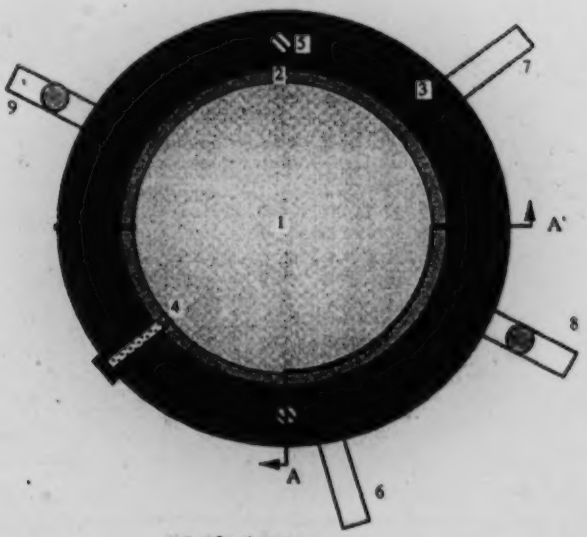

1 Coal Specimen
2 Teflon Liner
3 PVC tube
4 Resistance Temperature Detector (RTD)
5 Open Ended Screw
6 Bottom Coolant Feeding Port
7 Bottom Coolant Outlet Port
8 Pore Pressure Transducer Port
9 Drainage Port

Figure 3.4: Bottom Portion of the Cell (modified from Davila, 1992)

The RTD is a thin, flat shaped, ceramic encased, resistance temperature detector offering the advantage of being small in dimensions (2.3 × 2.0 × 1.0 mm) and providing a rapid, accurate and reliable surface temperature measurement. The temperatures of the boundary plates were also monitored with this in order to check if the applied temperature gradient is constant at any time. The RTDs are calibrated for every test using a cold bath with crushed ice and water at 0°C.

The electrical signals provided by the RTDs are recorded using the data acquisition system. The data are continuously recorded using the DOLPHIN data acquisition system. The experimental data are collected, using a time interval of 10 minutes during the whole test period. Two systems of this kind were prepared to carry out the laboratory program, and the data acquisition was common for both of them.

3.3.2 Sample Placement into the Freezing Cell

Due to the dimensions of the freezing cell, it was determined that the diameter of the sample should not exceed 9.50cm. The cell is cleaned to make sure that no dust is present. Vacuum grease is applied over the PVC jacket split sides and on the bottom, which has contact with the bottom plate. The inner part of the cell is covered with a lubricant to reduce wall friction that may develop during the freezing test. A low permeability filter paper is placed on the pedestal along with a porous stone that has been boiled and de-aired.

Once the sample is carefully transferred into the freezing cell, the system is completely sealed and saturated with water.

The sample is allowed to stay there under ambient conditions for 5 to 6 hours. A plate is put on top of it so that further instrumentation can be installed to measure the change in height of the sample during freezing. The zero reading for vertical displacement of the dial gauge is set at the 15 mm mark. The 15 mm mark is chosen arbitrarily so as to take into account any heaving or consolidation of the sample.

3.3.3 Assembling the Freezing Cell

The sealing of the sample in the freezing cell is achieved by means of O-rings placed in grooves in the wall of the top plate and at the wall of the pedestal in the bottom plate.

A porous stone is placed at the bottom. Now the specimen is placed on top of this porous stone. Another porous stone is placed on the top. RTDs are placed with the sample and it is made sure that they are touching the sample. At the end cell is filled with simple tap water and now it is ready to be frozen.

After the sample has been positioned in the cell, the surrounding PVC jacket is positioned and the RTD outlets are connected to the data acquisition system. Both temperature baths are in continuous circulation but only the bottom plate is receiving the coolant. This does not create any temperature gradient since both the bottom plate and the room are at the same temperature. The next step is the installation of the Linear Voltage differential Transducer (LVDT) rod with its core placed on top of the PVC jacket. The bearing ball is installed on top of the piston and then the hanger system assembled on top of the piston ram. The system is left for overnight under the weight of the hanger system only-.

The dead weight is placed on the hanger system and once again it is left to equilibrate for approximately 4 to 5 hours. At the end of this period of time, the specimen is ready to have the temperature gradient applied to start the uniaxial freezing of the sample.

Finally, a check of all the readings is carried out after the cold room temperature has equalized. The time and date of the start of the experiment is recorded. The door of the cabinet is closed and the initial readings from the data logger are recorded as reference points.

3.3.4 Freezing of the Sample

Freezing of the sample begins at an initial temperature gradient of 0.5°C per hour applied for the first 4 hours and then increased to 2°C per hour. Measurements from the RTDs

allow the position of the freezing front in the sample to be monitored continuously. After 24 hours the temperature gradient is further increased and maintained.

The measurement of the movement of the freezing front is very important as only this will enable us to find the position of the freezing front in the sample. As mentioned earlier that the two RTDs were placed with each sample, one at the top and one bottom so that the temperature at these points can be measured. Once the temperature on the top either reaches zero or ice can be seen on the top, the test was stopped. Sometimes, it was observed that due to the fluctuation in temperature in the freezing room the temperature shown by the top RTD was not consistent with the observation that ice has been formed on the top. Figure 3.5 shows a typical relationship between the time and the movement of the temperature inside the cell at top and bottom for freezing cell 1.

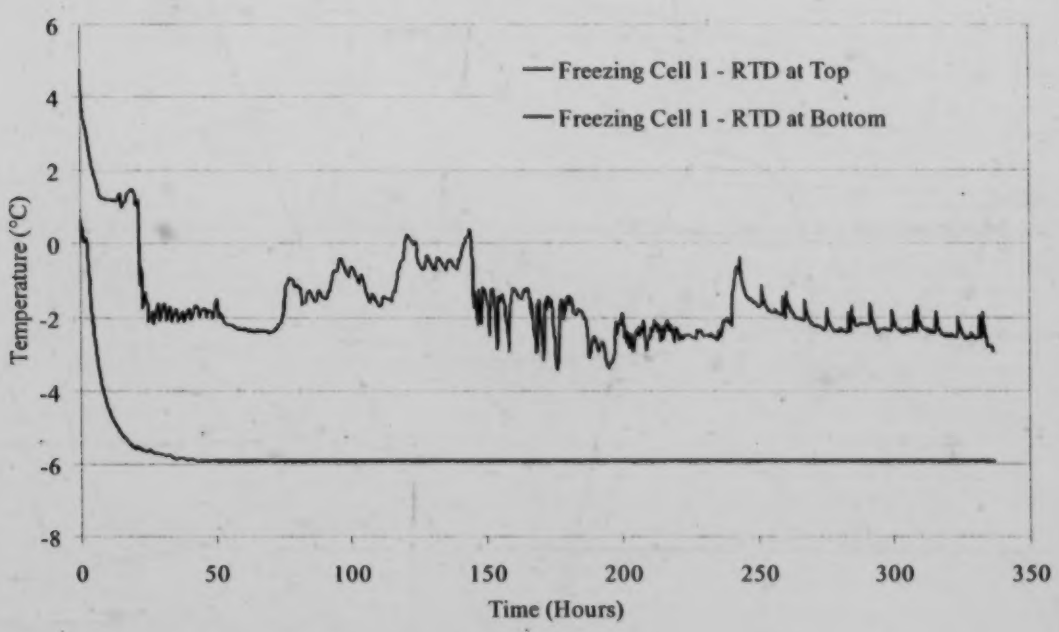

Figure 3.5: Graph between Temperature Gradient and Time in Cell

Once the samples have been frozen, that approximately takes 5 days, they are easily removed and placed in a freezing room at -35°C. The sample is cooled to -35°C to allow easier coring at room temperature and prevent the internal temperature of the sample to go above 0°C. If the temperature goes above 0°C sudden thawing of the sample may cause the fractures present in the sample to start opening up resulting in breakage of the sample.

After three days at -35°C, which is sufficient for the thermal equilibrium to be achieved, the samples were taken out of the freezing room to start the final coring of the samples to produce 62 mm diameter specimens. The specimen preparation was done as quickly as possible to ensure that the temperature of the specimen did not approach room temperature. After coring a specimen to the final diameter, they are once again placed in the freezing room but at a lower temperature. Now the temperature is increased in increments until the samples are at the room temperature within a week's time. Figure 3.6 to 3.11 shows the placement of the sample in a step by step approach as explained earlier while Figure 3.12 shows the final specimen.

Figure 3.6: Freezing Cell: Bottom Drainage Platen

Figure 3.7: Freezing Cell: Porous Stone at Base of the Cell

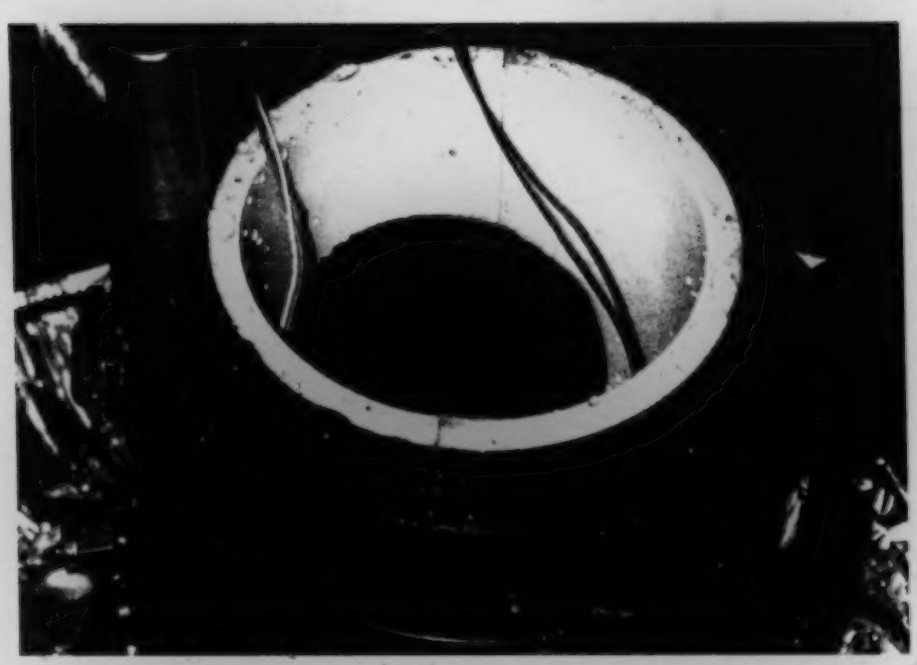

Figure 3.8: Coal Sample and RTDs in the Freezing Cell

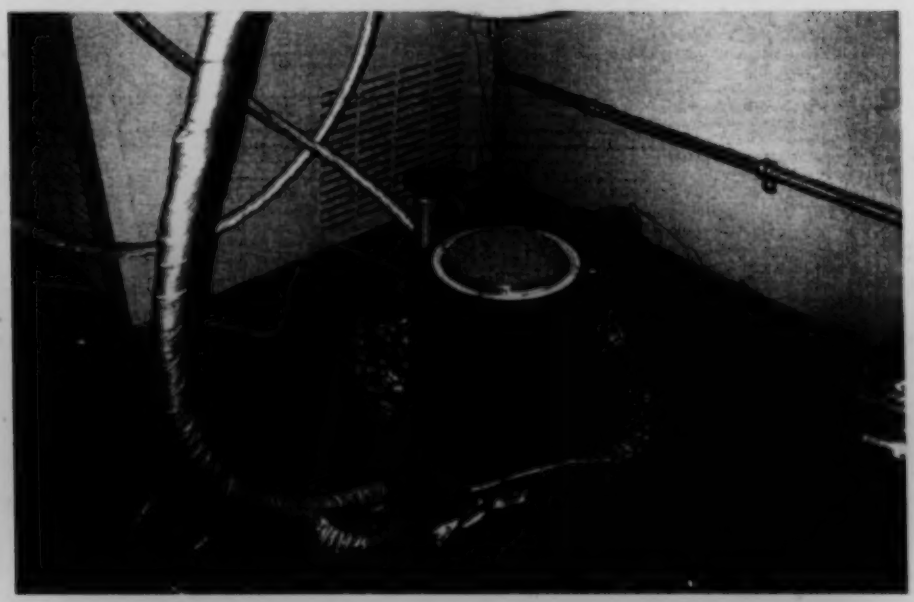

Figure 3.9: Freezing Cell: Top Porous Stone placed on Top of the Coal Sample

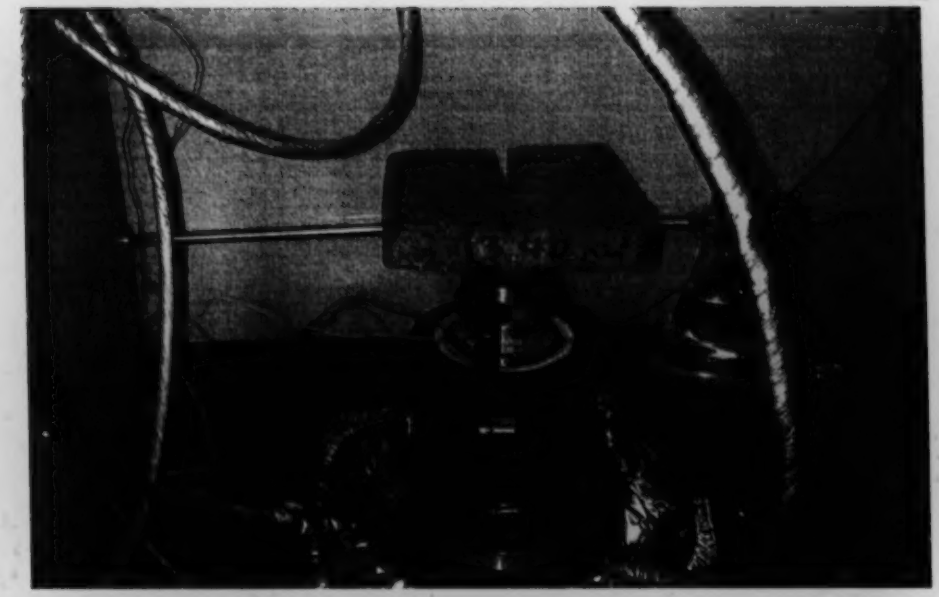

Figure 3.10: Weight Placed on Coal Sample for Confinement

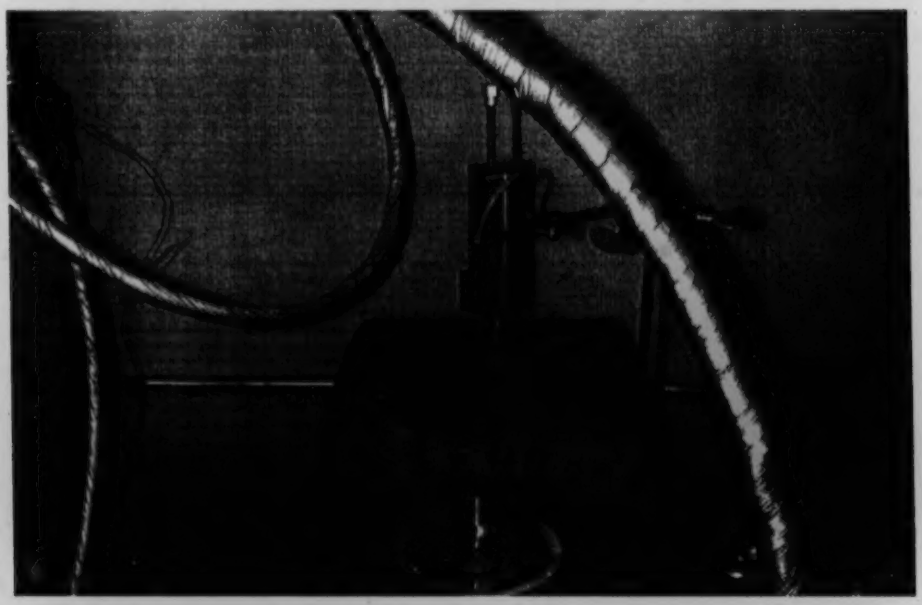

Figure 3.11: Installation of LVTD to Monitor Vertical Displacement during Freezing

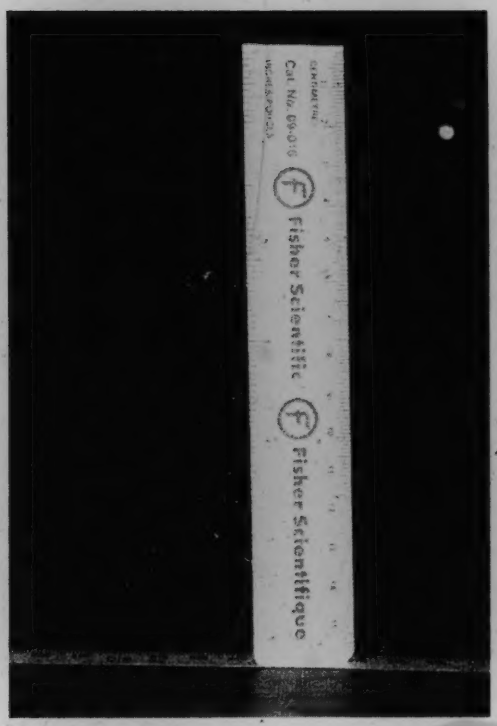

Figure 3.12: Frozen Coal Sample

3.3.5 Advantages

A significant advantage of freezing technique is that a workable specimen can be obtained from coal samples that are extremely fractured. The frozen samples are easy to handle and subsequent coring with any coring machine using chilled water can be easily undertaken. The frozen water will hold the specimen intact therefore minimizing the coring disturbance.

3.3.6 Disadvantages

A major unknown factor in utilizing the freezing technique is the alterations that may occur in the chemical signature of the water. A geo-chemical analysis of the water that is present in the seam was not available. Without understanding the original in-situ geo-chemical nature of the pore water in the seam, it is very difficult to replicate to assess its

variation during the freezing technique. If a change in water chemistry occurs, it may affect the adsorption capacity of the coal. Since the frozen specimens were not used in this research therefore the issue of water chemistry changes was not pursued. If freezing techniques are utilized water chemistry changes will require further research.

Temperature gradients also need to be monitored constantly because higher gradients tend to cause ice lensing leading to opening of the cracks and possible breakage of the samples. For low temperature gradients it can take more than a couple of weeks to freeze one sample.

Another point of concern is the thawing that may occur when the sample is removed from freezing room in order to core the specimen and sudden thawing may even break the sample.

3.4 Alternate method of Sampling

Al-Hawaree (1999) tried to sample coal from the same mine but pointed out that it was extremely difficult to get a good core length of the sample, due to the pervasive fracturing within the coal. However, it was decided that same method should be tried with some modification.

Large pieces of coal were put in a plastic lined tray full of plaster of paris. When the plaster of paris sets, it holds the coal sample securely and prevents movement during coring, aiding in the coring of high quality specimens. It also ensures that the cored sample is straight and has smooth edges. In this manner a workable sample can be obtained from the coal. To prevent the plaster from entering the coal fractures, the coal specimen was doubly wrapped in plastic sheet. If the plaster moves into the coal

fractures, it may open up the fractures when it sets and subsequent breakage of the sample can occur.

A portable coring machine available at the Civil Department, University of Alberta, was used for the coring and is shown in Figure 3.13. The core barrel length was such that even if the sample is broken within the core barrel, the required specimen size can still be cut from the broken core. In general 3 to 4 finished specimens were prepared. Figure 3.14 illustrates the condition of a cored specimen

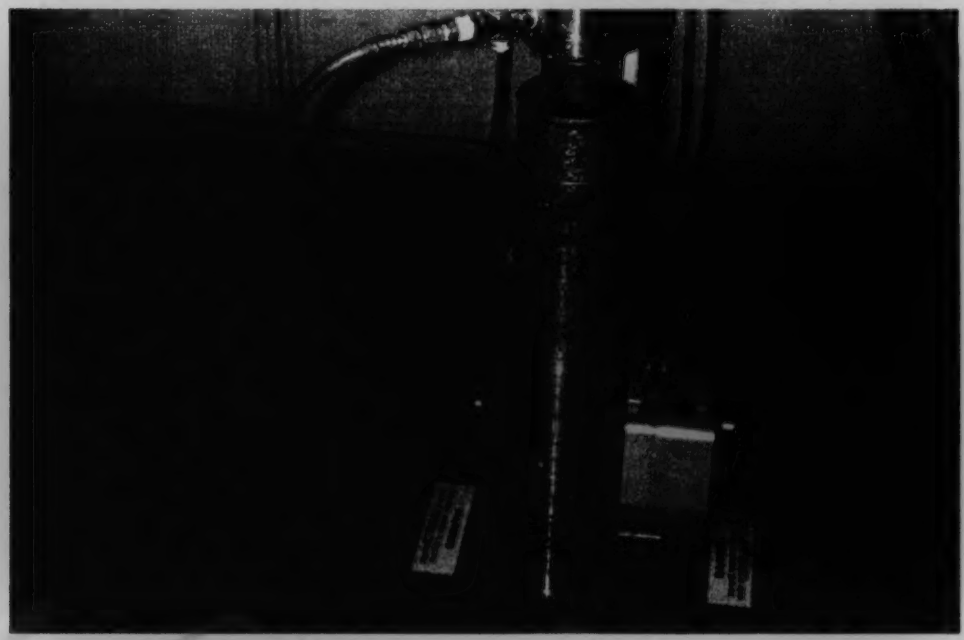

Figure 3.13: Coring Machine and Core Barrel

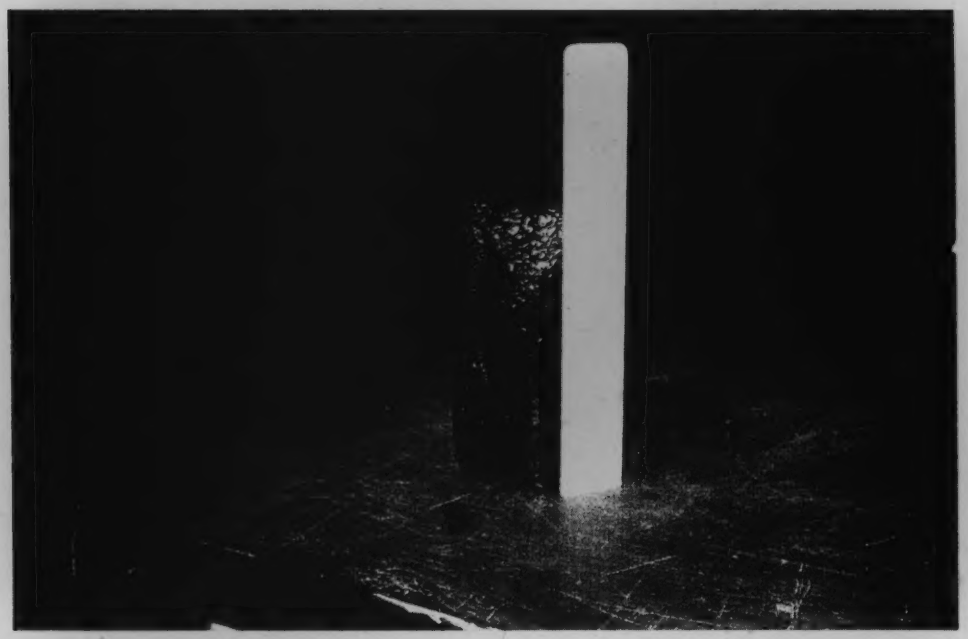

Figure 3.14: Coal Specimen Obtained Using the Coring Device

Once a core sample was obtained the final step in specimen preparation is to cut the specimens to the required size. This was a difficult procedure as usually some part of the sample was chipped at the end of the sawing run and the sample was rendered useless. This happened as a result of the stress concentration at the end of the coal specimen as the saw reached the edge of core sample end. Therefore, to obtain good quality samples, the core were put in an Acrylic tube and the tube was marked at 10±1mm. Tape was wrapped around the tube as well as on the open ends of the samples so as to keep the sample in place. Care was taken to not cut the tube all the way through. Leaving the tube intact ensures that coal is not broken at the end even when it is sawed all through the diameter. Specimens that were cut in this fashion had satisfactory dimensions. The usual size that was obtained was 10.5±0.75mm. Occasionally, the specimen that was obtained after sawing was not of constant thickness hence it was decided to machine the sample.

This was done to have a constant thickness of the sample so that when the sample is put into the cell it would not have any differential movement. Figure 3.15 to 3.20 illustrate the final steps in specimen preparation.

Figure 3.15: Core in Acrylic Tube

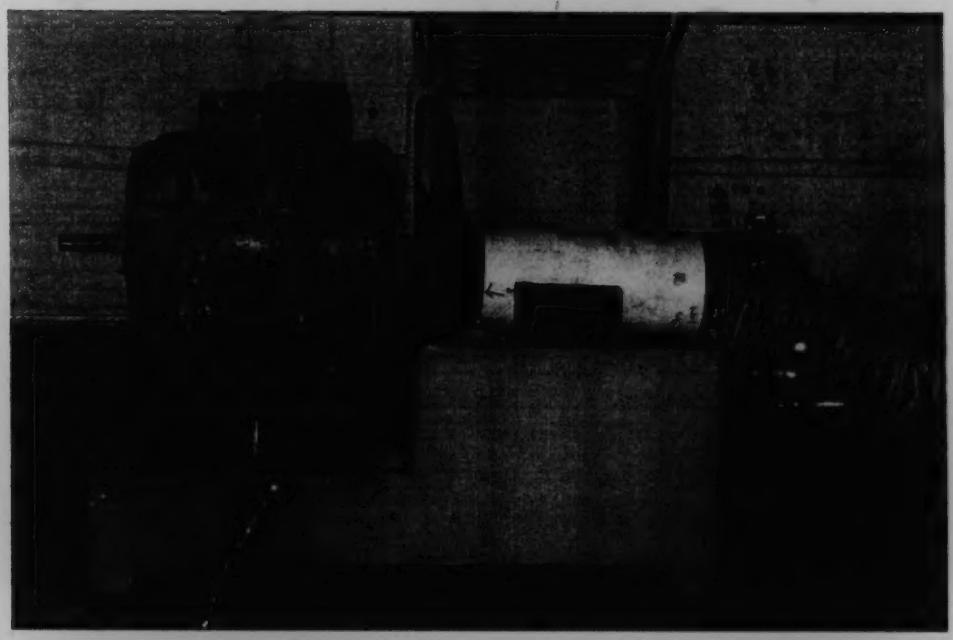

Figure 3.16: Sample Ready for Sawing

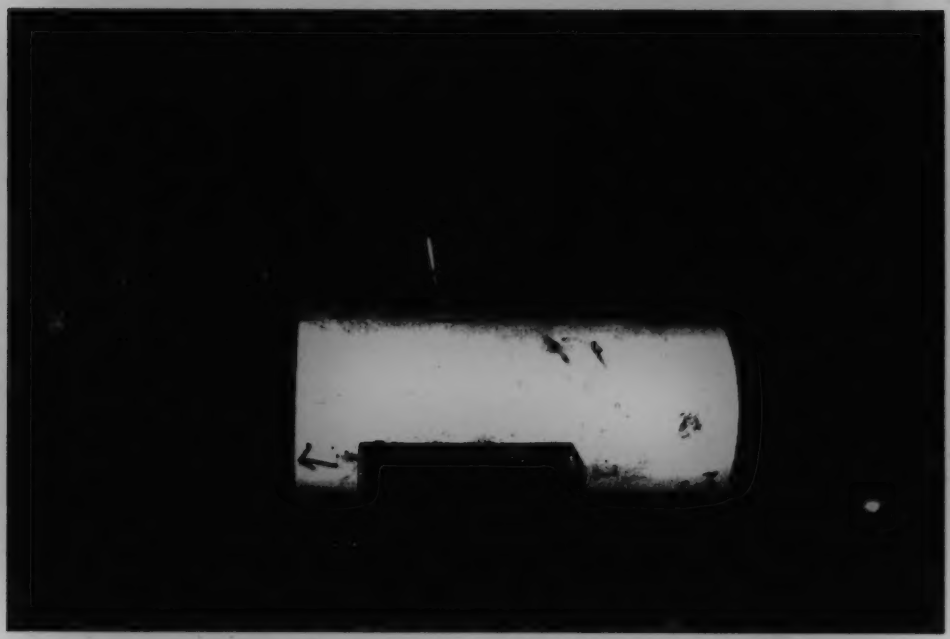

Figure 3.17: Sample being Sawed

Figure 3.18: Sample ready for Machining

Figure 3.19: Sample being Machined

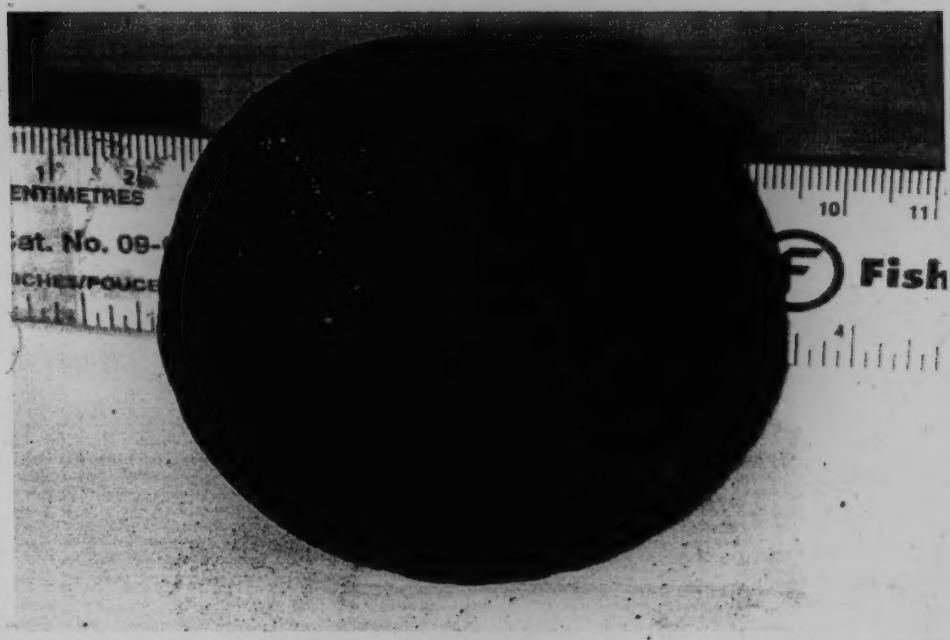

Figure 3.20: Prepared Sample

3.5 Summary for Intact Specimen Preparation

As discussed, possible changes in the pore water chemistry within the frozen coal sample led to the decision of not using this technique for the specimen preparation. From previous studies (Arri et al., 1992, Clarkson and Bustin, 2001) it was found that the presence of moisture in the coal matrix significantly changes the adsorption equilibrium characteristics of gases. Arri et al., (1992) further showed that the water present in the pores starts competing for the adsorption spaces present in the coal and also that the moist coal adsorption curves have greater variation than the dry coal adsorption curves. According to the model predictions by Clarkson and Bustin (2001), the presence of moisture in coal decreases the selectivity for carbon dioxide and water competes with gases for adsorption sites, and apparently occupies the higher energy sites that would

otherwise be occupied by carbon dioxide if the coal was dry. Hence taking these observations into consideration it was decided not to use the frozen samples in this study and recommend that further study of this phenomenon is required.

The samples that were obtained without freezing have been used in previous studies undertaken by Harpalani (1988) and Al-Hawaree (1999), and were found to be quite adequate. The second method used has fewer unknowns present although the question still remains about the quality of the sample. In this study only the adsorption testing was to be carried out therefore it was decided that these samples could be used. Another factor which contributed towards using the second technique was that the samples were easier to prepare and handle.

3.6 Sample Preparation for Crushed Coal

The selection and preparation of a crushed coal sample was a critical step in the experimental procedure. The procedure can be summarized as follows.

- Sample selection
- Sample crushing
- Proximate analysis

Samples for crushing can either be obtained from drill cuttings or cores. The disadvantage with drill cutting samples is that the depth of origin is not precisely known and as a result, samples that are selected may not be representative of the average reservoir properties of the entire producing interval. Generally samples are selected on the basis of depth and ash content. Relatively ash free samples are desirable for the experiments to minimize the influence of the non-coal material upon the results. Prior to performing an isotherm experiment, proximate analysis of the samples should be

conducted to determine the moisture, volatile matter, ash, and fixed carbon content of the coal. The purpose of undertaking proximate analysis is to quantify the mass of coal present in the sample that is to be used for the isotherm analysis. Generally it is preferable to use samples with an ash content of 15% or less to avoid non-coal affects upon the diffusion behavior.

Crushing is performed in order to reduce the experimental time by minimizing the distance gas molecules must diffuse through the matrix. In general, the internal surface area of 100 grams of bituminous coal ranges from 75,000 to 220,000 cm^2 (Jones et al., 1981).

Figure 3.21: Hand Crushed Sample

Figure 3.22: Crushing Machine used

Figure 3.23: Sample after being Crushed using the Crushing Machine

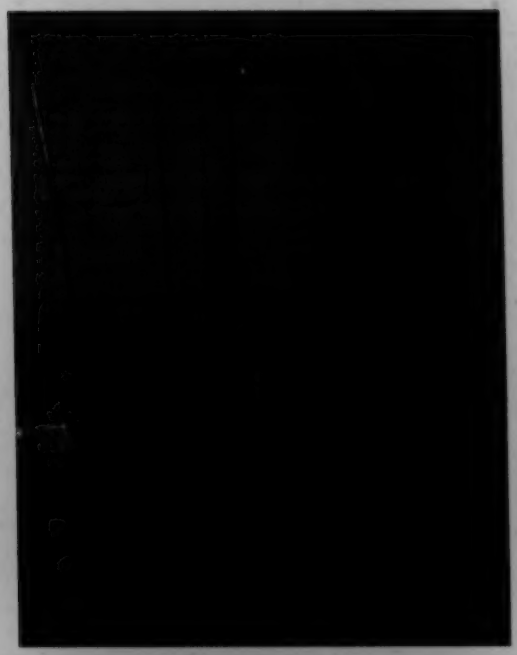

Figure 3.24: Sample being Passed through Sieve

Figure 3.25: Sample to be used in the Testing (passing sieve #60)

The external surface area of 100 grams of spherical coal particles (assuming a Density of 1.25 g/cc and 0.0250 cm in diameter (60 mesh)) is 240 cm^2. As a result, crushing the coal changes the surface area for gas adsorption.

The procedure given in ASTM D2013-86 (Reapproved 1994) was followed for the preparation of the samples for the adsorption testing of coal.

The sample was crushed by hand (stage crushed – Figure 3.21) to pass through 4 mesh (4.75 mm) sieve and four sub samples were obtained. A fraction passing #4 mesh was retained and other sub-samples were crushed using a crushing machine (Figure 3.22) to pass though an 8 (2.38 mm), 20 (0.841 mm) and 60 (0.25 mm) mesh sieve (Figure 3.23). The sieving process is shown in Figure 3.24. Only the fraction passing 4 and 60 mesh were used for isotherm analysis (Figure 3.25), according to the ASTM D2013-86 (Reapproved 1994)

3.7 Summary

As for all geotechnical / geo-environmental testing the quality of the specimen used in the testing has a significant impact on the experimental results. This is usually true for the analysis of adsorption behavior.

Assessment of the freezing technique for sample preparation appears to show that extremely high quality specimens of highly fractured coal can be obtained. Further study is needed to fully understand the geo-chemical processes that may occur in the sample during the freezing process. When these geo-chemical processes are understood and are shown to have a negligible impact on the adsorption and mechanical behavior of the coals, the freezing method may prove to be an ideal sampling procedure.

The crushed coal specimens were prepared according to the ASTM 2013-86 (Reapproved 1994).

Chapter 4: Experimental Setup

4.1 Introduction

This chapter describes the experimental design criteria, the experimental infrastructure and the experimental procedures followed in this research program.

4.2 Guiding principles

A triaxial cell remains the most common apparatus used in determining the geotechnical properties of a material. In geotechnical testing, a "true" triaxial cell allows for independent control of the three principal stresses. The most common form of a triaxial cell, however, has σ_2 and σ_3 equal by applying a hydrostatic cell pressure around a cylindrical specimen. This type of cylindrical compression test for studying changes in volume and the determination of pore pressure responses as well as dissipation rates under isotropic conditions is the most typical of triaxial applications in geotechnical engineering (Bishop and Henkel, 1964).

A triaxial cell concept that has been modified for isotropic stress conditions following design criteria is determined to be important in this type of testing within the framework of triaxial testing, the following design criteria are deemed important for successfully examining the constitutive response of coal:

- Capable of testing under a wide range of temperatures and pressures, indicative of geological storage situations;
- Re-saturation of specimens with compatible pore fluids (if needed);
- Incorporation of a true triaxial environment, to best replicate in-situ conditions;

- Designed with the intention of testing permeability, intact adsorption, and diffusion of gases under pressures indicative of deep saline aquifer conditions;
- Design should be adaptable to include the determination of gas permeability under conditions of deformation;
- Design should be flexible, and easily adjustable to accommodate a variety of core types and sizes;
- Ease of sample loading, reducing the set-up time required, and the minimization of sample preparation are desirable to avoid potential desiccation and sample disturbance prior to testing;
- Either a relatively gas impermeable membrane should be used, or alternatively, the gases must be insoluble in the cell fluid;
- Membrane should remain flexible enough so that the lateral confining pressure is not carried by the membrane; and
- An adequate sealing mechanism on the upper and lower end caps must be in place to ensure no leakage from the specimen into the cell fluid or vice versa.

The modification of the triaxial cell, taking the above points into considerations, has been undertaken previously by Ho (2002) and the same cell is used here for the testing of adsorption of gas on coal. While the details of the testing infrastructure can be found in Ho (2002) some of the salient features of the test equipment are discussed in the following sections since the testing procedure deviated substantially from the standard ASTM test methods.

4.3 Temperature Limits and Control

The experimental apparatus is capable of operating under a variety of temperatures, from room temperature to 60°C. The temperature of CO_2 at disposal is dependent upon the specific reservoir conditions i.e. depth of the reservoir, as well as the ground temperature. In this study the temperature was assumed to be 50°C and it was assumed that CO_2 will be disposed at a depth of about 200m.

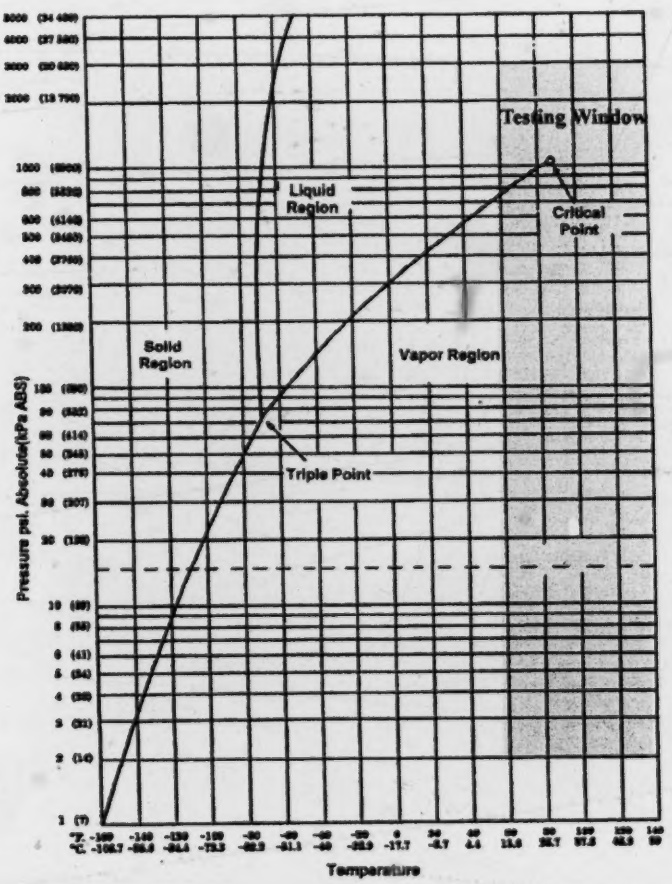

Figure 4.1: Applicability of Testing Framework in Field Conditions (Modified from the Handbook of Compressed Gases)

Range of temperatures, for which this testing equipment is valid, will enable CO_2 storage testing to occur under a variety of conditions. The testing range is illustrated in Figure 4.1, relative to the phase behaviour of CO_2.

Fluctuations in temperature have an effect on the gas properties such as density, viscosity as well as the gas solubility in water, rate of diffusion, and adsorption. Changes within 0.1°C can result in density fluctuations as great as 1% around the critical point of CO_2 (Span and Wagner, 1996). Fluctuations of temperatures in the testing window of 0.1°C will result in 10% difference in gas density. Temperature tolerance for diffusion is about 1°C. Strict temperature control is required to accurately and precisely measure the gas volumes. In measuring adsorption by volumetric means, the amount of gas adsorbed is calculated based on the temperature and pressure of the gas. Poor temperature control will result in large uncertainties in determining gas volumes.

To achieve the required temperature accuracy and stability, the triaxial cell, gas and water lines were all submerged under water in a constant temperature water bath. The water bath was monitored using Precision Platinum RTD Temperature Probes (Azonix 1011). A Proportional-Integral (PI) control system was set up to obtain tight control on the water bath. Two mixers were placed inside the bath to ensure uniform circulation of water throughout the bath. A 750 watt heating element was placed inside the water bath to supply the necessary heat to maintain a constant temperature. Power delivery to the heating element was provided by PCI data acquisition board which transmitted the voltage to 20mA converter, and solid state relay (SSR) driver. The Labview control system received information from the SSR driver, and the corresponding energy input

was provided to maintain a constant temperature. An overall accuracy in measurement was 0.02°C, while the accuracy of the control was determined to be 0.05°C.

4.4 Pressure Limits and Control

For all tests conducted in this research, an effective confining pressure of 3.75MPa was based on a saturated unit weight of 18.5kN/m^3 at a depth of 200 m. This testing apparatus is capable of testing to a maximum cell pressure of 20MPa and a maximum gas pressure of 10MPa at 50°C. The upper limit of pressure, both for water and gas, is due to the material of the cell. The cell could be easily modified to accommodate significantly higher pressures.

Control on pressure fluctuations is not as stringent as the regulations on temperature. ISCO 500D and ISCO 260D series syringe pumps, with Nitronic50 construction of all wetted parts, and a heavy duty graphite-impregnated Teflon seal, were used to deliver gas pressures to the cell. It is capable of operating to a maximum pressure of 25.9MPa (3750psi) to an accuracy of 0.5% of the full scale. Changes in the pressure can affect the rate of diffusion therefore stringent control of the pressures in syringe pumps is required. The syringe pump is preheated to 50°C, and is wrapped in insulation tape to minimise heat loss to the atmosphere as shown in Figure 4.2. All of the flow lines leaving the pumps pass through a heat exchanger, which is controlled by an ISOTEMP refrigerated circulating water bath, bringing up the temperature of the flow lines to the testing temperature, if required prior to entering the main temperature bath.

4.5 Cell Fluid

If a low solubility cell fluid is used it limits the mass transfer of CO_2 from the specimen when the cell fluid approaches its CO_2 saturation point. Therefore, change in

concentration of CO_2 with respect to time can be determined for a given volume of cell fluid. This rate of change can be calculated and accounted for in the laboratory analysis. However, solubilities which are too great will decrease the overall sensitivity of the analysis. Grozic (1999) tested gassy sands under triaxial configurations at relatively low pressures using viton coated latex membranes. Since testing was performed in 3-4 hours, it was concluded that minimal diffusive losses through the membrane would have occurred in that time, which allows for the use of water as the confining fluid. However, adsorption and diffusion tests on coal result in significantly longer test times.

Sobkowicz (1982) outlined a variety of options in altering the cell fluid to minimise the diffusion of CO_2 from the sample to the confining fluid, among them were low gas solubility fluids such as mercury, silicone oil and glycerol. Although silicone oil can be used to reduce the diffusive escape of most permeants, due to its viscous nature (Tavenas et al., 1983), its CO_2 solubility increases substantially with pressure, rendering it ineffective for CO_2 isolation systems (Wedlake and Robinson, 1979). A better cell fluid was determined to be glycerol ($C_3H_8O_3$) in preventing gas diffusion from the specimen (Sobkowicz, 1982). Solubility of CO_2 in glycerol is in the order of 10^{-5} mol/cm^3, only slightly lower than the CO_2 solubility in water at the same temperature (Vazquez et al., 1994). Although it has been exhibited that glycerol and silicone oil have lower CO_2 solubility than water but using glycerol or silicone oil results in an increase in the equipment set-up time in comparison to water. An additional error associated with the use of low solubility confining fluids is that the calculation of solubility with time can be altered by the presence of gas bubbles entrained in the cell fluid during set-up. Testing

conducted by Sobkowicz (1982) demonstrated that upon disassembly of the apparatus, trapped CO_2 between membranes and in the cell fluid (glycerol) was observed.

Expected experimental time will have a significant influence over the applicability of utilising a low solubility fluid as the confining fluid to prevent migration of gases from the specimen. Krooss and Leythaeuser (1988), and Rebour et al., (1997) suggest that the amount of gas loss due to solubility in cell fluids can result in a decrease in the sensitivity of the analysis. Solubility of CO_2 into the cell fluid should be much less than the CO_2 diffusion/adsorption in the sample materials.

Initial cell designs that were carried out at the University of Alberta attempted to incorporate a double-barrelled triaxial cell. In the double barrel design, the outer barrel houses the confining fluid (typically water), and the inner barrel contains mercury which prevented the diffusion of gases from the sample into the confining fluid, separated from the specimen by a latex membrane (Fredlund, 1973; Al-Hawaree, 1999). The double barrel technique is capable of preventing gas migration from the specimen to the cell fluid; however, it is a difficult test method to work with in terms of experimental set-up. The major drawback of using mercury in this kind of testing is that mercury is difficult to work with, hard to clean up, and a hazardous substance which requires significant laboratory equipment and safety precautions to handle properly. Any leaks in the membrane and/or membrane seal results in mercury entrainment into the sample, porous stones, and displacement into the flow lines. Leakage results in complicated cleanup procedures and in extreme cases may result in pump damage if proper mercury traps are not in place.

Given the inherent difficulties associated with cell fluids and CO_2 solubility, the test system was modified by Ho (2002), to utilize a special membrane system to eliminate solubility issues. The following section describes the details surrounding the selection and design of the membrane sealing system.

4.6 Membranes

Ho (2002) suggested changes in membrane material that can reduce the loss of gases from the specimen. Materials such as polyethylene film, Teflon film, copper and other metals all have lower diffusivity to gases than latex, which have been traditionally used in the triaxial testing, were suggested. If a relatively impermeable membrane is not available, a combination of low diffusivity membrane with a low solubility cell fluid may be suitable, depending on the specific test conditions.

Typical polyethylene heat shrink is made with linear low density polyethylene (LLDPE), however, not all LLDPE are equal. Varying properties in the LLDPE will result in varying gas diffusivity properties. Shrink film is usually made with LLDPE or VLDPE (very low density polyethylene). Essentially, lower the density of the polyethylene greater will be the gas migration rates. Other factors are thickness, film orientation and cross linking.

Ho (2002) studied the membranes that can be used in this type of testing in detail and observed that seamless thin walled copper and aluminium membranes have been used successfully in the testing of competent shale materials by Krooss et al. (1998), and Harrington and Horseman, (1999). However, thin walled larger diameter copper membranes can be difficult to procure.

The electroforming process, whereby molecules of copper are deposited onto a mandrel to the desired thickness and later removed, is capable of producing very thin walled seamless copper membranes of a variety of sizes. An inherent risk associated with electroformed copper is that poorly electroformed copper has inclusions and open porosity and can potentially enhance gas diffusivity. However, well-manufactured electroformed copper should be 100% dense, and will behave similar to wrought copper with the same grain size, which is practically impermeable to gas diffusive effects (Shelby, 1996).

4.7 Sealing Mechanisms

Even though the membrane selection is of utmost importance it is imperative to effectively seal the membrane against both the upper and lower end caps to ensure isolation of the cell fluid and pore fluid. Preventing communication between the gas (pore fluid) and the water (cell fluid) was difficult to achieve with an O-ring. The addition of hose clamps were unable to provide a uniform seal on the O-rings, and therefore provided zones whereby leakage could occur. It was determined that a sufficient seal could not be assured utilising these methods.

Ho (2002) tried to eliminate the sealing uncertainty associated with hose clamps by designing smooth seamless confining rings having bevelled edges. These confining rings were meant to secure the O-rings in the O-ring grooves, and therefore provide adequate sealing by providing a physical force. However, during testing Ho (2002) determined that the confining rings were cumbersome and difficult to work with. They were only able to provide seal part of the time, and their potential failure or success was not always easy to determine. In some cases, the seal was broken upon disassembly of the test cell.

Assembly of thin metal membranes utilising the confining rings was also prone to tearing of the metal. Utilising the confining rings required significant effort and time to set-up the apparatus and likely subjecting the specimen to significant disturbance and desiccation. In some cases, the sample showed signs of crushing and extreme disturbance upon disassembly. Consequently, confining rings were not incorporated in the final design of the experimental system.

Introduction of metal membranes resulted in increased difficulty in sealing the end caps due to their rigidity. It was determined by Ho (2002) that O-ring seals utilising some type of confining ring or split ring would not provide a reliable seal. The substantial increase in cost of copper membranes in comparison to latex or polyethylene membranes requires an increased reliability of the sealing mechanism, as membrane failure leads to higher experimental costs.

A sealing mechanism, modeled after a Swagelok fittings was designed by Ho (2002) to allow a rigid membrane to slide freely inside the seal until the fittings were tightened. This more sophisticated approach to sealing relies on a series of O-rings separated by brass washers, to provide an active compression against the copper membranes. The active seal is achieved by mechanical exertion of a force on a series of O-rings, creating an active seal between the copper tubing and the end caps. If required, a concentric silicon ring can be cast around the copper tubing as a back-up seal during the early stages of pressurization.

Copper membranes employed were specifically designed for the flow cell by electroforming. The copper membranes specifications were an inside diameter of 63.6mm ±0.03mm; a length of 70 mm ±0.5mm, and a thickness of 0.15mm ± 0.03 mm. A

thickness of 0.5mm is the maximum acceptable wall thickness in the current sealing design.

4.8 Plumbing

Tubing used was constructed from stainless steel and is capable of tolerating high pressures. The system was leak tested several times to ensure that there were no leaks at any of the tubing connections. The water line was tested at 15MPa of water pressure at room temperature and 50°C (test temperature). The gas lines were tested for 10MPa at room temperature as well as at 50°C (test temperature). The closed system was kept running for a week and no leakages were recorded during this process. This was one of the most important steps of the test procedure because in previous studies (Al-Hawaree, 1999, Ho, 2002) the leakage from the plumbing was always observed.

Furthermore, all the plumbing was wrapped in heat insulation material to ensure that the temperature did not drop below the testing temperature (50°C). If there was a high difference between the temperature of gas and the testing temperature then there would be sudden expansion or contraction of the gas that would make the results unreliable.

A spiral tube was placed inside the water bath and gas was passed through it to ensure that the temperature of the gas entering the specimen was at 50°C (test temperature).

4.9 Data acquisition system

A high performance data acquisition system was used to collect and record data during the tests. This data acquisition system consisted of a Desktop Intel based computer, HP 3497a signal acquisition hardware, and Labview software.

4.10 Calibration of Electronic Monitoring Devices

The electronic monitoring devices were calibrated prior to the start of the test program. Calibration checks were repeated periodically during the testing program and a second full suite of calibration was carried out half way through the testing program.

4.11 Experimental Procedure for Intact Sample

A series of permeability tests were conducted on the coal samples from the same mines by Al-Hawaree (1999). Al-Hawaree (1999) also tried to investigate the effect of adsorption of different gases (CO_2 and CH_4) on Coal Valley bituminous coal. Those tests were performed under different gas pressures to evaluate the behaviour over a range of injection pressures. The confining pressure was also varied between 6MPa and 16MPa to study the influence of different in situ confining stresses. Intact small coal samples of 1" diameter were used to reach adsorption equilibrium in short time. Using intact samples allows the separation of the effect of micro porous and macro porous effects on the coal behaviour.

In previous research studies, Ates et al., (1988) showed that adsorption time for small samples (54 mm diameter and 12.7 mm thickness) takes around 24 hours while Harpalani et al., (1993) concluded that coal saturation with gases takes a long time (four months for 3 ½" (90 mm) diameter sample). Consequently, small samples were used in this research to allow rapid saturation of the coal. The specimen dimensions were around 62 mm diameter and 10 mm height.

During the adsorption test, samples were left for longer times to assure full adsorption. This time period ranged between a minimum of 24 hours to a maximum of 240 hours and was ended only when the syringe pump stopped adding more gas to the sample or the

total amount of gas being pumped was less than a flow rate of 0.3 mL/hr of gas, which can be detected easily with this equipment. Based on this, a pressure increment was concluded when the amount of gas that entered the cell was less than 0.3 mL/hr over a period of 4 hours continuously. A secondary measure of 0.5% of the cumulative gas volume entering the cell over a 4 hour period was also used as equilibrium limit. Although volume change measurements are important variables to monitor during the adsorption and/or compressibility tests, the small size of the specimen prohibited these measurements and was expected that the volume change would be small.

After the preparation of the sample, as has been described previously, the sample is weighed using electronic balance, capable of weighing up to micro-gram. The dimensions of the sample are also taken using a vernier-calliper, capable of measuring up to fraction of a millimetre.

If any fractures are found on the sample, as found in this particular sample shown in Figure 4.4, they are filled with coal passing sieve#60. Coal passing sieve #60 is used because the same coal will be used for the crushed coal testing according to ASTM D2013-86 (Reapproved 1994).

A porous stone is placed on the top of a spacer (Figure 4.4) and sample is placed on top of this porous stone. Porous stones are used so that the gas pressure is equally distributed onto the surface of the coal specimen. Another porous stone is placed on the top and the whole assembly is placed inside the copper membrane (Figure 4.7).

This assembly and the sealing rings are gently placed on the top pedestal. A copper spacer ring is placed on the bottom pedestal followed by an O-ring then again a copper ring followed by another O-ring. These copper spacers and O-rings form the basis of the

sealing system. A stainless steel ring is then put on this whole assembly and tightened so that the copper rings as well as the O-rings compress to form a seal. Same procedure is followed is done with the bottom (Figure 4.18). This assembly is placed into the cell, the top cap is closed and now the sample is ready for placement into the triaxial cell for testing (Figure 4.19).

After placing the sample in the cell (Figure 4.20), it is filled with water already at test temperature of 50°C. The cell is now placed inside the temperature bath and water is filled in the temperature bath. The temperature of the water in the bath is maintained at 50°C (testing temperature). An initial pressure of 3.75MPa is applied as cell pressure. This effective confining stress of 3.75MPa is kept constant throughout the duration of the test.

Now the sample is ready to be back-saturated with helium gas. Back-saturation of the specimen with helium gas is now conducted in order to flush out all of the gases already present in the sample. A back-saturation pressure of 125kPa is used which is slightly higher than atmospheric pressure but lower than the first intended CO_2 adsorption pressure of 150kPa. Helium pressures above the atmospheric pressure ensure all gases are flushed out of the specimen and the dry helium gas also adsorbs the excess moisture present in the sample.

The setting with the helium pressure of 125kPa is left overnight to equilibrate. The valve at downstream side is opened and the gas is flushed. This flushing is undertaken because in this research only single gas adsorption is needed. If flushing is not done then the gases that were present in the sample before helium gas was passed through, would also become a factor in the final CO_2 adsorption analysis.

The pressure in the pump containing CO_2 is increased to 150kPa while the valve at the downstream side (Valve 2) of the pump is kept shut. This helps in determining the compression of gas inside the pump. After some time (about 10 minutes on average), when the pressure is stable, the valve on downstream (Valve 2) is opened while keeping the valve immediately before the cell (Valve 3 – not shown) closed. This helps in pressurizing the flow lines till Valve 3, before the testing cell. On average 30 minutes were required for the lines to be at constant pressure. After the flow lines are pressurized and are stable the valve is opened to allow CO_2 to contact the coal specimen and adsorption begins.

Figure 4.2: Valve Placement on the Pump

The first set of data for adsorption is taken at a CO_2 pressure of 150kPa. To maintain a constant effective stress, cell pressure is also increased by the same amount of pressure as the gas pressure. In order to maintain $\sigma_3' = 3.75$MPa, for CO_2 pressure of 150kPa, the confining pressure is increased to 3.9MPa. The data acquisition software (Labview) is set

at 10 second interval for the first 5 hours and then changed to 30 second intervals. When Valve 3 is opened, a drop in pressure is associated with the opening of the valve and this immediately begins to be compensated for by the gas in the upstream pump, which attempts to return to its constant pressure. If no adsorption was to occur, the pump would return to the constant pressure. But as adsorption begins to occur within the coal matrix, the pressure declines which is compensated for by pumping in more gas until a constant pressure is re-established. Equilibrium is achieved once no more gas is pumped into the specimen or satisfies the equilibrium criteria discussed previously. After the cut-off criterion for a particular CO_2 pressure is met, the gas pressure is increased to the next point followed by an increase in the cell pressure so that the effective stress for the test remains at 3.75MPa. This process is repeated for different CO_2 gas pressures of 250, 500, 1000, 2000 and 4000kPa.

After equilibrium is achieved at 4000kPa, the gas pressure is lowered in concert with the cell pressure. Once the ambient pressures are reached, the cell is dissembled; the specimen is removed, weighed, measured and prepared for a moisture content determination. Immediately after opening of the cell, cell fluid temperature is measured to check that the temperature inside the cell remained at the required testing temperature.

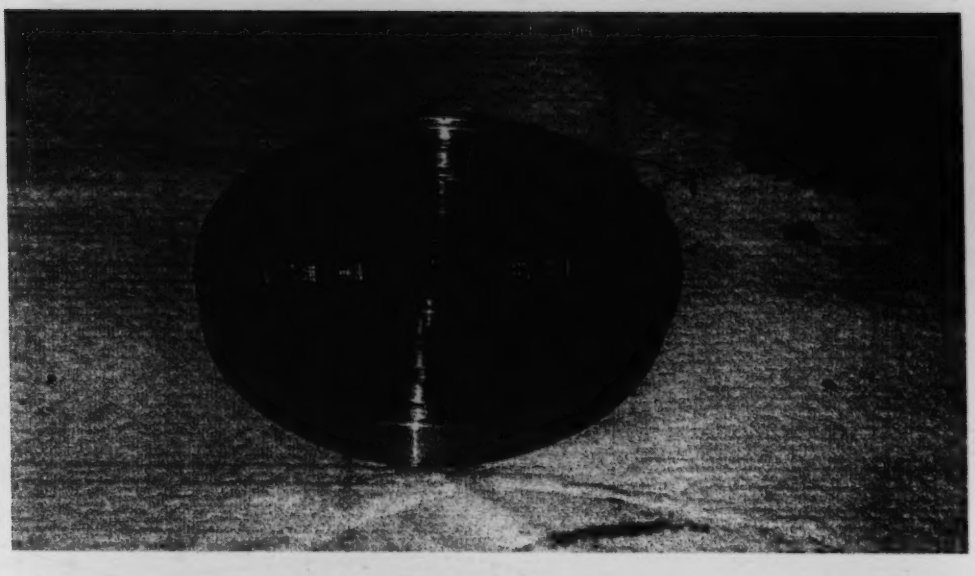

Figure 4.3: Spacer for the Bottom Pedestal

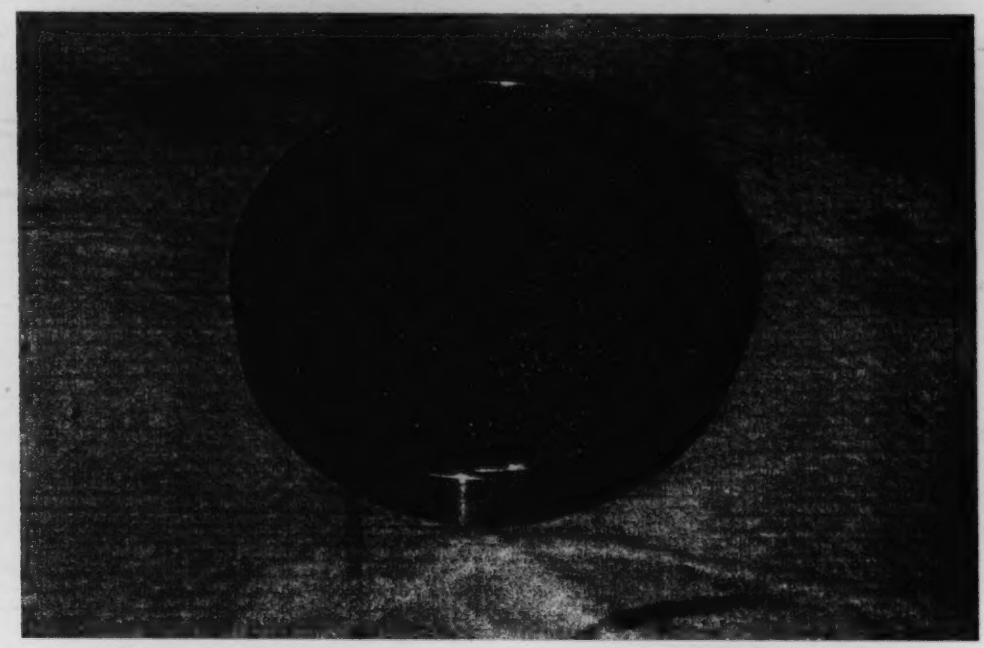

Figure 4.4.: Spacer with the Porous Stone

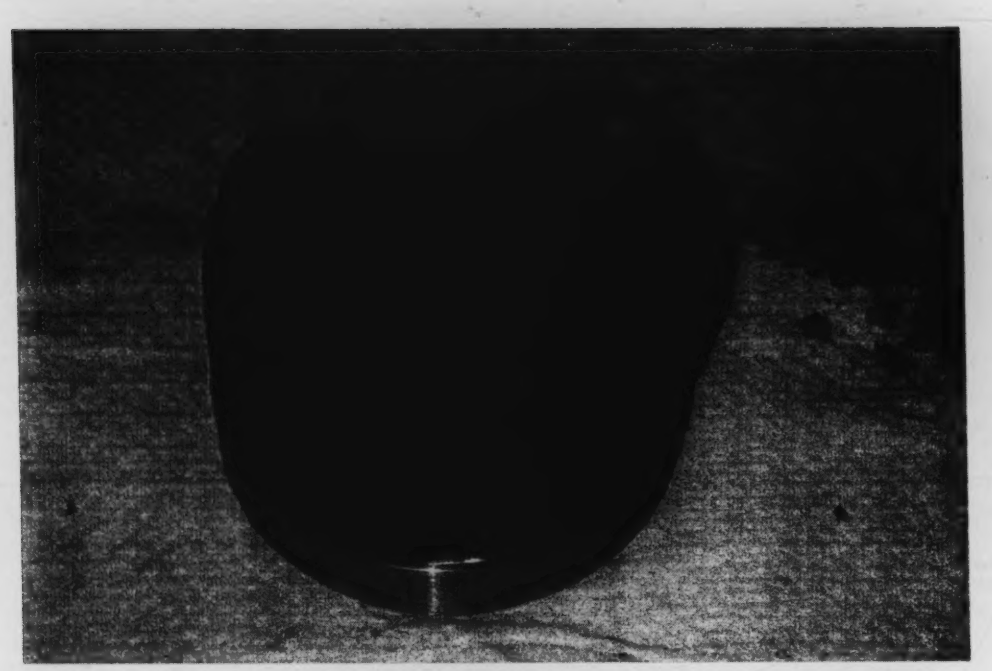

Figure 4.5: Sample placed on the Bottom Pedestal with Porous Stone

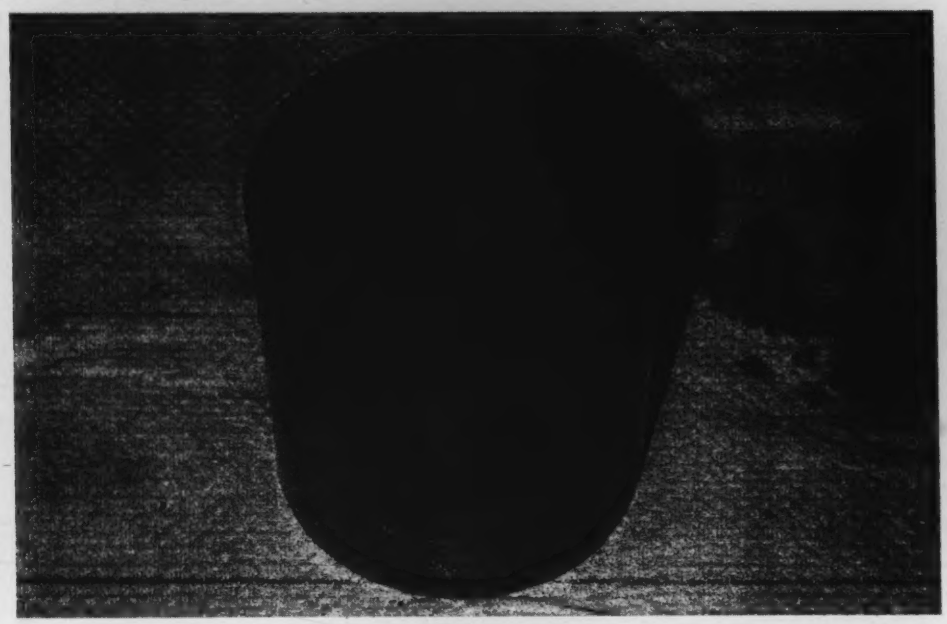

Figure 4.6: Sample in the Copper Tube

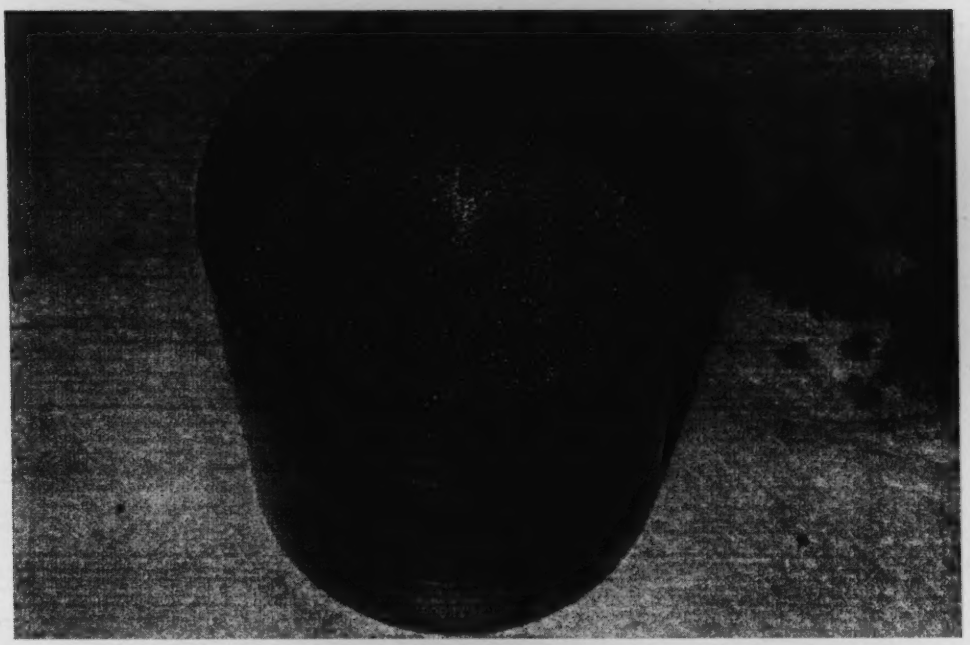

Figure 4.7: Top Porous Stone placed on the Sample

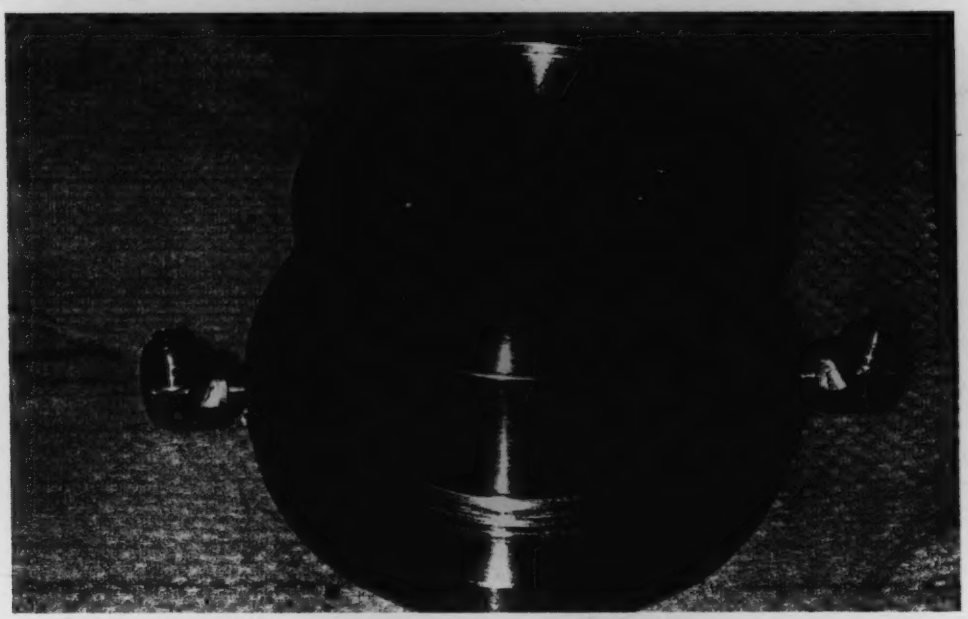

Figure 4.8: Top Pedestal

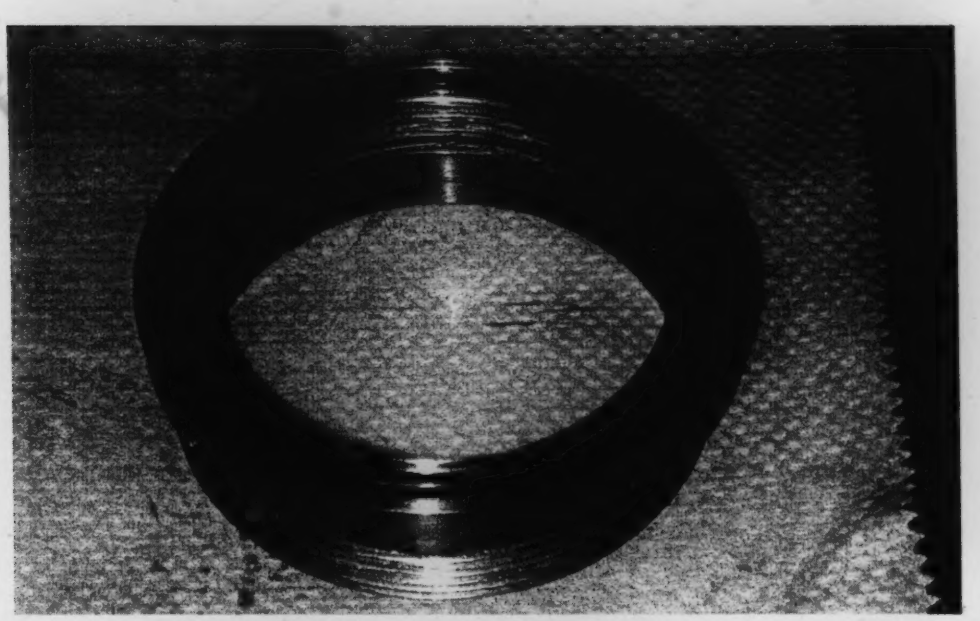

Figure 4.9: Swedgelok Fitting with O-Ring at the Bottom

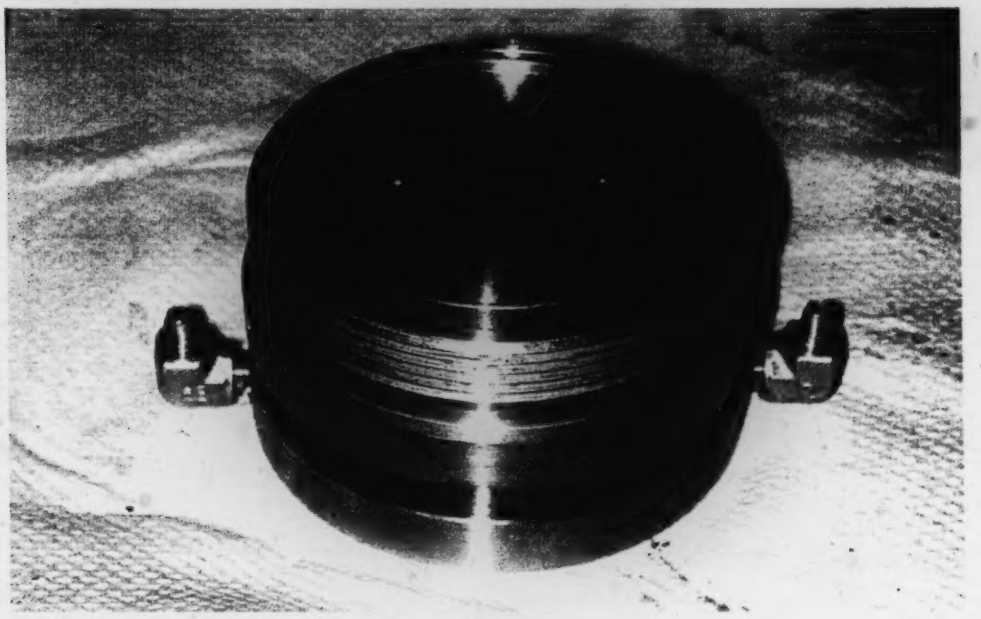

Figure 4.10: Fitting Placed on the Top Pedestal

Figure 4.11: Sample with Porous Stone and Copper Tube placed on the Top Pedestal

Figure 4.12: Copper Spacer and O-rings placed and are ready to be Tightened

Figure 4.13: Swedgelok Fitting being Tightened

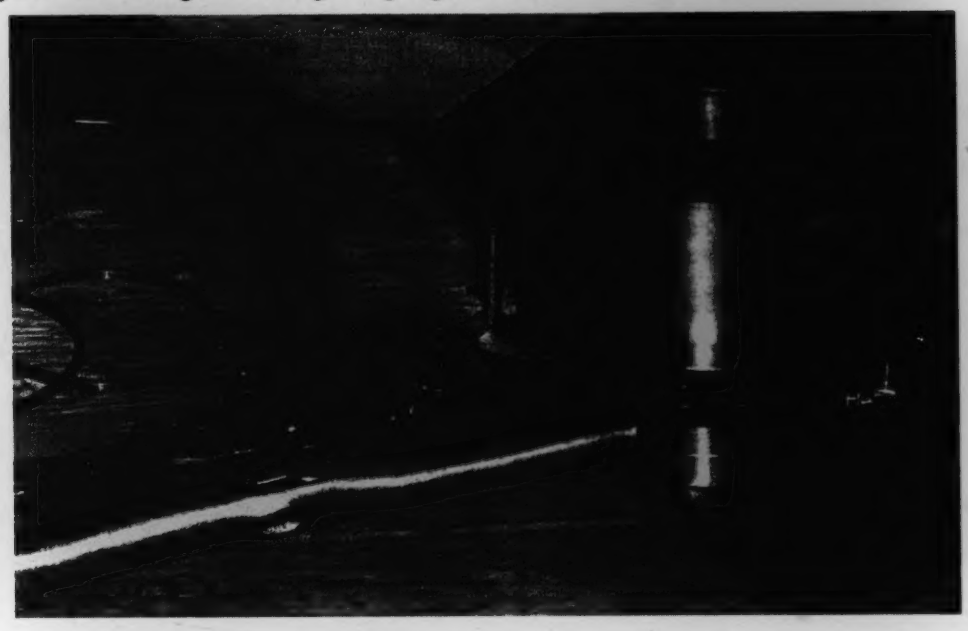

Figure 4.14: Top Portion being Tightened and ready for Placement

Figure 4.15: Bottom Portion ready for Placement of Sample

Figure 4.16: Swedgelok Fitting for Bottom Portion ready for Placement

Figure 4.17: Bottom Portion being placed

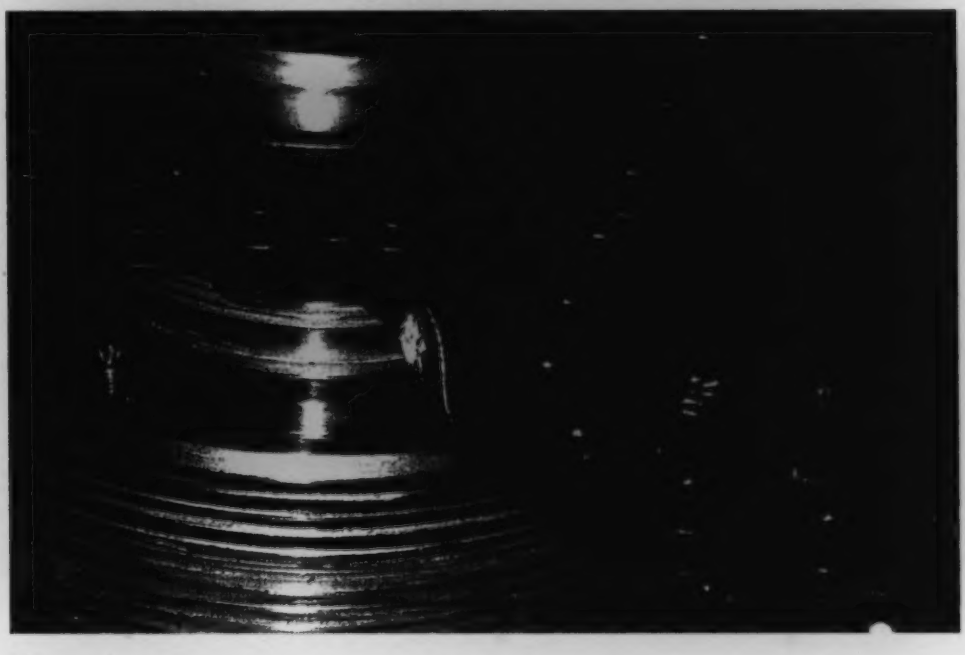

Figure 4.18: Bottom Portion being Tightened in place

Figure 4.19: Top Ports Being Connected for Gas Input

Figure 4.20: Testing Cell ready for Placing into the Water Bath

4.12 Experimental Procedure for Crushed Sample

As the objective of this research is the comparison of CO_2 adsorption isotherms of intact and crushed coal specimens, the same testing procedure used for intact specimens was used for the crushed coal specimens.

The samples were crushed by hand first to pass through #4 mesh and four sub-samples were obtained. One sub-sample passing #4 sieve was retained while the others were crushed to pass through sieve #8, #20 and #60. The testing for the adsorption isotherm was carried out on the crushed sample passing through sieve #60 (ASTM D2013-86 (Re-approved 1994)).

The setup of the cell is similar in operation as for the intact sample. After the preparation of the crushed coal sample, the sample is weighed using an electronic balance, capable of weighing up to micro-gram. Moisture content of the sample is also determined at this point and recorded. The moisture content is determined according to ASTM D 3173-00 and ASTM D 3302-02. The detailed calculations of the moisture content are provided in Appendix F.

As before, a porous stone is placed on the top of the steel spacer. This assembly is put in the copper membrane, which serves as a container for the crushed coal specimen. A small steel rod is used to slightly compact the crushed coal until it fills all the space within the copper membrane.

Whole assembly including the copper membrane and the sealing rings is placed on the bottom pedestal of the triaxial cell. The copper spacer ring is placed around the membrane followed by an O-ring then again a Copper ring followed by another O-ring. A stainless steel ring is then put on this whole assembly and is tightened so that the copper

rings as well as the O-rings form a seal. Same is done with the top pedestal and similarly steel ring is tightened. This assembly is placed into the test cell and the top cap is closed. After placing the sample into the cell, it is filled with water at 50°C and a confining pressure of 3.75MPa is applied. The cell is placed inside the temperature bath and the temperature of the water in the bath is maintained at 50°C (testing temperature).

As with the intact specimen the crushed specimen is back-saturated with helium gas. Pressures of helium higher than atmospheric pressure make sure that all of the atmospheric gases are flushed out. This setting, maintaining helium pressure at 125kPa, is left overnight. The valve at downstream side is opened and the gas is flushed out. For all the tests no coal was seen exiting the downstream valve indicating that the porous stones were retaining the crushed coal as expected. At this point, the same CO_2 adsorption pressures, used for intact testing, are used for the crushed coal tests.

To aid in comparing the intact versus crushed coal test results, it was decided that the time for the testing should be the same as for intact specimen so that any time-dependency related to the adsorption of gas on crushed coal is eliminated.

The sealing system in this study proved very effective. The moisture content was found to be the same before and after each test. Also it was observed that no water was present in the sample after it was opened. Unfortunately pictures of the sample after opening were not be taken in detail but Figure 4.24 gives good view how the sample looked like after opening the cell. The lumps present in the sample (Figure 4.25) were dry in nature and were only in the form of lumps due to high cell pressure applied in this study. The average moisture content of the samples before test was 7.083% while after the test it was

near 7.212%. Results for the moisture content calculations are presented below while detailed moisture calculation and the procedure is presented in Appendix F.

Table 4.1: Moisture Content Calculation for Crushed Sample (According to ASTM D 3173-00 and ASTM D 3302-02)

Sample	Total Moisture Content (%)	
	Before testing	After testing
Crushed Sample 1	7.0188	7.1978
Crushed Sample 2	7.1465	7.2269

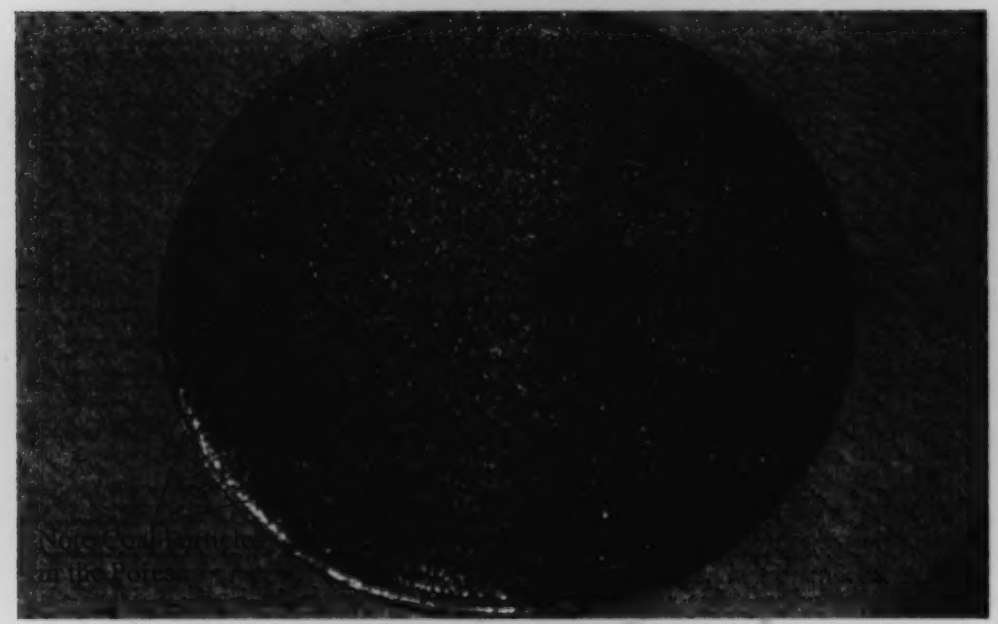

Figure 4.21: Porous Stone after Opening

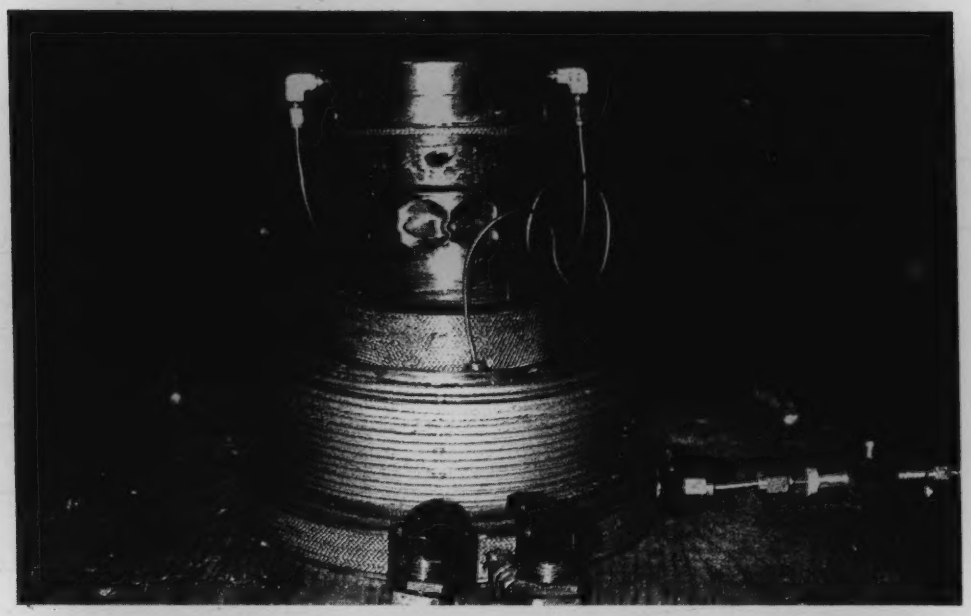

Figure 4.22: Copper Membrane Dismembered due to High Cell Pressure

Figure 4.23: Dismemberment of the Tubing

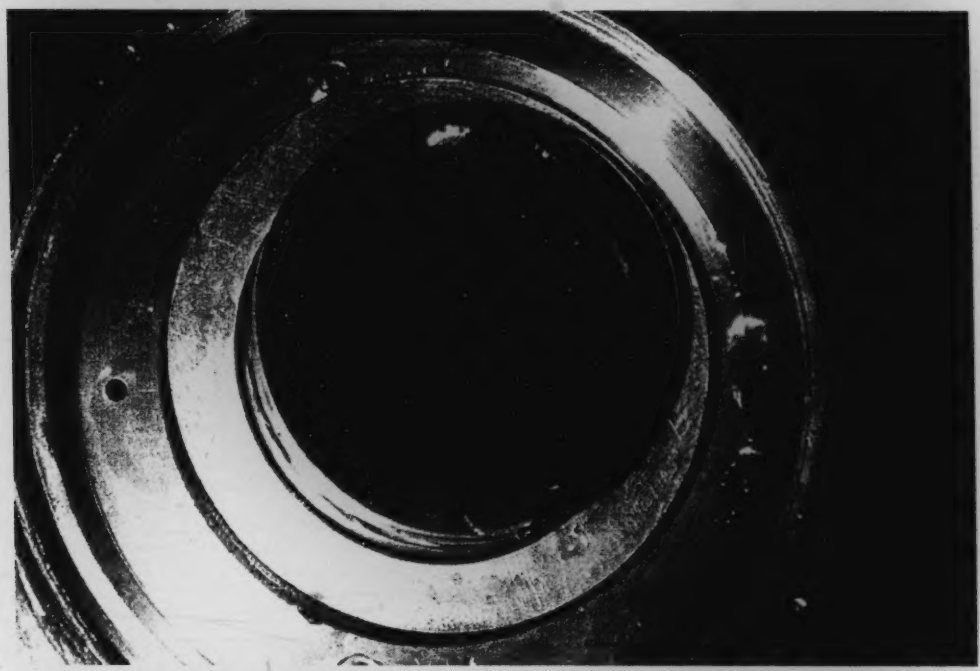

Figure 4.24: Sample inside the Copper Membrane after the Cell is Opened

Figure 4.25: Sample is Lumped due to Excessive Cell Pressure

4.13 Summary

The ability to operate under a variety of pressures and temperatures increases the flexibility of the triaxial testing system. It was determined that the tolerable limit of temperature changes in the laboratory was less than 0.1°C. Tolerance of changes in pressure were determined to be less stringent, and within the accuracy of the syringe pumps chosen for the experimental set-up.

Due to the longer time periods required in the testing of CO_2 adsorption on intact coal samples, gas diffusion through the membrane will always be a concern.

The membranes and the mechanisms used to seal the samples are likely to be one of the most important factors in the experimental design for determination of slow transport processes. Utilizing a low solubility cell fluid alone will not provide adequate enough measures against CO_2 migration into the cell fluid. Although a variety of membranes can be and have been used in this type of testing, the most suitable are gas impermeable metal membranes. Adaptations of the sealing mechanism are required if stiffer seals, such as metals are to be used. Therefore, due to the low diffusion rates, the likelihood that adsorption will be diffusion limited, and the total amount of CO_2 adsorbed will be small, the membrane and sealing mechanisms must ensure that gas migration is lower than the observed fluxes.

Traditional O-ring seals alone, typically used in triaxial cells were not capable of providing a sufficient seal. Previously designed confining rings increased the opportunity for tearing of the copper membrane. Although, many of these sealing mechanisms are able to provide seal some of the time, the probability of an adequate seal should be greater, given the time required for a setup, and the cost of the membranes. Therefore,

confining rings, hose clamps, split rings were all abandoned for a more secure and sophisticated means of sealing, modeled after the Swagelok fitting.

Chapter 5: Results and Discussion

5.1 Introduction

Existing numerical models do not properly handle coal reservoir properties (e.g. diffusion of multiple gas components between the coal matrix and the cleats, swelling/shrinkage of the coal matrix and its effect on permeability, multi-component gas sorption, water movement between the matrix and the cleats) (Law, 2002 – personal communication). Of particular interest for this research program is that the currently available reservoir simulation models do not fully incorporate the phenomena of swelling and shrinkage of coal with the variation in the gas content as a result of changes in the composition of sorbed gas and pressure. To appropriately study the process of swelling and shrinkage of coal, it is necessary to conduct adsorption tests on intact coal specimens. Almost all the literature for adsorption isotherms has been generated on crushed coal specimens. Consequently, prior to addressing the swelling / shrinkage phenomena, it is imperative to understand the possible differences that may exist for adsorption tests on intact versus crushed coal specimens. This chapter presents the test results of such a program and discusses the implications of these results on adsorption behaviour of coals.

5.2 Physical Properties of Samples

This section presents a comparison of the physical properties of the intact samples used in the testing program. It has been assumed that the diameter of the intact sample does not change during the test due to the lateral confinement provided by high cell pressure and the copper membrane. As expected, the average diameter of the sample measured before and after the testing were the same. The height, however, decreased by 1.25% in response

to the application of an effective confining stress of 3.75 MPa. These height changes lead to an increase in the average bulk density of the sample of about 2.75%. Table 5.1 shows the comparison of the readings for intact sample 1, while Table 5.2 shows the same for intact sample 2.

Table 5.1: Physical Properties of Intact Sample #1 (IS1)

Intact Sample #1 Before Testing							
Description	**1**	**2**	**3**	**4**	**5**	**6**	**Average**
Diameter (mm)	62.23	62.02	62.21	62.19	62.19	62.25	62.18
Height (mm)	10.70	10.80	10.50	10.70	10.70	10.70	10.68
Area (mm^2)	3041.51	3021.02	3039.56	3037.60	3037.60	3043.47	3036.79
Volume (mm^3)	32544.16	32627.02	31915.38	32502.32	32502.32	32565.13	32442.06
Mass (g)	47.15	47.13	47.14	47.15	47.14	47.14	47.14
Bulk Density (g/cm^3)	1.45	1.44	1.48	1.45	1.45	1.45	1.45
Moisture Content (%)							4.36

Intact Sample #1 After Testing							
	1	**2**	**3**	**4**	**5**	**6**	**Average**
Diameter (mm)	62.20	62.18	62.23	62.12	62.19	62.17	62.18
Height (mm)	10.49	10.40	10.52	10.56	10.67	10.66	10.55
Area (mm^2)	3038.58	3036.63	3041.51	3030.77	3037.60	3035.65	3036.79
Volume (mm^3)	31874.70	31580.95	31996.69	32004.93	32411.19	32360.03	32038.14
Mass (g)	47.86	47.84	47.85	47.84	47.84	47.85	47.85
Bulk Density (g/cm^3)	1.50	1.51	1.50	1.49	1.48	1.48	1.49
Moisture Content (%)							4.39

It is evident from Table 5.1 and Table 5.2 that the moisture content of the samples before and after the test did not change significantly. This shows that the sealing mechanism worked properly during the testing.

Table 5.2: Physical Properties of Intact Sample #2 (IS2)

Intact Sample #2 Before Testing							
Description	**1**	**2**	**3**	**4**	**5**	**6**	**Average**
Diameter (mm)	62.18	62.16	62.15	61.10	62.08	62.14	61.97
Height (mm)	10.69	10.68	10.56	10.59	10.59	10.69	10.63
Area (mm^2)	3036.63	3034.67	3033.70	2932.06	3026.87	3032.72	3016.11
Volume (mm^3)	32461.58	32410.28	32035.87	31050.52	32054.55	32419.78	32070.28
Mass (g)	44.43	44.43	44.43	44.43	44.43	44.43	44.43
Bulk Density (g/cm^3)	1.37	1.37	1.39	1.43	1.39	1.37	1.39
Moisture Content (%)							4.00

Intact Sample #2 After Testing							
Description	**1**	**2**	**3**	**4**	**5**	**6**	**Average**
Diameter (mm)	62.15	62.32	62.17	61.03	62.08	62.06	61.97
Height (mm)	10.48	10.28	10.58	10.45	10.56	10.65	10.50
Area (mm^2)	3033.70	3050.32	3035.65	2925.34	3026.87	3024.92	3016.13
Volume (mm^3)	31793.18	31357.29	32117.18	30569.80	31963.75	32215.40	31669.40
Mass (g)	45.10	45.10	45.10	45.08	45.09	45.10	45.09
Bulk Density (g/cm^3)	1.42	1.44	1.40	1.47	1.41	1.40	1.42
Moisture Content (%)							4.06

5.3 Temperature Variation

The average temperature variation as a function of pressure for both sets of tests performed on the intact samples as well as crushed samples is shown in Figure 5.1. The temperature varies between a maximum of 49.98°C and a minimum of 49.91°C. The total variation between the temperatures is less than 0.1°C for all the tests over a period of about 3000 hours (4 months). The maximum deviation of the test from the standard temperature of 50°C is only 0.09°C, which is within the expected range of deviation.

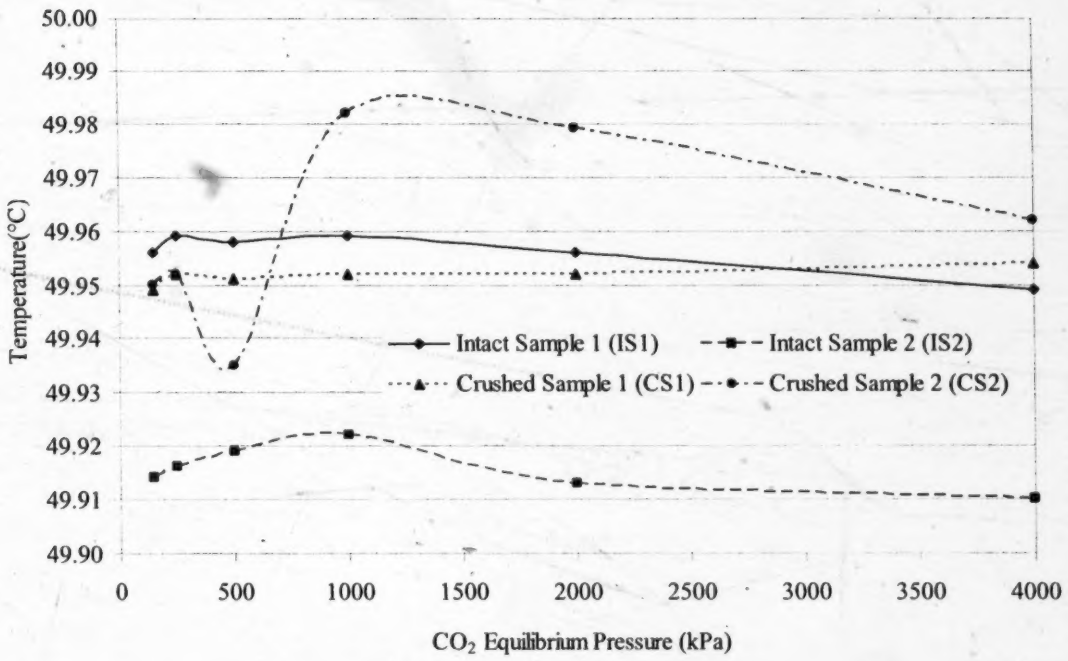

Figure 5.1: Temperature Variation with Pressure for Intact and Crushed Sample Tests – Note Vertical Scale is a Total Span of 0.1°C while the Resolution of RTDs is ±0.02°C

5.4 Gas Compressibility Factor

All the test results reported in this thesis were carried out at a temperature higher than standard temperature (25°C) and pressure (101.25kPa) hence it is appropriate that the results obtained should be converted to standard temperature and pressure (STP) conditions. For completeness the following section summarizes the methodology for these conversions.

Starting with the ideal gas law

$$\frac{PV}{T} = Const \tag{5.1}$$

where P is the pressure in kPa, V is the volume of the gas in mL and T is the temperature in °K, two different test conditions can be compared using;

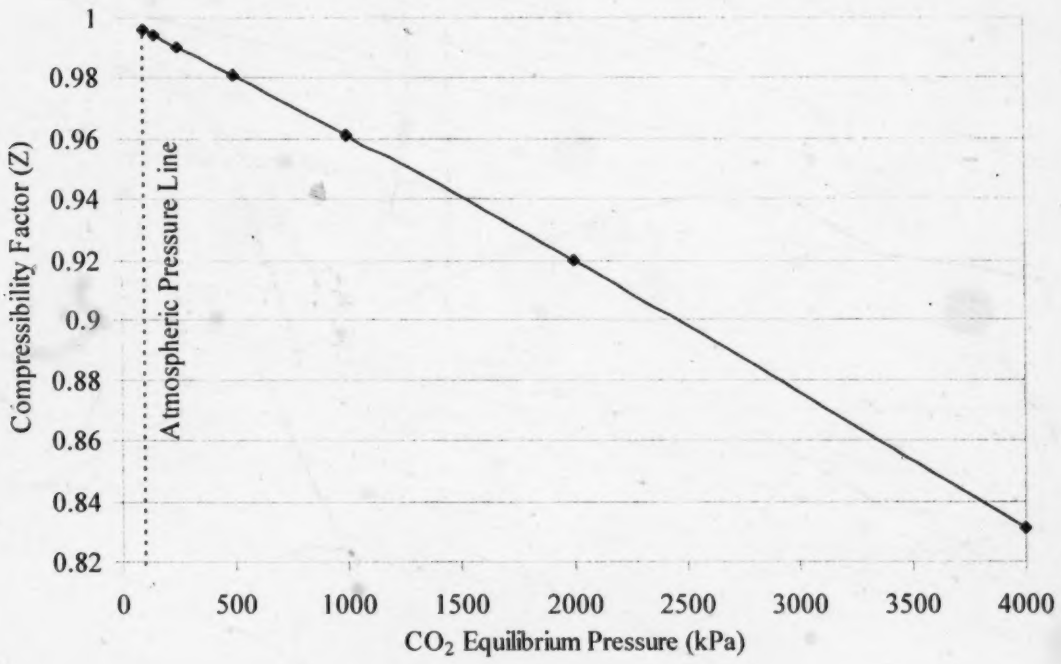

Figure 5.2: Graph between Compressibility Factor and Pressure at 50°C

$$\frac{P_1V_1}{T_1} = \frac{P_2V_2}{T_2} \tag{5.2}$$

As pressure increases or decreases, the gas change volume. Using a compressibility factor to account for this, Equation 5.2 can be modified to obtain

$$\frac{P_1V_1}{Z_1T_1} = \frac{P_2V_2}{Z_2T_2} \tag{5.3}$$

where Z is the factor used to give the compressibility of the gas at that condition of temperature and pressure.

The compressibility factor (Z) can be found from the following equation

$$Z = \frac{PV}{RT} \tag{5.4}$$

where R is the gas constant with a value of 8314 kPa-cm^3/K

Table 5.3: Relationship of Compressibility Factor against Pressure

Intact Sample 1 (IS1)			Intact Sample 2 (IS2)		
Temp	CO_2 Pressure	Compressibility Factor	Temp	CO_2 Pressure	Compressibility Factor
°C	kPa	Z	°C	kPa	Z
50.000	101.25	0.9960	50.000	101.25	0.9960
49.956	150	0.9941	49.914	150	0.9941
49.959	250	0.9903	49.916	250	0.9903
49.958	500	0.9806	49.919	500	0.9806
49.959	1000	0.9610	49.922	1000	0.9609
49.956	2000	0.9201	49.913	2000	0.9200
49.949	4000	0.8306	49.910	4000	0.8305

Crushed Sample 1 (CS1)			Crushed Sample 2 (CS2)		
Temp	CO_2 Pressure	Compressibility Factor	Temp	CO_2 Pressure	Compressibility Factor
°C	kPa	Z	°C	kPa	Z
50.000	101.25	0.9960	50.000	101.25	0.9960
49.949	150	0.9941	49.950	150	0.9941
49.952	250	0.9903	49.952	250	0.9903
49.951	500	0.9806	49.935	500	0.9807
49.952	1000	0.9610	49.982	1000	0.9609
49.952	2000	0.9201	49.979	2000	0.9200
49.954	4000	0.8306	49.962	4000	0.8306

$$Z = \frac{\text{Pressure (kPa)}}{\text{Temperature (K)}} \times \frac{\text{Molecular Mass of Gas (g)}}{\text{Density of Gas (g/cm}^3\text{)}} \times \frac{1}{\text{R}} \tag{5.5}$$

Figure 5.2 shows how the compressibility Z varies from 101.25 kPa to 4000 kPa for a constant temperature of 50°C. For all the pressures and temperatures encountered during the test program, Table 5.3 provides the complete listing of the variation in Z.

5.5 Crushed Coal Adsorption Isotherms

To understand the characteristics of the intact specimen adsorption isotherms, adsorption isotherms are required for the crushed coal equivalent of the intact specimen. Equivalent refers to conditions such as coal rank and moisture content. For crushed coal, adsorption isotherms specimens are usually prepared following ASTM Test Method D2013-86 (Reapproved 1994) which for completeness has been included in Appendix I. This sample preparation method has been followed as closely as possible, and was explained in Chapter 4.

Table 5.4 provides the gas inflow test data for crushed coal specimen 1 (CS1) and 2 (CS2). Note that the test duration for CS1 is substantially shorter than for CS2. Due to a power shutdown event in the Civil Engineering Building, the time increments selected for CS1 were reduced dramatically in order to complete the test prior to the power shutdown. Interestingly, both samples were able to retain an almost equal amount of the injected gas. While the CS1 test was accelerated due to the power issue, the CS2 test was conducted over the same duration as the tests conducted for intact specimen.

Equilibrium conditions for the crushed coal tests were identical to the intact test conditions: less than 0.3 mL/hr over a period of 4 hours. For the crushed coal tests, even CS1, equilibrium was usually attained within 30 minutes. Utilizing the procedures outlined in Section 5.4, Table 5.5 provides the equilibrium adsorption data at standard temperature and pressure conditions. Figure 5.3 illustrates the detailed procedure of calculations.

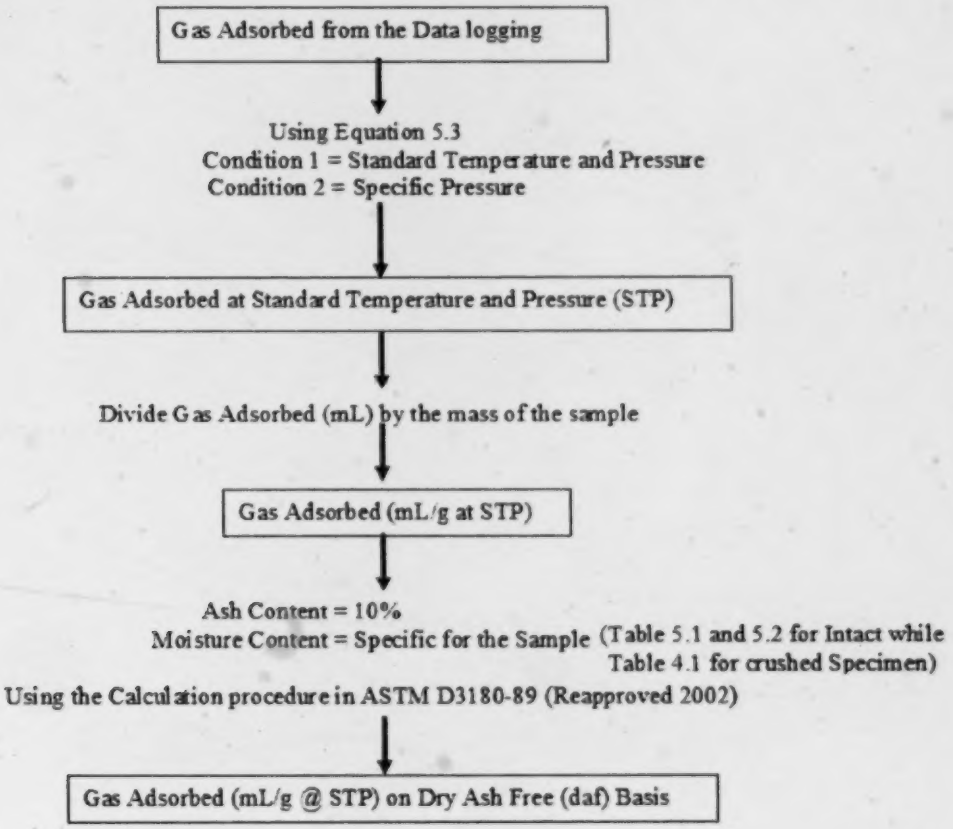
Gas Adsorbed from the Data logging
Using Equation 5.3
Condition 1 = Standard Temperature and Pressure
Condition 2 = Specific Pressure
Gas Adsorbed at Standard Temperature and Pressure (STP)
Divide Gas Adsorbed (mL) by the mass of the sample
Gas Adsorbed (mL/g at STP)
Ash Content = 10%
Moisture Content = Specific for the Sample (Table 5.1 and 5.2 for Intact while Table 4.1 for crushed Specimen)
Using the Calculation procedure in ASTM D3180-89 (Reapproved 2002)
Gas Adsorbed (mL/g @ STP) on Dry Ash Free (daf) Basis

Figure 5.3: Step by Step Procedure of Calculating the final Adsorbed Volume of the Gas

After testing the first sample, when the cell was opened, it was observed that due to high cell pressure applied, the copper membrane has been excessively deformed. The mass of sample used for the first test was 21.90 g. It was suspected that because of the small sample mass, excessive deformation may lead to development of cracks and the sealing system, which is mechanical in nature, may not work properly. Therefore in the second test the mass of the sample was increased to 49.94 g.

Table 5.4: Gas Adsorption Test Data for Crushed Specimen (CS1 and CS2)

CO_2 Pressure (kPa)	Time (hrs)		Gas inflow (at Test conditions) (mL)			
	Crushed Sample 1 (CS1)	Crushed Sample 2 (CS2)	Crushed Sample 1 (CS1)		Crushed Sample 2 (CS2)	
			Total Gas Volume	Adsorbed Volume	Total Gas Volume	Adsorbed Volume
150	21.764	47.950	63.375	14.522	63.988	15.135
250	62.559	126.047	126.000	31.785	166.828	72.613
500	85.831	212.136	155.280	29.952	188.843	63.515
1000	109.864	354.364	191.324	26.108	229.484	64.268
2000	133.131	514.481	200.628	14.434	229.821	43.627
4000	156.584	685.089	199.226	4.366	205.967	11.107

Table 5.5: Gas Behavior at STP for Different Pressures for Crushed Samples (CS1 and CS2)

CO_2 Pressure (kPa)	Gas Adsorbed @ STP (mL)		Volume of Gas Adsorbed @ STP/Mass of Sample (mL/g)	
	Crushed Sample 1 (CS1)	Crushed Sample 2 (CS2)	Crushed Sample 1 (CS1)	Crushed Sample 2 (CS2)
150	17.214	24.439	0.786	0.489
250	84.887	242.252	3.876	4.850
500	219.195	519.486	10.009	10.401
1000	448.757	1044.517	20.491	20.914
2000	691.727	1750.832	31.586	35.057
4000	838.596	2032.064	38.292	40.688

Figure 5.4 illustrates the shape of the adsorption isotherms measured for both crushed coal specimens. Even though CS1 and CS2 were under and effective confining stress of 3.75 MPa, the measured isotherms are very similar in shape to the crushed isotherms reported in the literature.

It is interesting to note that the crushed coal specimens tested in this research had very similar low pressure adsorption response as reported by Bustin et al., (1997). Secondly, CS1 and CS2 had significantly different coal solids mass (21.90 versus 49.94 g, respectively) yet when adsorbed volumes were normalized to the solids mass, almost identical adsorption curves were obtained. This speaks to the repeatability of this test procedure even for the conditions of high effective stresses.

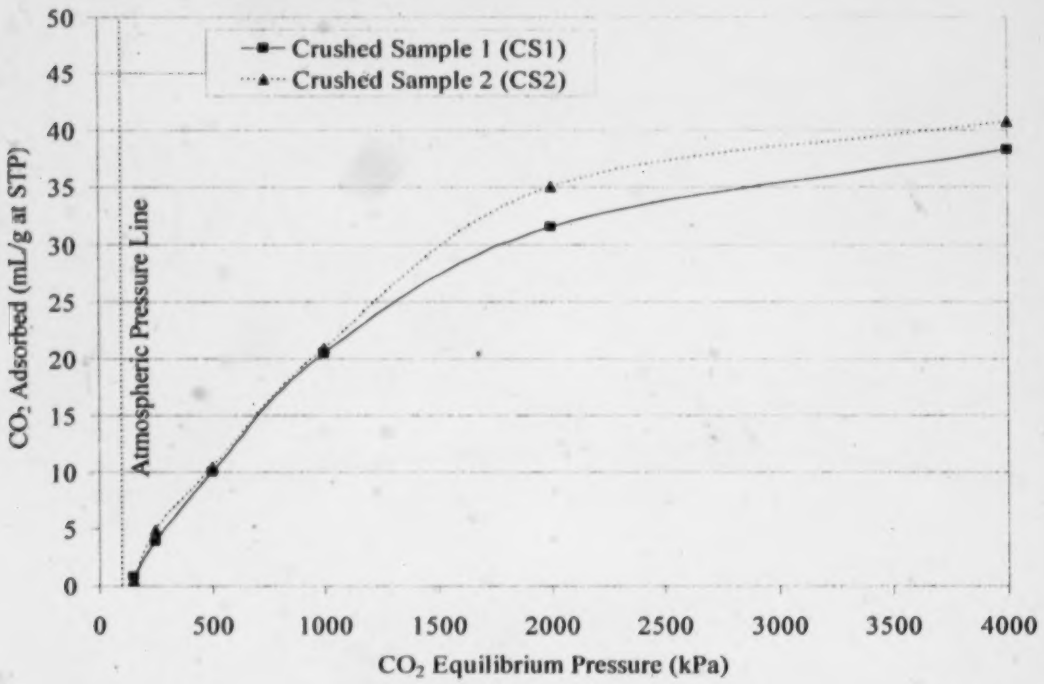

Figure 5.4: Crushed Specimen Adsorption Curves at STP Conditions (non daf Basis)

Table 5.6: Gas Behavior at STP for Different Pressures for Crushed Samples (daf Basis)

CO_2 Pressure (kPa)	Volume of Gas Adsorbed @ STP/Mass of Sample (mL/g)		Volume of Gas Adsorbed @ STP/Mass of Sample (mL/g)	
	Crushed Sample 1 (CS1)	Crushed Sample 2 (CS2)	Crushed Sample 1 (CS1) (daf Basis)	Crushed Sample 2 (CS2) (daf Basis)
150	0.786	0.489	0.647	0.402
250	3.876	4.850	3.190	3.988
500	10.009	10.401	8.238	8.553
1000	20.491	20.914	16.865	17.199
2000	31.586	35.057	25.997	28.830
4000	38.292	40.688	31.516	33.461

In previous studies reported in the literature regarding adsorption of gas on coal, adsorption curves are converted to a dry, ash free (daf) basis. For the purpose of correlating the results with other studies, the results obtained from the crushed coal test were converted to daf basis. These conversions are provided in Table 5.6 and the adsorption isotherm shown is replotted in Figure 5.5.

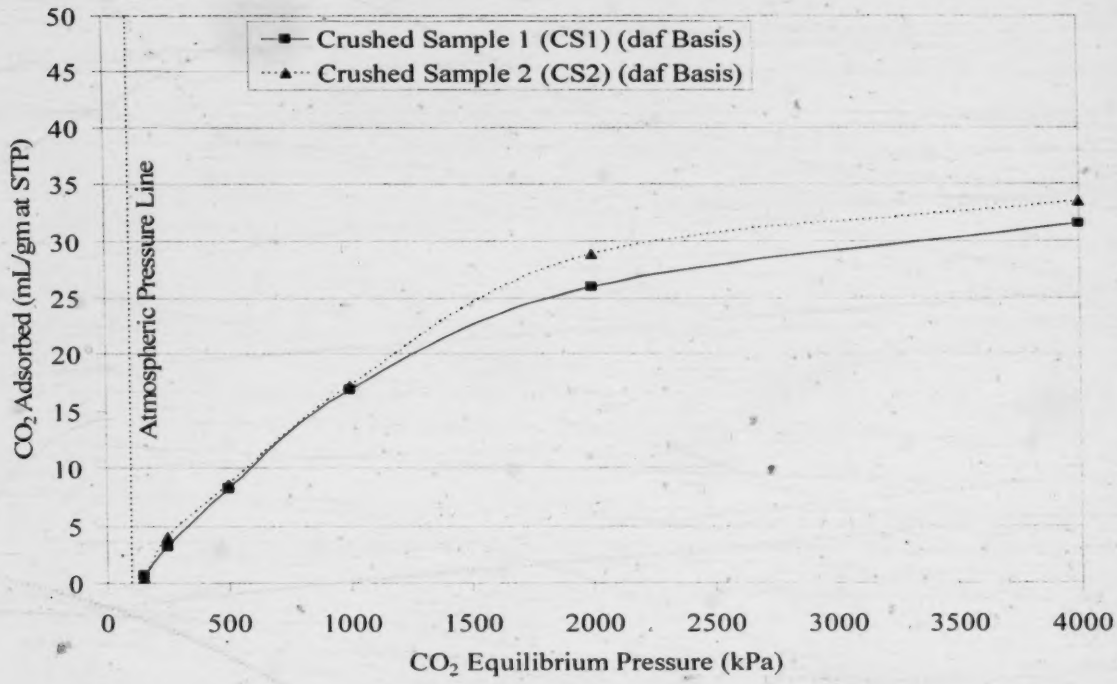

Figure 5.5: Crushed Specimen Adsorption Curves at STP Conditions (daf basis)

5.6 Leakage Integrity Test

The test procedure adopted in this research, by necessity, utilized small volume specimens. Consequently, concern over system leakage contributing to apparent adsorption volumes demanded a separate leakage integrity test.

Utilizing a non-adsorbing copper specimen (63.4mm diameter and 12.3mm high), a test following the exact procedure followed for the intact specimen test was conducted. Table 5.7 provides the details of the gas injected during the leakage integrity test. To illustrate the nature of the system integrity for the pressure step 1000 to 2000kPa, Figure 5.6 demonstrates the stability of the sealing mechanism and clearly shows that the initial gas inflow is associated with gas compression in the void volume or "dead volume" of the testing system. The remaining pressure steps for the leakage integrity test are illustrated in Appendix C

Table 5.7: Test Data for Leakage Integrity Test

Cell Pressure	CO_2 Pressure	Time (hrs)		Gas inflow	Average Temp	Cumulative Gas inflow @ STP
kPa	kPa	Incremental	Cumulative	mL	°C	mL
3900	150	68.267	68.267	73.835	49.952	100.722
4000	250	94.633	162.900	244.926	49.936	655.000
4250	500	118.021	280.921	335.441	49.928	2153.014
4750	1000	142.922	423.843	185.383	49.913	3739.199
5750	2000	179.208	603.051	328.664	49.493	9095.858
7750	4000	176.346	779.397	157.148	49.711	12998.685

Figure 5.6 shows the compression of the gas in the cell. It should be remembered that the gas is being compressed while some volume of the gas is also being stored in the cell as

there are spaces between the dummy sample and the membrane as well as in the porous stone. This is called the cell volume.

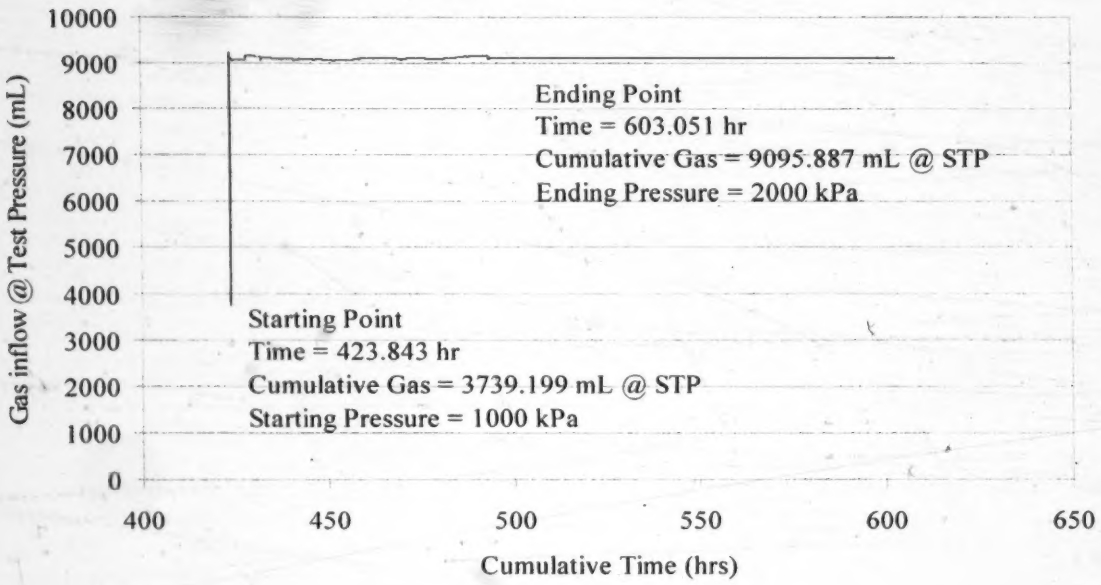

Figure 5.6: Relationship between Gas inflow at STP and Cumulative Time for Pressure Increment of 1000 kPa to 2000 kPa

The theoretical compression curve for CO_2 using ideal gas law is given in Figure 5.6. While at first glance it is evident that both, theoretical and experimental curves are not the same. It should be noted that in theoretical curve there is no consideration for the non-ideal behaviour of the gas and the experimental problems like the temperature fluctuation, even if it is as very low as 0.09°C must be accounted for in the experimental compression curve. For the theoretical compression data initial volume of the gas was taken as 13L and then it was compressed using the procedure discussed in section 5.4 and the subsequent compression data is plotted (Figure 5.7).

The experimental compression curve (Figure 5.7) was developed at STP using the calculation procedure discussed in Section 5.4. The test temperature was taken as 50°C while the standard temperature was 25°C. The compressibility factor was calculated using Span and Wagner Equation of State (1996).

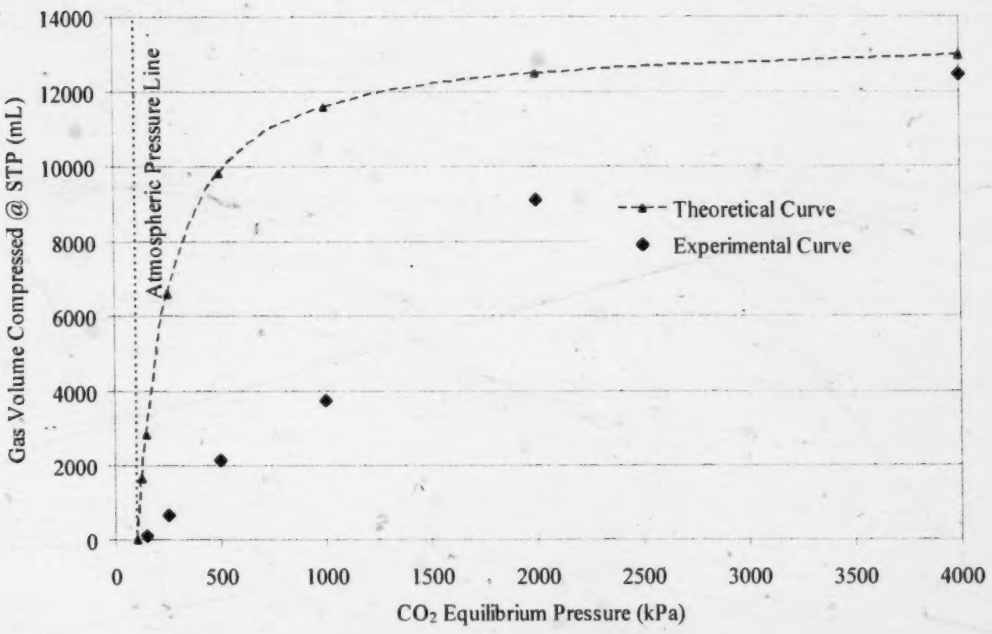

Figure 5.7: Graph showing Theoretical Curve and Experimental Data

Figure 5.7 shows the data from both theoretical calculations based on the Ideal Gas Law, and the experimental data. The primary reason behind the difference is this CO2 under test conditions behave as a Real Gas and does not obey the Ideal Gas Law.

5.7 Test Results for Intact Coal Sample

Table 5.8 provides the measured volume of gas inflow, at test conditions for intact specimen 1 (IS1) and intact specimen 2 (IS2). The duration of each test was approximately 700 hours each and the total maximum gas volume inflow for one pressure increment was almost equal at 220mL. It is pertinent to note that the total gas volume inflow at any one particular pressure includes compressed volume as well as the adsorbed volume of the gas. The duration or length of time is important in this type of test because increased times may allow some diffusion through the cell membrane for each test although for the current cell, the use of copper membrane efficiently eliminates this occurrence. As well, pressure maintenance and physical limitations (e.g. seals) of the pump equipment are also a crucial factor for long test duration.

Table 5.8: Time and Total Gas in for Different Pressures for Intact Samples

CO_2 Pressure (kPa)	Time (hrs)		Gas inflow (at test conditions) (mL)			
			Intact Sample 1 (IS1)		Intact Sample 2 (IS2)	
	Intact Sample 1 (IS1)	Intact Sample 2 (IS2)	Total Gas Volume	Adsorbed Volume	Total Gas Volume	Adsorbed Volume
150	72.667	46.128	74.832	13.368	72.222	10.758
250	156.923	100.944	146.321	-*	124.033	18.638
500	230.817	178.775	175.453	48.388	160.817	33.752
1000	372.011	324.481	213.887	63.542	203.171	52.826
2000	514.619	510.658	213.669	56.488	231.968	74.787
4000	716.097	728.881	221.010	16.675	219.433	15.098

* upstream valve inadvertently left closed during pressure increment

The results presented in Table 5.8 illustrate several important aspects of adsorption testing on intact coal specimens. It has been mentioned that a sample as small as 89mm

(3 ½") in diameter can take about 4 months to come to equilibrium (Harpalani et al., 1993) while other researchers (Ates et al., 1988) have shown that the adsorption time for small samples (54mm diameter and 12.7mm thickness) takes around 24 hours. Recall that the dimensions of the intact specimens in this test program were 62.2mm diameter and 10.6mm height. Based on the work of Ates et al., (1988), it would be reasonable to expect the equilibrium conditions within 24 hours. For both intact specimens, equilibrium conditions were achieved at around 40 hours at a minimum gas pressure of 150kPa and around 150 hours at the maximum gas pressure of 4000kPa. This implies that at higher gas pressures more time is needed for this criterion to be fulfilled. At pressures up to 2000kPa most of the micro-pores, responsible for the adsorption of the gas on coal, have been filled and therefore swelling of coal must occur to accumulate further adsorption (Stefanska, 1988, Levine, 1993) and as a result at higher gas pressures attaining equilibration takes more time.

Curves for total gas inflow versus pressure are presented in Appendix D for intact sample 1 and Appendix E for intact sample 2.

In terms of detecting equilibrium conditions, the minimum measurement limit for volumetric flow rate within pumps is 0.005mL/min. Therefore, a flow rate of 0.3mL/hr of gas can be detected and used as a threshold limit. A pressure increment was concluded when the amount of gas that entered the cell was less than 0.3mL/hr over a period of 4 hours. A secondary measure of equilibrium of 0.5% of the cumulative gas volume entering the cell over a 4 hour period was also selected.

At test conditions, Figure 5.8 provides a clear picture of how the adsorbed gas volume changes with increasing CO_2 pressure. As the gas pressure is increased micropore

locations within the specimen fill to a limiting amount and as the pressure exceeds 1000 and 2000MPa, the incremental value of gas that can be adsorbed begins to decrease. Recall that for these tests, σ_m' (effective stress – 3.75MPa) remained constant during the test

Using the procedure presented in Section 5.4, the data shown in Figure 5.9 presents the adsorption data at STP conditions. As well, the adsorbed volumes are normalized to the mass of the coal specimen, including the mass of water. This is presented in Table 5.9

Table 5.9: Gas Behavior at STP for Different Pressures for Intact Samples

CO_2 Pressure (kPa)	Gas Adsorbed @ STP (mL)		Volume of Gas Adsorbed @ STP/Mass of Sample (mL/g)	
	Intact Sample 1 (IS1)	Intact Sample 2 (IS2)	Intact Sample 1 (IS1)	Intact Sample 2 (IS2)
150	18.238	14.678	0.387	0.330
250	-*	56.838	-*	1.279
500	243.246	207.694	5.160	4.675
1000	797.028	667.974	16.907	15.034
2000	1714.115	1898.544	36.361	42.731
4000	2054.343	2172.773	43.578	48.903

* upstream valve inadvertently left closed during pressure increment

The general shape of this isotherm is quite different from the conventional Langmuir type isotherms, especially at lower equilibrium pressures. The reason being that at lower pressures, due to the presence of moisture in the specimen it is difficult for CO_2 to get adsorbed onto the surface of coal

At gas pressures below 250kPa negligible volumes of CO_2 are being adsorbed whereas beyond 250kPa, the process of adsorption is occurring at a reasonably constant rate till about 2000kPa. Beyond 2000kPa most of the micro-pores spaces have been filled

therefore very little amount of gas volume is adsorbed. Consequently, the curves start to flatten showing that the sample has almost reached its capacity.

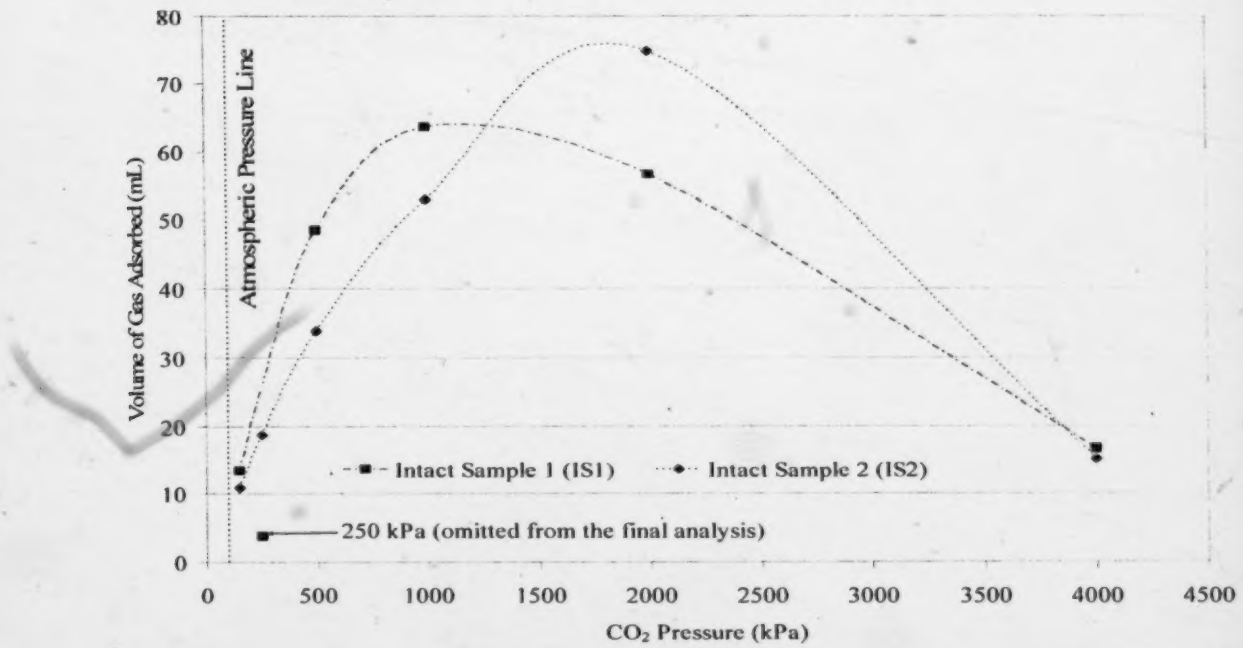

Figure 5.8: Intact Specimen Adsorption Curves (At Test Conditions)

The slight difference in adsorbed volumes between IS1 and IS2 are likely due to small variations in the structure of each specimen, small irregularities in specimen shape and variation in specimen moisture content.

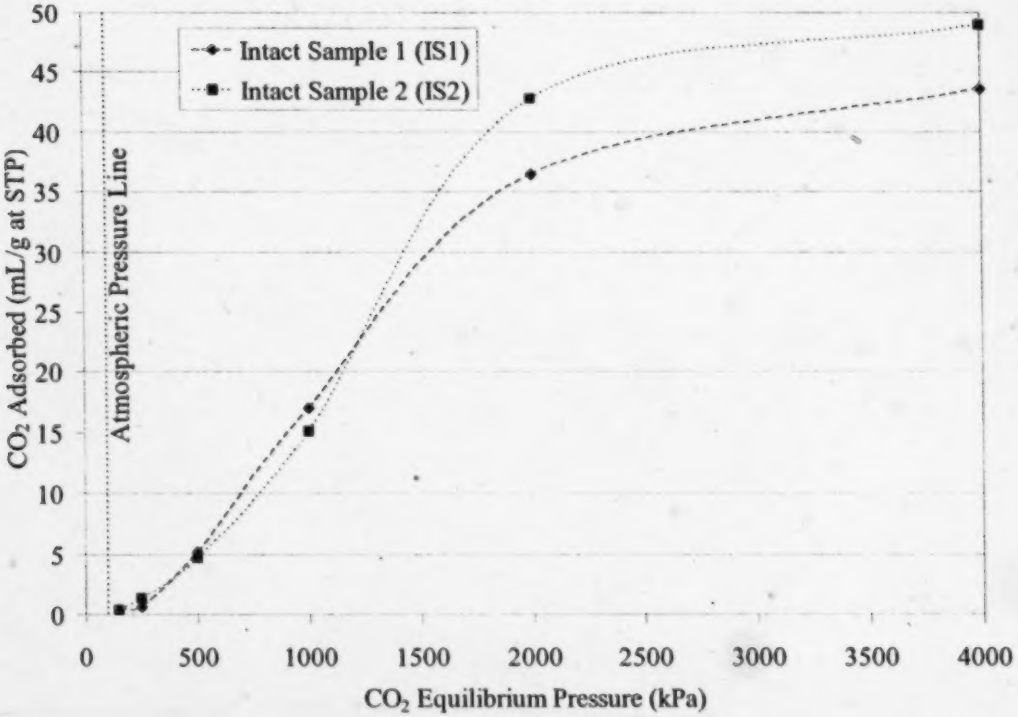

Figure 5.9: Intact Specimen Adsorption Curves at STP Conditions (non daf Basis)

In general, most adsorption curves in literature are presented at dry ash free (daf) basis. For the purpose of this research, which primarily focuses on a comparison of intact and crushed coal isotherms, the data for intact samples is also converted to dry ash free basis and presented in Table 5.10 and plotted in Figure 5.10.

Table 5.10: Gas Behavior at STP for Different Pressures for Intact Samples (daf Basis)

CO_2 Pressure (kPa)	Volume of Gas Adsorbed @ STP/Mass of Sample (mL/g)		Volume of Gas Adsorbed @ STP/Mass of Sample (mL/g) (daf Basis)	
	Intact Sample 1 (IS1)	Intact Sample 2 (IS2)	Intact Sample 1 (IS1) (daf Basis)	Intact Sample 2 (IS2) (daf Basis)
150	0.387	0.330	0.329	0.282
250	-*	1.279	-*	1.092
500	5.160	4.675	4.391	3.992
1000	16.907	15.034	14.389	12.839
2000	36.361	42.731	30.946	36.491
4000	43.578	48.903	37.088	41.762

* upstream valve inadvertently left closed during pressure increment

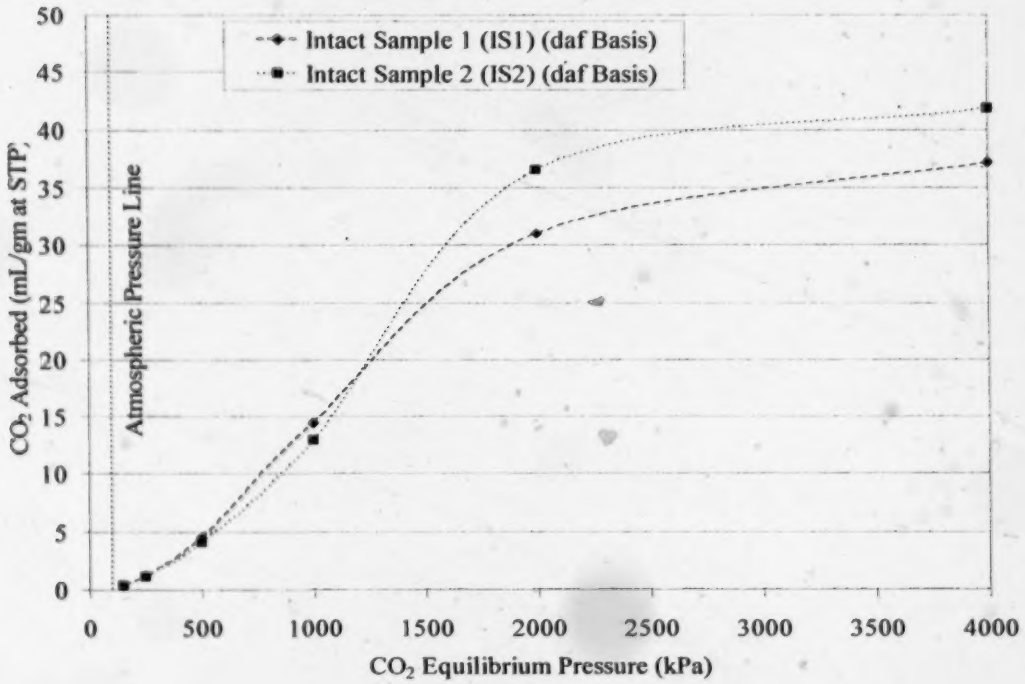

Figure 5.10: Intact Specimen Adsorption Curves at STP Conditions (daf Basis)

Figure 5.11 shows the results from this study for both crushed and intact samples and the adsorption results reported in the literature.

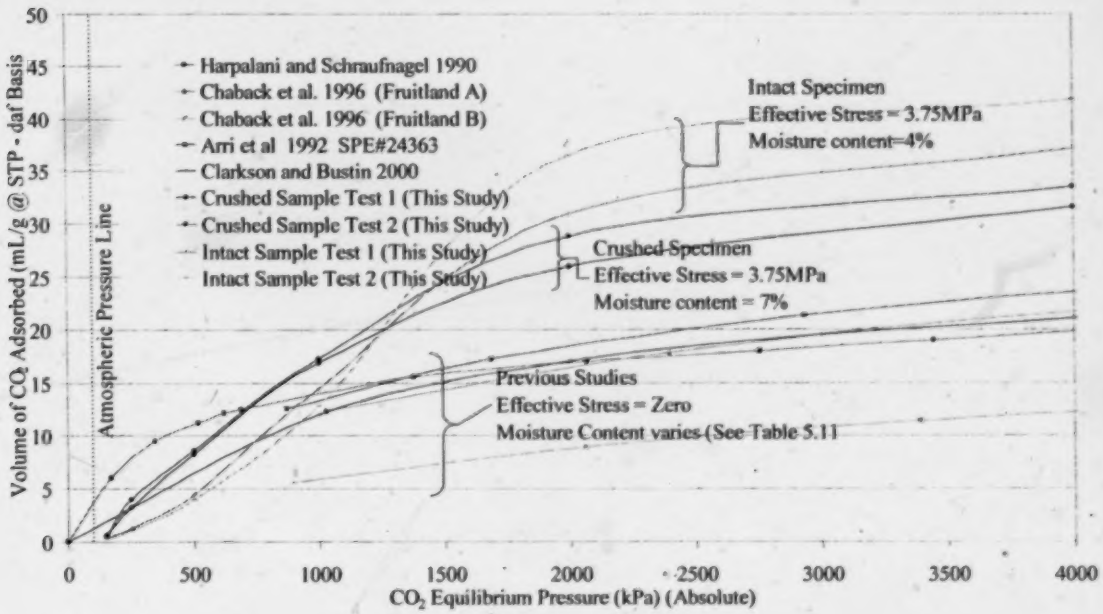

Figure 5.11: Graph Showing the Relationship between Results from this Study and Previous Studies (Dry Ash Free (daf) Basis)

Table 5.11 presents the specimen properties taken from the previous studies.

Based on the results presented in Figure 5.11 the following section discusses the possible difference in adsorption mechanism between crushed and intact coal specimens.

Table 5.11: Specimen Properties for Various Other Studies

	Harpalâni and Schraufnagel, 1990	Chaback et al., 1996				Arri et al., 1992		Clarkson and Bustin, 2000
Description of Specimen		Fruitland A		Fruitland B				
Basis	Moisture Free	Moisture Free	daf	Moisture Free	daf	As Received	daf	dry basis
Ash Content	5.1	21.76	-	13.28	-	16.08	-	13
Eq. Moist		2.27	-	2.27	-	2.27		2.4 @ 30C
Moisture	0.6							
Volatile Matter	23.7	20.76	25.53	36.75	42.38	18.69	22.89	
Fixed Carbon	71.2	57.48	73.47	49.97	57.62	62.96	77.11	
Carbon		66.75	85.31	71.56	82.52	67	82.06	
Oxygen		6.31	8.06	8.5	9.8	7.03	8.61	
Sulfur		0.69	0.89	0.42	0.48			
Sample M.C								
Coal Rank	*	Low Volatile Bituminous				Low Volatile Bituminous		Medium Volatile Bituminous
Gas Pressure (σ_1)	Atmospheric to 6.9MPa	148psi to 778psi		130 psi to 1250psi		100 to 1600 psi		up to 8MPa
Cell Pressure (σ_3)	**	**				**		**
Test Temp	**	46°C				46.3°C		30°C
Carried on	Sample passing 28 ~ 48 mesh	Sample passing 63 ~ 300 mesh				Sample passing 63 ~ 300 mesh		Sample passing 60 mesh
Reflectance						1.32		
Mass used		60g						

* Sample from Piceance basin (High Volatile to Medium Volatile)

** Not Mentioned

Table 5.12 presents the same properties for the coal used in this study. This is taken from Al-Hawaree (1999)

Table 5.12: Specimen Properties for Coal used in this Study (Al-Hawaree 1999)

Coal	Property	Test	Result	Unit	ASTM Method	Classification
Luscar Coal Mine	Moisture	Moisture Content	7.2	%weight	ASTM D5142	High Volatile Bituminous C
	Proximate Analysis	Moisture	5.55	%weight	ASTM D5142	
		Ash	10.52	%weight		
		Volatile Matter	28.44	%weight		
		Fixed Carbon	55.49	%weight		
	Ultimate Analysis	Carbon	67.72	%weight	ASTM D5373	
		Hydrogen	4.74	%weight		
		Sulfur	0.27	%weight	ASTM D4239M	
	Reflectance	Reflectance Index	0.584			

5.8 Discussion of the results for Intact and Crushed Sample

In general, the crushed coal adsorption isotherms measured in this research are very similar in shape and indicating a slightly larger capacity than the crushed coal adsorption isotherms measured by other researchers even for coals of similar rank.

Within the scope of this thesis, it was important to demonstrate the ability to measure adsorption curves very similar to those measured by conventional methods. Similar crushed coal isotherms provided some measure of proof that the experimental system performed satisfactorily, the use of constant pressure techniques to measure CO_2 volumes adsorbed within the coal was reliable and that adsorption isotherms could be measured under elevated effective confining stresses.

The main objective of this thesis research was a comparison of adsorption behavior associated with crushed and intact coal specimen, the "proof" provided by the crushed coal testing results gave additional confidence in comparing crushed versus intact behaviour.

Forgoing the successful execution of the crushed and intact specimen adsorption tests, several significant factors must be considered in comparing the test results

1. Effective Confining Stress
2. Oxidation of the coal specimen;
3. Moisture content of the specimen; and
4. Structure of coal.

The issues are discussed in the following section

5.8.1 Effective Confining Stress

Cell pressure plays an important part in the fact that the adsorption onto the coal surface is dependent on the surrounding pressure. Most of the prior studies regarding the adsorption have been carried out on crushed coal therefore overburden pressure never played a major role in these results. Another reason that the overburden pressure was not applied previously is that the methodology used in the previous studies of constant volume cannot allow a pressure to be applied.

When the coal is present in the seam it is under overburden pressure which is released when it is bought to the surface. The release of this overburden pressure opens the fractures present especially in the intact coal specimen hence increasing the surface area available for the adsorption of the gas. When the overburden pressure is simulated in the laboratory testing this can close the crack that opened up while the overburden pressure was released and this can provide us with results more reflective of the field conditions.

5.8.2 Oxidation of the Sample

It is fully expected that all specimen prepared for this test program underwent laboratory oxidation (weathering) due to the exposure of the block samples to air during storage. During oxidation, oxygen replaces hydrogen chemically and it is extremely difficult for carbon dioxide at low pressures to replace oxygen, which due to its nature is bonded or chemisorbed to the structure of the coal (Berkowitz, 1979). In general, high activation energies would be required to desorb the oxygen from the coal surfaces. It is likely that at low pressure (< 500 kPa), CO_2 does not posses enough free energy to replace the oxygen present in the coal but at higher gas pressures CO_2 can successfully compete for the

adsorption sites present on the surface of the coal. At pressures higher than 500 kPa, the crushed coal isotherms behave similarly to previous results reported in the literature.

Mastalerz and Bustin (1997) have noted that natural and laboratory oxidation will effect adsorption in different ways. Natural oxidation of coal that occurs in situ in the presence of groundwater will result in small decrease in adsorption whereas ex-situ (laboratory) oxidation due to specimen storage in air will result in higher adsorption capacities. Given that the specimen used in this testing program underwent oxidation in laboratory environment therefore it is likely to be one of the reasons that the adsorption capacities measured on the crushed coal specimen are higher than test results reported in the literature.

While no specific measurements were made to quantify the degree of oxidation in the specimen, it was assumed that the intact specimen was exposed to an equivalent degree of oxidation as the crushed coal specimens since all samples were taken from the same block samples. while it is recognized that crushing the coal creates additional surface area relative to intact coal, it is expected that the degree of oxidation per unit surface area was the same.

5.8.3 Moisture Content

According to ASTM D 2013-86 (Reapproved 1994) adsorption testing must be conducted at equilibrium moisture content for the coal.

From previous work (Harpalani and Chen, 1993, Harpalani and Chen 1995) on the coal of similar rank the equilibrium moisture content was determined as 2.8%. Although in this study equilibrium moisture content was not determined but it is assumed that,

because the coal rank is similar i.e. high bituminous, therefore the equilibrium moisture content would be in the same range of below 3%.

In this study, tests were carried out on samples that were weathered (oxidized) as well as air-dried. The air-dried moisture content of the samples was found to be 7% in the crushed sample and approximately 4% for the intact coal samples. Previous studies have correlated the moisture content to the adsorption capacity and it has been shown (Joubert et al. (1973, 1974), Curl (1978), Arri et al., (1992)) that the adsorption capacity of a coal sample increases with a decrease in moisture content. At higher moisture contents, CO_2 has a more difficult time competing with the bound water for adsorption sites on the coal surface.

Based on moisture contents alone, the crushed coal specimen should display a lower adsorption capacity, than the intact specimens. As shown in Figure 5.10, this is indeed true at higher CO_2 equilibrium pressures, above approximately 1500 kPa, but at lower equilibrium pressures, the intact specimen despite having lower moisture content exhibit lower adsorption capacities. This indicates that additional mechanisms are occurring within the intact specimen to affect the adsorption capacities.

5.8.4 Structure of Coal

Effect of particle size has also been studied in various previous studies (Flood, 1966, Gregg 1967, Berkowitz 1979, Mahajan 1991). As has been discussed earlier the oxidation of the sample also depends upon the particle size. While the particle size decreases the oxidation of the sample increase as the surface area directly available to the oxygen increase dramatically (Beier, 1983, Mikula et al., 1983, Ingram and Rimstidt, 1984). According to ASTM method for Analysis of the coal samples (ASTM D 2013-86

(Reapproved 1994)), only this is mentioned that the coal should be passing Sieve #60. It is prudent to believe that the many particles that passed through Sieve 60 would be passing through smaller sieves implying that more surface area is available for the adsorption of the gas. Correlation of the effect of smaller particles of coal on the rate and path of adsorption cannot be ignored. The smaller particles would be highly oxidized while bigger particles would not. Consequently this can play an important part in obtaining a different path for the adsorption.

Investigation carried out for the sorption phenomenon proved that the solids of non-rigid structure expand under a gas or a vapour atmosphere (DeGance et al., 1993) and as coal belongs to this group of solids therefore it is applicable for this study too. According to Stefanska (1990) expansion in the direction perpendicular to the bedding is larger than that in the direction parallel to it. This is due to the fact that a CO_2 particle located between the planes causes more intensive displacement in the direction perpendicular to the bedding as the energetic resistance in that direction is smaller. According to various studies carried out previously (Moffet and Weale, 1955, Stefanska 1988, DeGance et al., 1993, St. George and Barakat, 2001) the expansion in direction perpendicular to bedding increases at a lower rate and exceeds the expansion parallel to bedding not until several hours. The expansion of a solid depends on the diameter of an absorbing gas. Expansion can be explained by the fact that the majority of the pores slats and cracking is parallel to the bedding and the expansion in the first minutes is caused by the adsorption so the overall expansion of the sample is also greater than in the perpendicular direction. It has been pointed out that the method used for determining the swelling due to adsorption does not influence the amount of adsorbed CO_2 however there are differences in time

needed to achieve the equilibrium state of sorption (Stefanska, 1990). Twhen the gas penetrates the coal, coal swells this swelling results in lose in strength implying that longer times are needed to achieve the equilibrium state when the gas pressure is higher.

At higher CO_2 pressure sorption will not take place without coal swelling accompanied by the resultant new sorption spaces ready to be filled. Also according to previous studies (Stefanska et al., 1988, Stefanska 1990, Levine 1993) the process of CO_2 sorption on bituminous coal takes place in the micro-pore region of the macro-molecular elements of the coal substances but it does not cause their permanent deformation. In other words, sorption on the bituminous coal is a lattice sorption. Therefore, process of coal saturation is not governed by the micropore spaces being filled with gas but rather by structural changes in the coal substances, resulting in an increase of sorption space (Stefanska, 1990) and hence resulting in swelling of the sample.

Further study into this phenomenon is required to study the mechanism.

Chapter 6: Conclusions and Recommendations

6.1 Introduction

Accurate gas content determination is critical for the economic assessment of the coal gas reservoir and coal production forecasts. Gas capacity is typically obtained from canister desorption tests carried out on samples of the reservoir. The use of accurate equilibrium analysis on the coal is required to obtain reasonable gas-in-place values.

Coal, a compositionally complex material, contains both organic and inorganic components. This compositional heterogeneity is present on all scales, from molecular level to seam scale. This heterogeneity in coal properties impart heterogeneity in other physical properties of coal and subsequently may lead to inaccurate assessment of gas reservoir. Understanding of the variation in coals properties is important to model the seam characteristics like adsorption/desorption of coal under gas pressures and swelling of the coal during the adsorption. The goal of this study was to understand the adsorption behavior of intact coal under effective stresses and compare it to the better understood crushed coal adsorption characteristics.

6.2 Conclusion

6.2.1 Coal Sampling Techniques

Two different methods, freezing and direct coring, were used for the creation of test specimens from block samples of coal. Even though the frozen samples were not used, the freezing technique was shown to work well in the preparation of coal specimens. A study of possible geo-chemical changes of the pore fluid require future study and to

confirm the usability of the freezing technique for sampling of highly fractured coal samples.

6.2.2 Adsorption Test Results

The isotherms for intact coal samples clearly show a different path to reach almost the same final result. In a larger picture the difference between the total adsorption capacity of crushed coal and the intact coal is minor.

The results from both intact and crushed samples are compared to the previous studies and clearly show the kinematic behavior of the coal when tested in its intact condition thus simulating the field conditions.

It is safe to assume that due to oxidation, structure of the coal and different testing procedure adopted as well as application of effective stresses used in this study the capacity for the coal to adsorb CO_2 is different for intact versus crushed specimens.

The gas storage capacity of coal is significantly affected by the moisture content during the experiment. This phenomenon of storage capacity being moisture related has been observed for various other studies (Joubert, 1973, Joubert, 1974, Mavor et al., 1990).

The effect of sample moisture content as well as the nature of the sample (intact or crushed) should be further studied so as to fully comprehend the extent to which the sample state affects the adsorption capacity of the coal.

6.2 Practical Application of Research

The major practical application of this research is the determination of adsorption characteristics of in situ coal samples in order to improve production and injection behavior of the coalbed methane reservoir

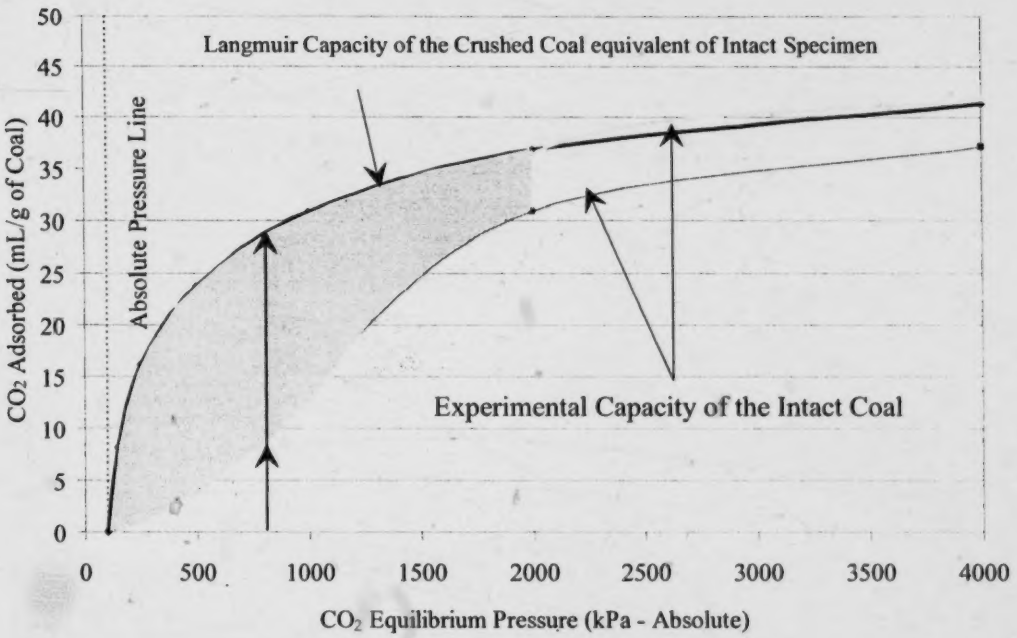

Figure 6.1: Difference in Langmuir Capacity and Experimental Capacity of Intact Coal

Figure 6.1 schematically illustrates the anticipated difference between the crushed and intact coal specimens. At low equilibrium pressures, the intact structure of the coal prevents CO_2 from assessing adsorption sites which are otherwise available in crushed coal specimens. Hence, intact coal specimens exhibit a lower absolute adsorption volume. At higher pressures, when CO_2 can penetrate a greater volume of micropores, the behavior for intact specimens approaches the behavior of crushed coal specimens. In conjunction with absolute adsorbed volumes, the kinetic adsorption (and by inference, desorption) are slower for intact coal specimens at lower pressure regimes. These variations in adsorptions or desorption kinetics may have a dramatic influence on reservoir producibility and subsequent economic projection for a CBM (Coalbed Methane) or ECBM (Enhanced Coalbed Methane) project

6.3 Recommendations

The following recommendations may be useful for future geomechanical studies of the sequestration process of CO_2 in coalbeds:

6.3.1 Experimental Procedure

Further tests on intact samples should be performed including tests for the mixture of CO_2 and methane to further understand the behavior of the coal.

Volume change measurements are important for understanding the shrinkage and swelling phenomena in coals. These were not undertaken in this study so a study should be conducted to understand shrinkage and swelling phenomena and their effect on the adsorption characteristics of the gas.

6.3.2 Scale Effects

This study was performed on intact coal samples. Further research should include complete constitutive testing to examine the impacts of coal structure specially the coal fracture system. Testing larger samples will also improve volume change response during adsorption.

6.3.3 Risk Assessment

It is important to quantify the risk of different geological disposal methods for greenhouse gases and their impact on the environment. Additional research should be conducted to identify risk events and their consequences as well as the probability of their occurrence.

References

Al-Hawaree, M., 1999. Geomechanics of CO_2 sequestration in coalbed methane reservoirs. MSc. Thesis, University of Alberta. 196p.

Al-Taweel, A.M., Farag, H.A., Kwak, J., Hamza, H.A. and Falk, M., 1982. Adsorption: a tool for characterizing coal oxidation. Coal: Phoenix of the 80's. Ottawa, Canada, Canadian Society for Chemical Engineering, **1**: 125-130

Arri, L.E., Yee D., Morgan, W.D., and Jeansonne M.W., 1994. Modelling Coalbed Methane Produstion with Binary Gas Sorption, SPE Paper number 24363, SPE Rocky Mountain Regional Meeting held in Casper, Wyoming, May 18-21.

ASTM. 1990. Standard Test Methods for Proximate Analysis of the Analysis Sample of Coal and Coke by Instrumental Procedure (D 5142-90). *In* 1990 Annual Book of ASTM Standards. ASTM, Philadelphia. **5**(5): 444-448.

ASTM. 1992. Standard Test Method for Determination of Pore Volume and Pore Volume Distribution of Soil and Rock by Mercury Intrusion Porosimetry (D4404-84 In 1997 Annual Book of ASTM Standards. ASTM, Philadelphia. **4**(8): 582-586.

ASTM. 1992. Standard Test Method for Surface Area of Catalysts (D3663-92). In 1992 Annual Book of ASTM Standards. ASTM, Philadelphia. **5**(3): 642-645.

ASTM. 1993. Standard Test Methods for Instrumental Determination of Carbon, Hydrogen, and Nitrogen in Laboratory Sample of Coal and Coke (D5373- 93). In 1993 Annual Book of ASTM Standards. ASTM, Philadelphia. **5**(5): 459-462.

ASTM. 1994. Standard Method of Preparing Coal Samples for Analysis (D2013-86 Reapproved 1994). In 2001 Annual Book of ASTM Standards. ASTM, Philadelphia. **5**(5): 149-160.

ASTM. 1997. Standard Test Methods for Specific Gravity of Soils (D 854-92). In 1997 Annual Book of ASTM Standards. ASTM, Philadelphia. **4**(8): 88-91.

ASTM. 2000. Standard Test Method for Moisture in the Analysis Sample of Coal and Coke (D3173-00). In 2001 Annual Book of ASTM Standards. ASTM, Philadelphia. **5**(5): 303-305.

ASTM. 2002. Standard Practice for Calculating Coal and Coke Analysis from As-Determined to Different basis (D3180-89 Reapproved 2002). In 2002 Annual Book of ASTM Standards. ASTM, Philadelphia. **5**(5): 331-333.

ASTM. 2002. Standard Test Method for Total Moisture in Coal (D3302-02). In 2002 Annual Book of ASTM Standards. ASTM, Philadelphia. **5**(5): 335-341.

Ates, Y., and Barron, K., 1988. The effect of gas sorption on the strength of coal. Mining Science and Technology, **6**, 291-300.

Bailey, R.T., and McDonald, M.M., 1993. Carbon dioxide capture and use for EOR in Western Canada: 1. General overview. Energy Convers. Manage. **34:** 1145–1150.

Banerjee, B., and Bhattacharyya, N.C., 1988. Changes in Physio-Chemical Properties of Coal due to insitu weathering of coal seams. Fuel Science and Technology. **7:** 1-2.

Bartosiewicz, H., and Hargraves, A.J., 1985. Gas properties of Australian coal. Proc Aust. Inst. Metal. **290:** 71-77.

Beier, E., 1983. Gas exchange of black coal and other substances when stored for decades in contact with air, *In* Proceedings: International conference on coal science Pittsburgh, PA, USA, 15-19 August 1983, 735-738.

Bell, G.J., and Rakop, K.C., 1986. Hysteresis of Methane/Coal Sorption Isotherms. SPE 15454, paper presented at the 61st Annual Technical Conference and Exhibition of the SPE, New Orleans, LA., 1986. 1-10.

Berkowitz, N., 1979. An Introduction to Coal Technology, Academic Press, 345p

Bishop, A.W. and Henkel, D.J., 1964. The measurement of soil properties in the triaxial test. Edward Arnold Ltd. 228p.

Brewer, P.G., Friederich, G., Peltzer, E.T. and Orr, F.M., Jr., 1999. Direct Experiments on the Ocean Disposal of Fossil Fuel CO_2, Science, **284:** 943-945.

Bruce, D.J., 1998. Global warming: public health and the debate about science and policy, Journal of Environmental Health. **60**(10): 9-19.

Brunauer, S., 1943. Adsorption of Gas and Vapors. Princeton University Press, 1943. 511p.

Brunauer, S., Emmet, P.H., and Teller, E., 1938. Adsorption of Gases in Multimolecular Layers. Journal of American Chemical Society. **60:** 309-319.

Bustin, R. M., Cameron, A. R., Grieve, D. A., and Kalkreuth, W. D., 1985. Coal petrology, its principles, methods, and application. Geological Association of Canada Short Course Note. 273p.

Bustin, R.M., 1997. Importance of Fabric & composition on the stress sensitivity of Permeability in some coals, Northern Sydney Basin, Australia: Relevance to Coalbed methane Exploration, AAPG Bulletin. **81**(11): 1894-1908.

Bustin, R. M. and Clarkson, C. R., 1998. Geological controls on coalbed methane reservoir capacity and gas content. International Journal of Coal Geology, **38:** 3-26.

Clarkson, C. R. and Bustin, R. M., 1999. The effect of pore structure and gas pressure upon the transport properties of coal: A laboratory and modeling study. 1. Isotherms and pore volume distributions. Fuel, **78**(11): 1333-1344.

Clarkson, C. R. and Bustin, R. M., 2001. Binary gas adsortion/desorption isotherms: effect of moisture and coal composition upon carbon dioxide selectivity over methane. Int. J. of Coal Geology, **42:** 241-271.

Crank, J., 1975. The mathematics of diffusion, 2nd Ed. Oxford University Press. 414p.

Crosdale, P.J., Beamish, B.B., and Valix, M., 1994. Coalbed methane sorption related to coal composition, Int. J. of Coal Geology, **35:** 145-158.

Crosdale, P. J., Beamish, B. B. and Valix, M., 1998. Coalbed methane sorption related to coal composition. International Journal of Coal Geology, **35:** 147-158.

Curl, S.J., 1978. Methane prediction in Coal Mines, Report No. ICTIS/TR04,IEA Coal Research, London.

Davila, R.S., 1992. The influence of fines content and specific surface acrea on freezing sandy soils. MSc Thesis University of Alberta, 232p.

DeGance, A. E. Morgan, W. D., and Yee, D., 1993. Investigation of adsorption, dilatometry and strength of low rank coal III. Investigation of simultaneous sorption together with expansion and desorption together with contraction kinetics of coal under the influence of CO_2, Fluid Phase Equilibria, **82:** 215-224.

Derbyshire, F., Davis, A., and Lin, R., 1991. Two-component concept of coal structure, in Schobert, H. H., et al., eds., Coal science II ACS Symposium Series 461, American Chemical Society, Washington, D.C., 72-88.

Diessel, C.F.K., 1992. Coal- bearing depositional Systems. Springer-Verlag. 56-68.

Ettinger, I.L., 1958. Systematic handbook for the determination of the methane content of coal seams from the seam pressure of the gas and the methane capacity of coal: National Coal Board, Moscow, Translation No. A1606/SHE. 58-95.

Faiz, M.M., and Cook, A.C., 1991. Influence of coal type, rank and depth on the gas retention capacity of coals in the southern coalfield, NSW. *In* Bomberry, W.J., Depers, A.M. (Editor): Gas in Australian Coals. Symposium Proceedings vol. 2. Geological Society of Australia, 19-29.

Faiz, M.M., Aziz, N. I., Hutton, A.C., and Jones, B.C., 1992. Proceedings, Symposium on Coalbed Methane Research and Development in Australia, Townsville, 1992, 9-20.

Felder, R.M., and Rousseau, R.W., 1986. Elementary principles of chemical processes, 2nd Edition. John Wiley & Sons. 668p.

Flood, A.E (Editor): 1966. The Solid-Gas Interface, Marcel Dekker Inc., New York, **1**, 514p.

Fogg, P.G.T., and Gerrard, W., 1991. Solubility of gases in liquids: a critical evaluation of gas/liquid systems in theory and practice. John Wiley & Sons, USA. 332p.

Francis, D., 1998, Extreme Weather and Climate Change. Climate Change Digest, Environment Canada. 76-87.

Francis, W., 1961. Coal: Its Formation and Composition, Edward Arnold (Publishers): Ltd., London. 806p.

Frederick, L.H., and Steinberg, M., 1981. Control of Carbon Dioxide Emissions from a Power Plant (and Use in Enhanced Oil Recovery). Report Environment Canada, 343p.

Fredlund, D.G., 1973. Volume change behaviour of unsaturated soils. PhD Thesis. University of Alberta. 490p.

Gregg, S.J., 1967. The Surface Chemistry of Solids. Reinhold, New York. 839p.

Grozic, J.L.H., 1999. The behaviour of loose gassy sand and its susceptibility to liquefaction. PhD Thesis. University of Alberta. 287p.

Gunter, W.D., Bachu, S., Law, D., Marwaha, V., Drysdale, D.L., Macdonald, D.E., and McCann, T.J. 1995. Technical and economic feasibility of CO_2 disposal in aquifers within Alberta Sedimentary Basin. Canada. Energy Conversation. **37:** 1135-1142.

Gunter, W.D., Gentzis, T., Rottenfusser, B.A., and Richardson, R.J.H. 1997. Deep Coalbed Methane in Alberta, Canada: A Fuel Resource with A Potential of Zero Greenhouse Gas Emissions. Energy Convers. Mgmt. 1997. **38:** 217-222.

Gunter, W.D., Wiwchar, B., and Perkins, E. H. 1997. Aquifer Disposal of CO_2 Rich Greenhouse Gases: Extension of the Time Scale of Experiment for CO_2 Sequestration Reactions by Geomechanical Modelling. Mineralogy and Petrology. **59:** 121-140.

Gunther, J., 1965. Etude de la liason Gaz-Carbon (Investigation of Coal Gas Bond). Revue de l'Industrie Minerale. **47:** 693-700 (in French) (Translated using www.BabelFish.com).

Handbook of Compressed Gases, 1985. Kersti Ahlberg (ed.): AGA AB Sweden, 582p.

Hansen, J. E., Sato, M., and Ruedy,R., 1998. Global climate data and models: A reconciliation, Science, **281**(5379): 930-932.

Harrington, J.F., and Horseman, S.T., 1999. Gas transport properties of clays and mudrocks. In: Aplin, A.C., A.J. Fleet, and J.H.S. Macquaker (eds). Muds and mudstones: physical and fluidflow properties, Geological Society, London, Special Publications, **15:** 107-124.

Harpalani, S., 1988. Specimen Preparation for Testing of Coal, Technical Note, International Journal of Rock Mechanics Mining Science and Geomechanical Abstract, **25**(5): 327-330.

Harpalani, S., and Chen, G., 1993. Coal Slippage and Matrix Shrinkage Effects on Coal Permeability. International Coalbed Methane Symposium, May 17-21, 1993, Birmingham, Alabama, 285-294.

Harpalani, S., and Chen, G. 1995. Estimation of changes in fracture porosity of coal with gas emission. Fuel, **74**(10): 187-196.

Harpalani, S., and Chen, G., 1997. Influence of gas production in duced volumetric strain on permeability of coal, Geotechnical and Geological Engineering, **15:** 303-325.

Harpalani, S., and Pariti, U.M. 1993. Study of Coal Sorption Isotherms Using a Multicomponent Gas Mixture. Proceedings, International Coalbed Methane Symposium. 1993. 151-160.

Harpalani, S., and Scraufnagel, R. A., 1990. Measurement of Parameters impacting methane recovery from coal seams, Int. J. of Mining and Geological Engg., **8:** 369-384.

Herod, A. A., Stokes, B. J., and Radeck, D., 1991. Coal structure and mass spectrometry: volatiles in peat and coals: Fuel, **70:** 329-340.

Hill, D.W., 1977. The influence of temperature and load on moisture transferin freezing soils. MSc Thesis University of Alberta, 236p.

Herzog, H., Eliasson, B., anf Koarstad, O., 2000. Capturing Greenhouse Gases. Scientific American, **282**(2): 72-79.

Ho, A., 2002, Experimental Methodology Used to Investigate Transport Processes in Cap Rock. MSc Thesis, University of Alberta, 135p.

Houghton, J., 1997. Global warming the complete briefing. 2nd Ed. Lion Publishing Inc., Oxford, England. 251p.

Ingram, G.R., and Rimstidt, J.D., 1984. Natural weathering of coal. Fuel, **63**(3): 292-296.

International Energy Annual 2001: Coal, Department of Defence, USA *http://www.eia.doe.gov* last accessed October 2003.

Johnson, J.W., Nitao, J.J., Steefel, C.I., and Knauss K.G. 2001. Reactive transport modeling of geologic CO_2 sequestration in saline aquifers: the influence of intra-aquifer shales and the relative effectiveness of structural, solubility, and mineral trapping during prograde and retrograde sequestration. Pre-print from: First National Conference on Carbon Sequestration U.S. DOE, Washington, D.C. 60p.

Jones, R.H., 1981. Developments and applications of frost susceptibility testing. Engineering Geology, **18:** 269-280

Joubert, J. I., Grien, C. T. and Bienstock, D. 1973. Sorption of methane in moist Coal. Fuel, **52:** 181-185

Joubert, J. I., Grien, C. T. and Bienstock, D, 1974. Effect of moisture on the methane capacity of American coals, Fuel, **53:** 186-191

Kaiser, P .K., 1979. Time Dependent Behaviour of Tunnels in Jointed Rock Masses. Ph.D. thesis, Department of Civil Engineering, University of Alberta, Edmonton, Alberta. 341p.

Kaji, R., Hishinuma, Y., and Nakamura, Y., 1985. Low Temperature oxidation of coals: effects of pore structure and coal composition, Fuel, **64**(3): 297-302

Konrad, J.M., 1980. Frost heave Mechanics. PhD Thesis. University of Alberta. 289p.

Krooss, B.M., and Schaefer. R.G., 1988. Experimental measurements of the diffusion parameters of light hydrocarbons in water saturated sedimentary rocks – I A new experimental procedure. Organic Geochemistry, **11**(3): 193-199.

Krooss, B.M. and Leythaeuser, D., 1998. Experimental measurements of the diffusion parameters of light hydrocarbons in water saturated sedimentary rocks – II results and geochemical significance. Organic Geochemistry, **12:** 91-108.

Kyle, B.G. 1992. Chemical and process thermodynamics, 2nd Edition. Prentice-Hall, USA. 567p.

Ladd, C.M., 1998. What global warming?, Mechanical-Engineering, **120**(11) 8-18.

Lamberson, M. N., and Bustin R.M., 1993, AAPG Bull, **77:** 2062-2068.

Law, B. E. and Rice, D. D. (Editors): 1993. Hydrocarbons from Coal. AAPG, Tulsa, Oklahoma, 119-132.

Lemmon, E.W., M.O. McLinden and D.G. Friend. 2001. Thermophysical Properties of Fluid Systems *In*: NIST Chemistry WebBook, NIST Standard Reference Database Number 69 Linstrom, P.J. and W.G. Mallard (Eds). National Institute of Standards and Technology, Gaithersburg MD, 20899 (http://webbook.nist.gov).

Levine, J. R., 1993. Coalification: The Evaluation of Coal as Source Rock and Reservoir Rock for oil and Gas in Law, B. E., and Rice, D. D., eds., Hydrocarbons from Coal, AAPG Studies in Geology #38, the American Association of Petroleum Geologists, Tulsa, Oklahoma, USA. 493p.

Loy, S.J., Cates, L.R., and Cox, J.N., 1987. oxidized coal problems. Coal prep 87: 4th International Coal preparation conference, Lexington, KY, USA, 27 April 1987, Aurora, CO, USA. Industrial Presentations West, 231-240

Mahajan, O. P., 1991. CO_2 surface area of Coal: The 25 Year Paradox. Carbon, **29**(6): 735-742

Mageau, D.W., 1978. Moisture migration in frozen soil. MSc Thesis, University of Alberta. 139p.

Mastalerz M., and Bustin, R.M., 1997. Variation in the chemistry of macerals in coals of the Mist Mountain Formation, Elk Valley coalfield, British Columbia, Canada. International-Journal-of-Coal-Geology. **33**(1): 43-59.

Mavor, J.M., and Vaughn, J.E. 1998. Increasing Coal Absolute Permeability in the San Juan Basin Fruitland Formation. Society of Petroleum Engineers, 201-206.

McPherson, B.J.O.L., and Cole, B.S., 2000. Multiphase CO_2 flow, transport, and sequestration in the Powder River Basin, Wyoming, USA. Journal of Geochemical Exploration, **69-70**: 65-69.

Meyers, R., 1982. Coal Structure, Academic Press. 340p.

Mikula, R.J., Mikhail M.W., and Munoz V.A., 1983. The influence of coal structure on handling and processing characterisation. Proceedings: 1983 International Conference on Coal Science, Pittsburgh, PA, USA, 15-19 August 1983. DE8401339 Pittsburgh, PA, USA, Pittsburgh Energy Technology Center, 709-712.

Moffat, D. H. and Weale, K. E., 1955. Sorption by coal of methane at high pressures. Fuel, **34:** 449-462.

Mukhopadhyay, P. K., and Hatcher, P. G., 1993. Composition of Coal, in Law, B. E., and Rice, D. D., eds., Hydrocarbons from Coal, AAPG Studies in Geology #38, the American Association of Petroleum Geologists. Tulsa, Oklahoma, USA. 493p.

Nandi, S. P., and Walker, P. L., Jr., 1966. Diffusion of Argon from coals of different rank, in Gould, R. F., eds., Coal Science: Washington, D.C., American Chemical Society, Advances in Chemistry Series, **55:** 379-385.

Neill, P.H., and Winans, R.E., 1986. The application of inverse gas chromatography to coal and oxidized coal. ACS Symposium Series, **391:** 290-305.

Neill, P.H., and Winans, R.E., 1989. Coal weathering: chemical processes and pathways. Chemistry of Coal Weathering. Amsterdam, The Netherlands, Elsveier Science Publishers, 1-32.

Noonan, D.K.J. 1972. Fractured Rock Subjected to Direct Shear. M.Sc. Thesis, University of Alberta, Edmonton, Alberta. 218p.

Pandolfo, A.G., Johns, R.B., Dyrkacz, G.R., and Buchanan, A.S., 1989. characterization of isolated maceral group concentrates and the behaviour of maceral lithotypes towardsaerial oxidation. Proceeding of the maceral '89 symposium, North Ryde, NSW, Australia, CSIRO Division of Coal Technology, 9.1-9.9

Patching, T.H., 1970. The retention and release of Gas in coal – A review, CIM Bulletin, **63:** 1302-1308.

Pearce, J.M., Holloway, S., Wacker H., Nelis M.K., Rochelle C., and Bateman K., 1996. Natural occurrences as analogues for the geological disposal of carbon dioxide. Energy and Conversion Management, **37**(6-8): 1123-1128.

Perkins E.H. and W.D. Gunter. 1996. Mineral traps for carbon dioxide, *In:* Hitchon, B (editor) Aquifer disposal of carbon dioxide hydrodynamic and mineral trapping-proof of concept. 93-112.

Puri, R., and Siedle, J.P., 1992. Mesurement of Stress dependent permeability in coal and its influence on coalbed methane production, In Situ, **16**(3): 183-202.

Rebour, V., Billiotte J., Deveughele M., Jambon A., and le Guen, C., 1997. Molecular diffusion in water-saturated rocks: A new experimental method. Journal of Contaminant Hydrology, **28:** 71-93.

Reucroft, P. J. 1986. Gas Induced Swelling in Coal. Fuel, **65:** 816-820.

Ryan, B., 1992. An equation for estimation of maximum coalbed-methane resource potential, British Columbia geological Survey, geological Fieldwork 1991, Paper 1992-1, 393-395.

Sawyer, C.N., McCarty, P.L., and Parkin, G.F., 1994. Chemistry for Environmental Engineering, 4th Edition, McGraw Hill Inc, 658p.

Schopf, J. M., 1956. A definition of coal, Economic Geology, **51:** 521-527.

Shelby, J.E. 1996. Handbook of gas diffusion in solids and melts. ASM International, USA. 240p.

Sobkowicz, J.C. 1982. The mechanics of gassy sediments. PhD Thesis University of Alberta. 531p.

Span, R., and Wagner, W., 1996. A new equation of state for carbon dioxide covering the fluid region from the triple-point temperature to 1100 K at pressures up to 800MPa. Journal of Physical Chemistry Reference Data, 1509-1596.

St. George, J. D., and Barakat. M. A., 2001. The change in effective stress associated with shrinkage from gas desorption in coal. International Journal of Coal Geology, **45:** 105-113.

Stacy, W.O., and Jones, J.C., 1986. The swelling and adsorption characteristic of Victorian brown Coals. Fuel, **65**(8): 45-68.

Stefanska, G. C., Czaplinski, A. and Brzoska, K., 1988. An influence of the CO_2 pressure on adsorptional and dilatometric property of high rank coals , Archives of Mining Sciences, **33**(3): 299-311.

Stefanska, G. C., 1990. An Influence of CO_2 and CH_4 on changes of sorption and dilatometric properties of bituminous coals, Archives of Mining Sciences, **35**(1): 105-113.

Stevens, S.H., Fox C.E., and Melzer L.S., 2000. McElmo Dome and St. Johns natural CO_2 deposits: analogs for geologic sequestraion. Fifth International Conference on Greenhouse Gas Control Technologies, Cairns, Queensland, Australia, August 13-16, 317-321.

Stevens, S.H., Pearce J.M., and Rigg A.J, 2001. Natural analogs for geologic storage of CO_2: an integrated global research program. Pre-print from: First National Conference on Carbon Sequestration U.S. DOE, Washington, D.C. 12p.

Suggate, R. P., 1990. Variability in Type III organic matter at the initiation of diagenesis, in Nuccio, V. F. and Barker, Ch. E., eds., Applications of thermal maturity studies to energy exploration: Denver, Colorado, Rocky Mountain Section, Society of Economic Palaeontologists and Mineralogists, 45-52.

Tavenas, F., Jean P., Leblond P., and Leroueil S., 1983. The permeability of natural soft clays. part I: Methods of laboratory measurement. Canadian Geotechnical Journal, **20:** 629-644.

Teo, K.C., Finora, S., and Leja, J., 1982. Oxidation states in surface and buried coal from the Fording River deposit. Fuel, **61**(1): 71-76.

van Heek, K. H., 2000, Progress of coal science in the 20th century, Fuel, **79:** 1-26.

van Krevelen, D.W., Blom, L., and Edelhausen, L., 1957. Fuel, **36:** 135-147.

van Krevelen, D. W., 1994. Coal (reprinted from 1961 edition): Amsterdam, Elsevier, 514p.

Vazquez, U.G., R.F. Chenlo, G.G Pereira, and L.J. Peaguda. 1994. Solubility of CO_2 in aqueous solutions of saccharose, glucose, fructose, and glycerin. Journal of Chemical and Engineering Data vol. 39, no. 4, 639-642.

Ward, C. R., 1984. Chemical composition of coal, in Coal geology and Coal Technology Melbourne Ward C. R. (ed.): Blackwell Publishers, 74-112.

Wedlake, G.D. and Robinson D. B., 1979. Solubility of carbon dioxide in silicone oil. Journal ofChemical and Engineering Data. **24**(4): 305-306.

White, S.P., Weir G.J, and Kissling W.M.. 2001. Numerical simulation of CO2 sequestration in natural CO_2 reservoirs on the Colorado Plateau. Pre-print from: First National Conference on Carbon Sequestration U.S. DOE, Washington, D.C. 12p.

Winans, R.E., and Neill, P.H., 1987. Application of Inverse gas chromatography to fluidity studies. Coal research conference vol. 1. Wellington New Zealand, 2-4 November 1987, Wellington New Zealand, Coal Research Association Paper 3-11

Yokokawa, C., Ohnishi, Y., and Oda, H., 1989. Variation of Hygroscopic characteristics of coal caused by slight air oxidation. 1989 International Conference on coal science, Tokyo Japan, 22-27 October 1989, Tokyo Japan, NEDO. 1039-1042.

Young, D.M., and Crowell, A.D. 1962. Physical adsorption of gases. Page 1, London Butterworth. 426p.

APPENDIX A – Graphs between Total Gas Inflow and time for Crushed Sample 1 for each pressure increment

The following pages contain Graphs between Time and Total Gas inflow for each Pressure range for the Crushed Sample 1.

Pressures start from 150kPa and goes on to 4MPa.

The time is presented in hours while the Total Gas inflow is in mL. The total gas Inflow includes the compressed and adsorbed gas.

Total Gas Inflow, Total time for which the pressure increment was applied and the pressure increment are written on the graph to make them easier to recognize

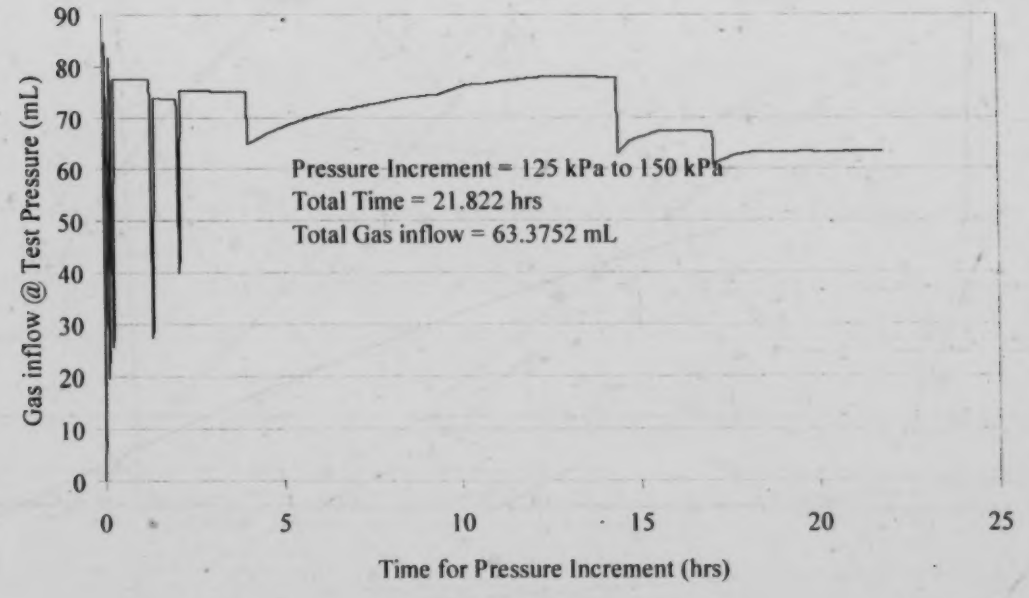

Figure A.1: Relationship Between Total Gas Inflow and Time for Pressure increment of 125kPa to 150kPa

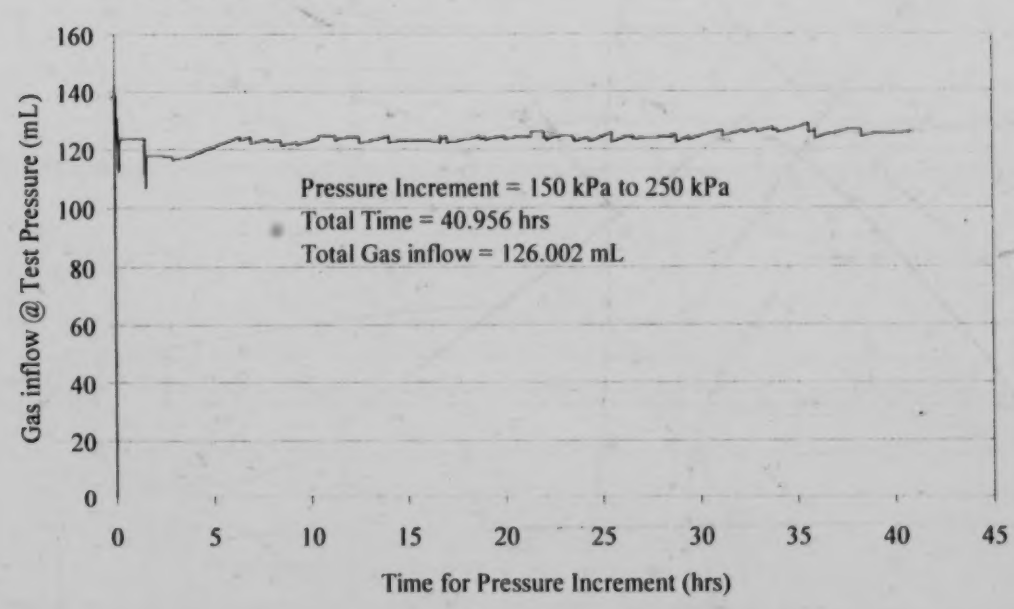

Figure A.2: Relationship Between Total Gas Inflow and Time for Pressure increment of 150kPa to 250kPa

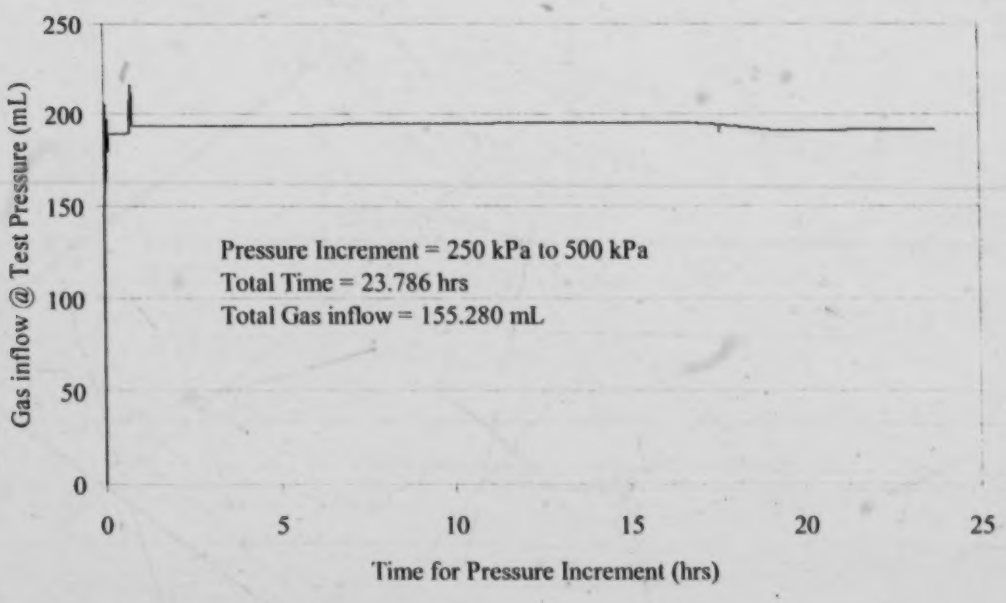

Figure A.3: Relationship Between Total Gas Inflow and Time for Pressure increment of 250kPa to 500kPa

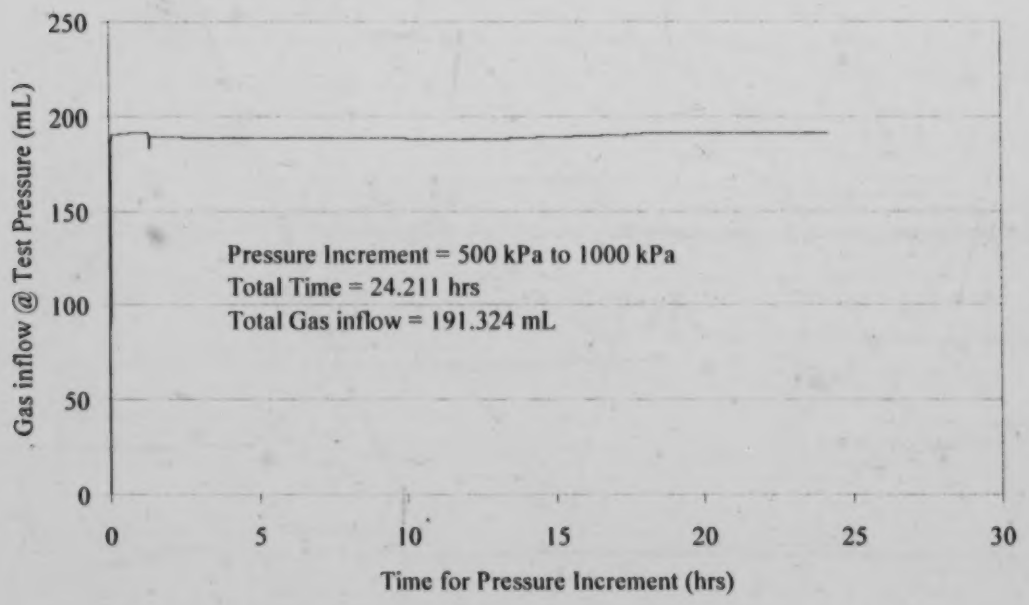

Figure A.4: Relationship Between Total Gas Inflow and Time for Pressure increment of 500kPa to 1000kPa

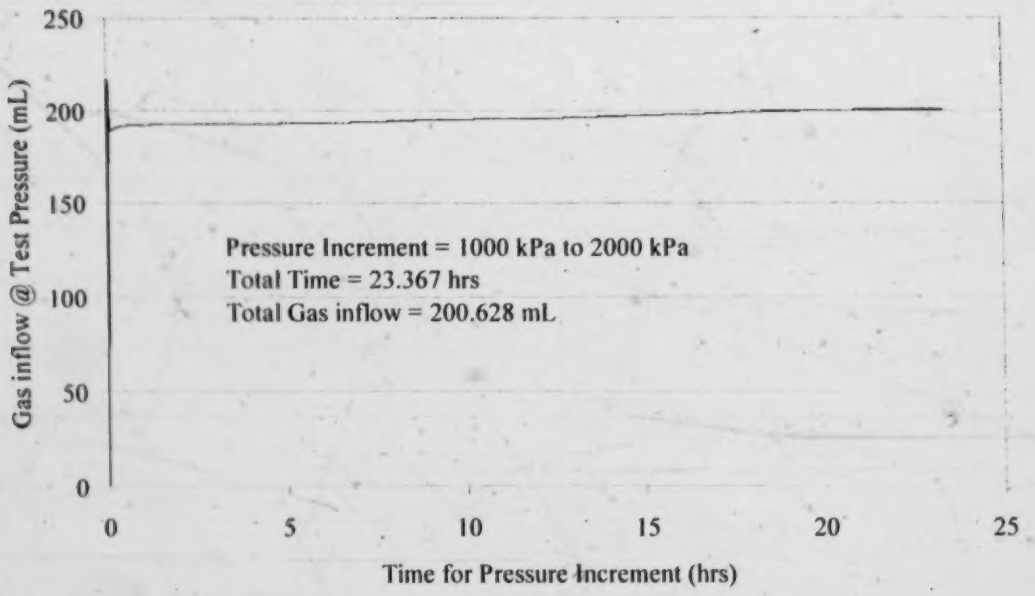

Figure A.5: Relationship Between Total Gas Inflow and Time for Pressure increment of 1000kPa to 2000kPa

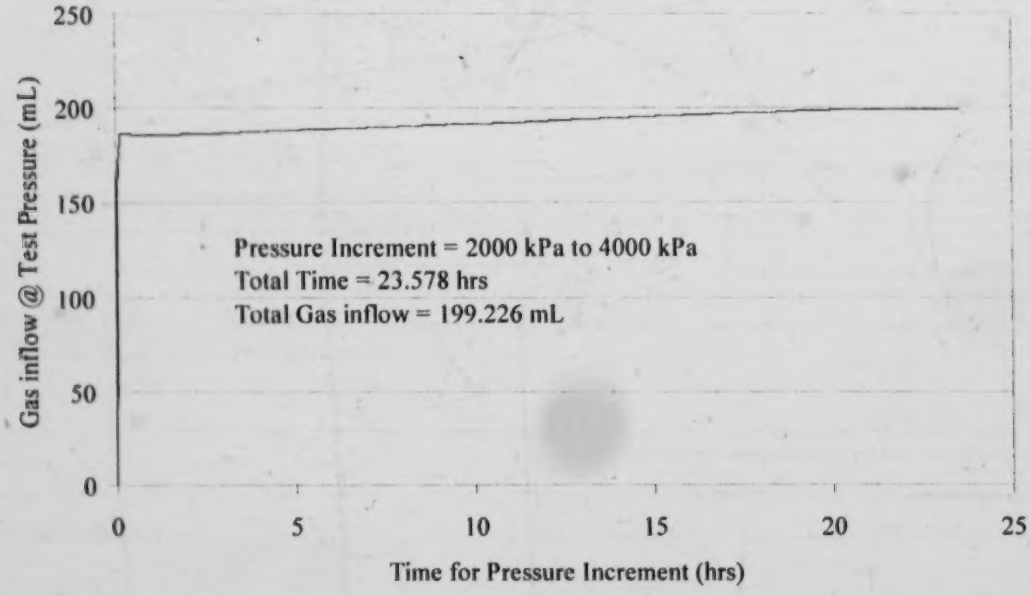

Figure A.6: Relationship Between Total Gas Inflow and Time for Pressure increment of 2000kPa to 4000kPa

APPENDIX B – Graphs between Total Gas Inflow and time for Crushed Sample 2 for each pressure increment

The following pages contain Graphs Between Time and Total Gas Inflow for each Pressure range for the Crushed Sample 2.

Pressures start from 150kPa and goes on to 4MPa.

The time is presented in hours while the Total Gas Inflow is in mL. The total gas Inflow includes the compressed and adsorbed gas.

Total Gas Inflow, Total time for which the pressure increment was applied and the pressure increment are written on the graph to make them easier to recognize

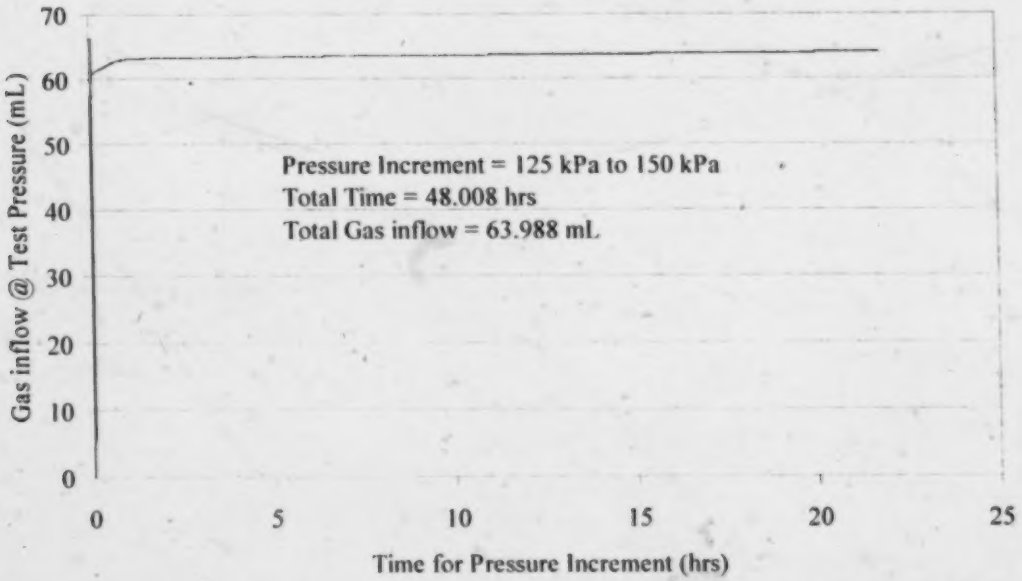

Figure B.1: Relationship Between Total Gas Inflow and Time for Pressure increment of 125kPa to 150kPa

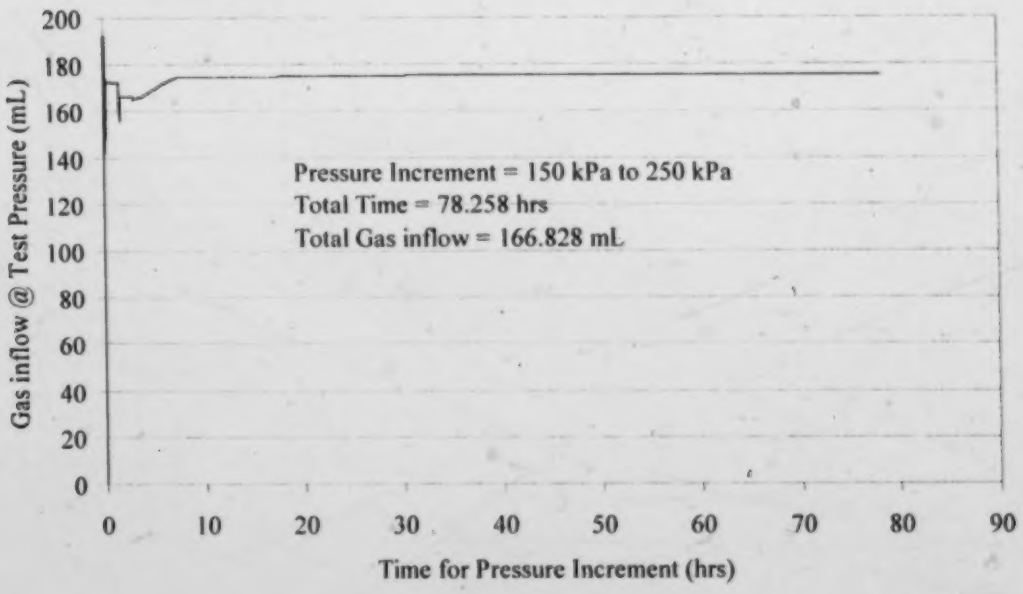

Figure B.2: Relationship Between Total Gas Inflow and Time for Pressure increment of 150kPa to 250kPa

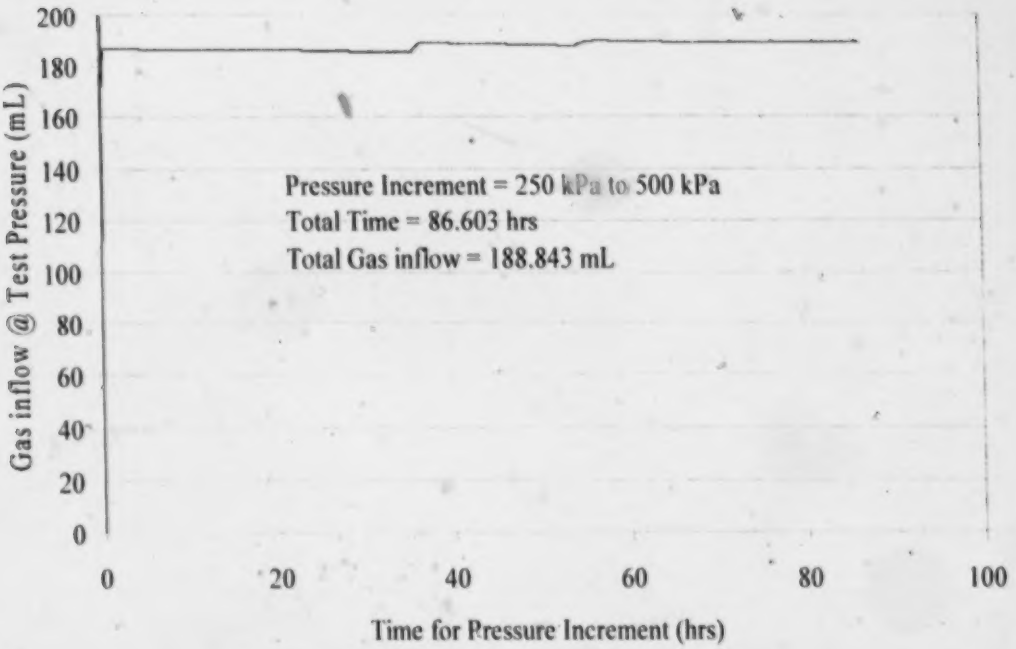

Figure B.3: Relationship Between Total Gas Inflow and Time for Pressure increment of 250kPa to 500kPa

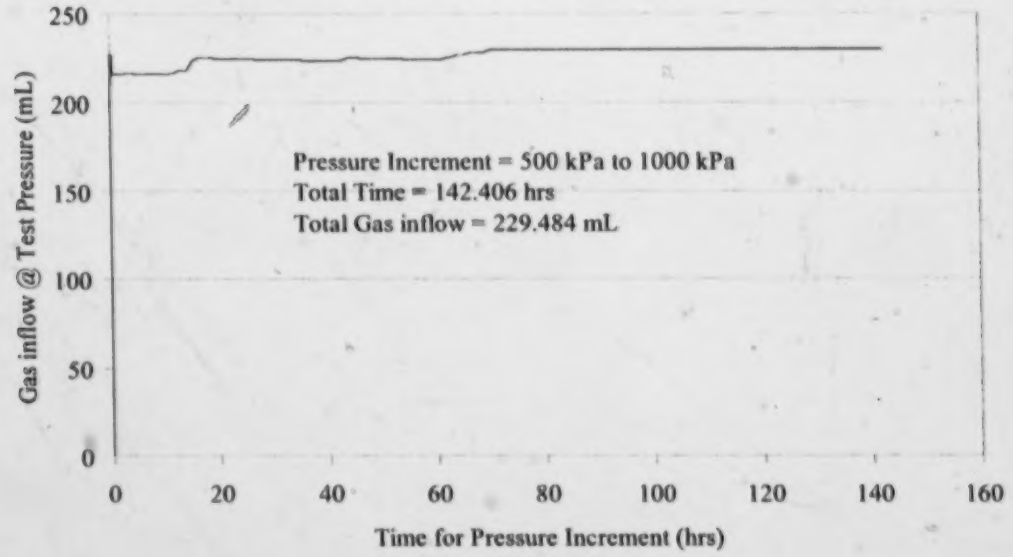

Figure B.4: Relationship Between Total Gas Inflow and Time for Pressure increment of 500kPa to 1000kPa

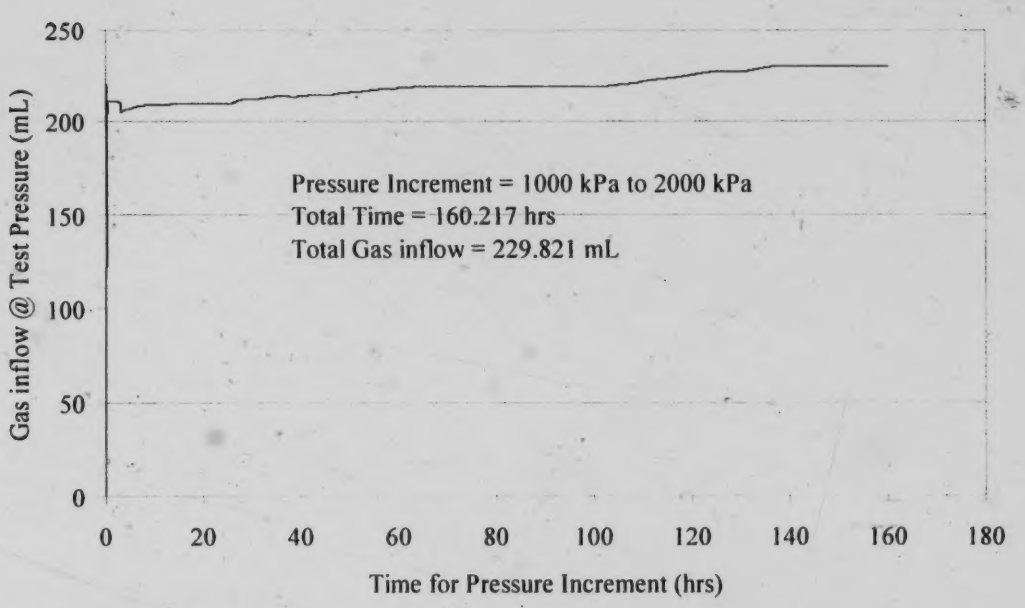

Figure B.5: Relationship Between Total Gas Inflow and Time for Pressure increment of 1000kPa to 2000kPa

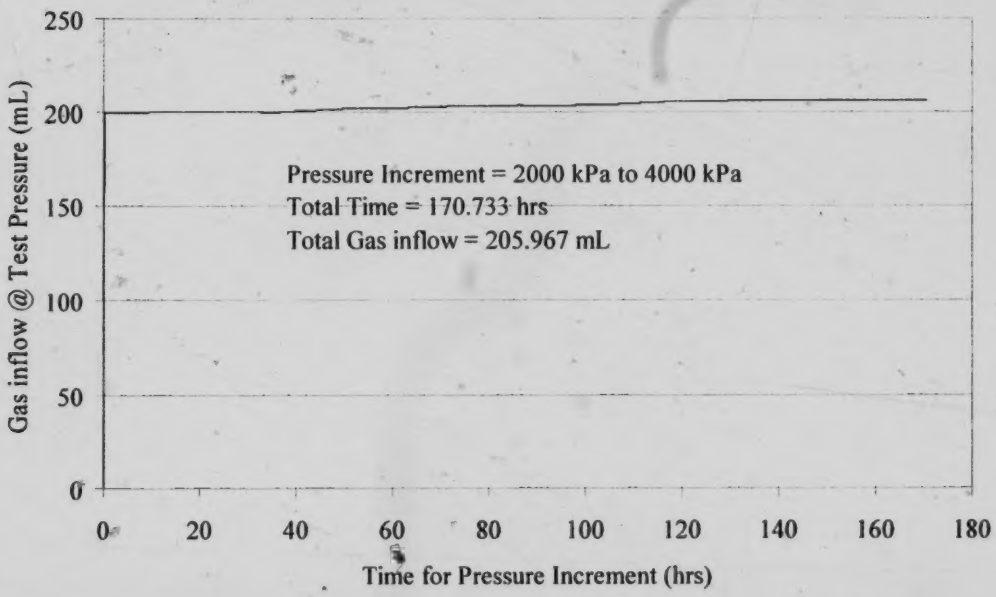

Figure B.6: Relationship Between Total Gas Inflow and Time for Pressure increment of 2000kPa to 4000kPa

APPENDIX C – Graphs between Total Gas Inflow and time for Leakage integrity Test for each pressure increment

The following pages contain Graphs Between Time and Total Gas Inflow for each Pressure range for the Leakage Integrity Test.

Pressures start from 150kPa and goes on to 4MPa.

The time is presented in hours while the Total Gas Inflow is in mL. The total gas Inflow includes the compressed and adsorbed gas.

Total Gas Inflow, Total time for which the pressure increment was applied and the pressure increment are written on the graph to make them easier to recognize

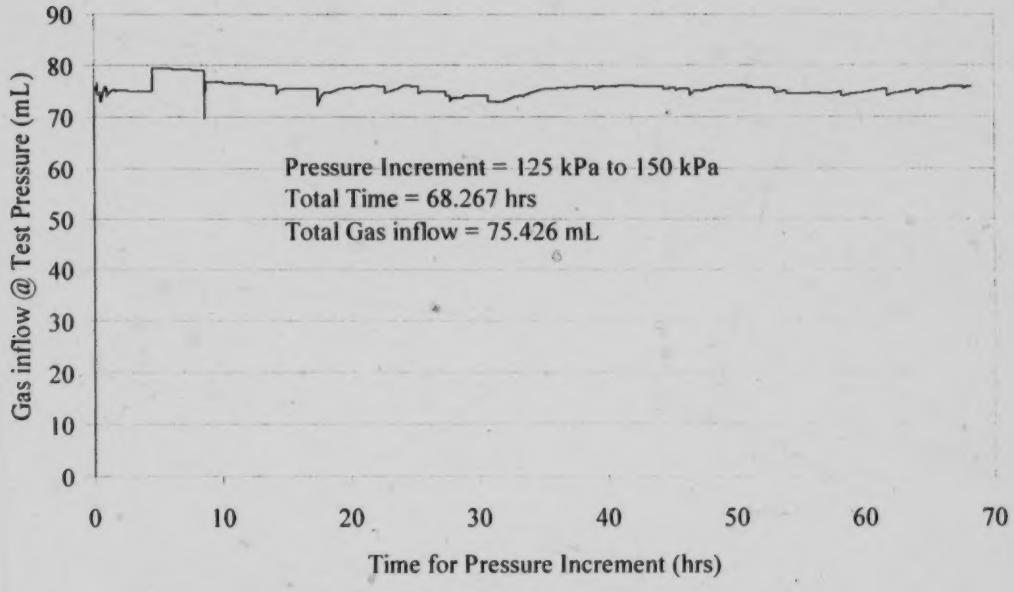

Figure C.1: Relationship Between Total Gas Inflow and Time for Pressure increment of 125kPa to 150kPa

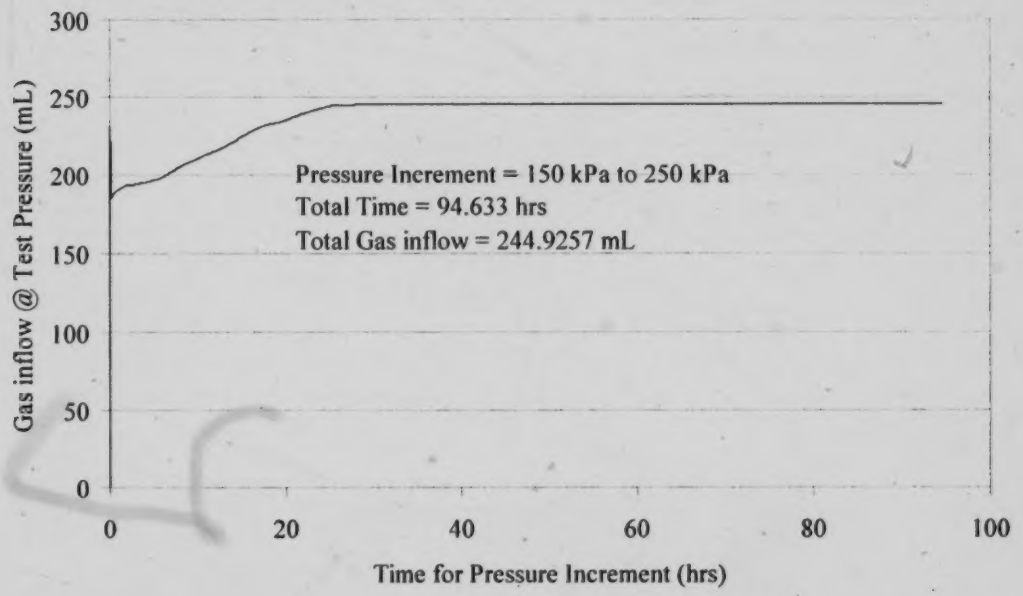

Figure C.2: Relationship Between Total Gas Inflow and Time for Pressure increment of 150kPa to 250kPa

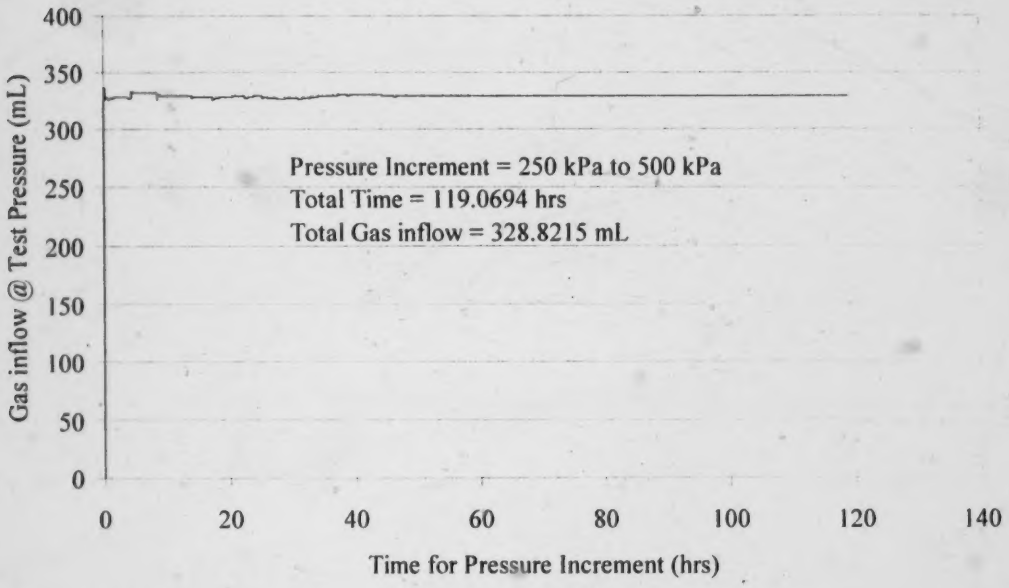

Figure C.3: Relationship Between Total Gas Inflow and Time for Pressure increment of 250kPa to 500kPa

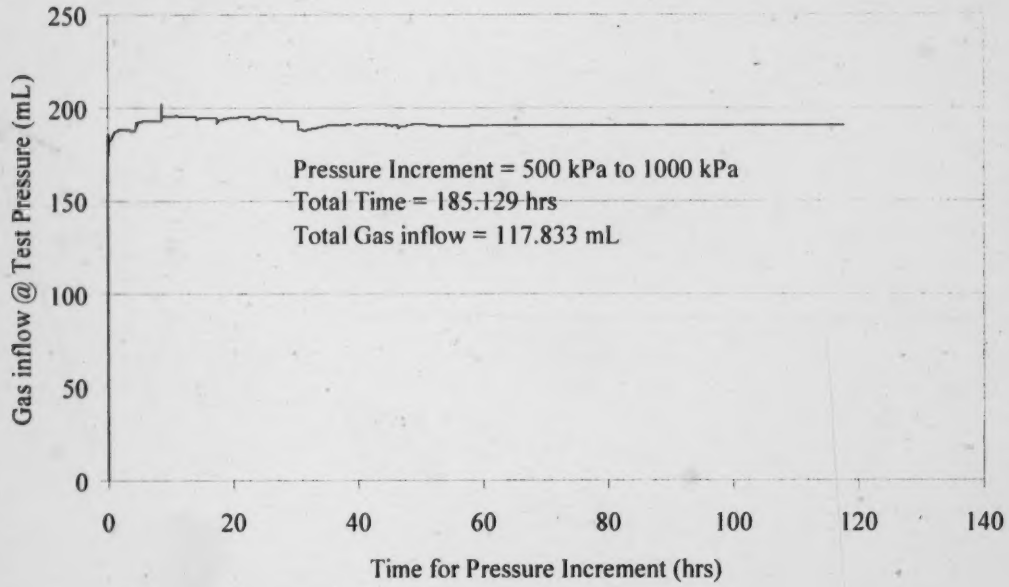

Figure C.4: Relationship Between Total Gas Inflow and Time for Pressure increment of 500kPa to 1000kPa

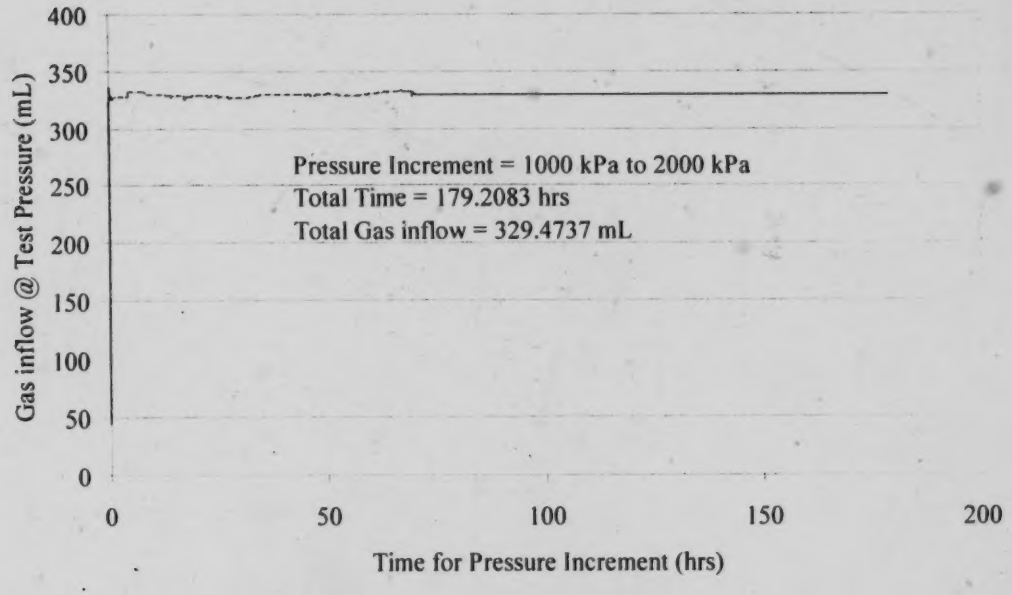

Figure C.5: Relationship Between Total Gas Inflow and Time for Pressure increment of 1000kPa to 2000kPa

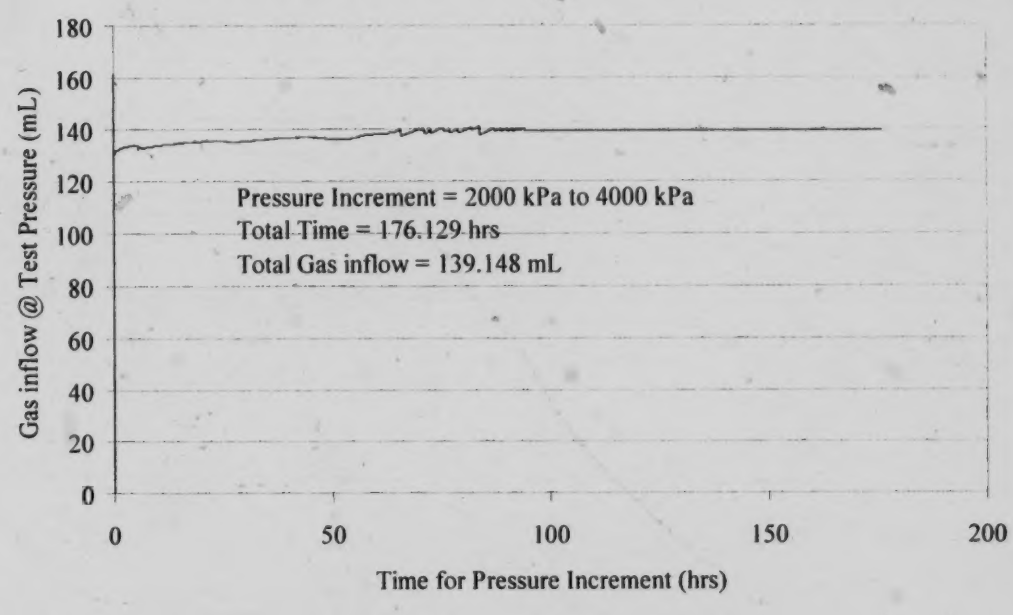

Figure C.6: Relationship Between Total Gas Inflow and Time for Pressure increment of 2000kPa to 4000kPa

APPENDIX D – Graphs between Total Gas Inflow and time for Intact Sample 1 for each pressure increment

The following pages contain Graphs Between Time and Total Gas Inflow for each Pressure range for the Intact Sample 1.

Pressures start from 150kPa and goes on to 4MPa.

The time is presented in hours while the Total Gas Inflow is in mL. The total gas Inflow includes the compressed and adsorbed gas.

Total Gas Inflow, Total time for which the pressure increment was applied and the pressure increment are written on the graph to make them easier to recognize

The relationship Between the Gas Inflow and time for pressure increment of 150kPa to 250kPa is not presented as the valve was not opened and the data only represents the total gas compression at this pressure increment.

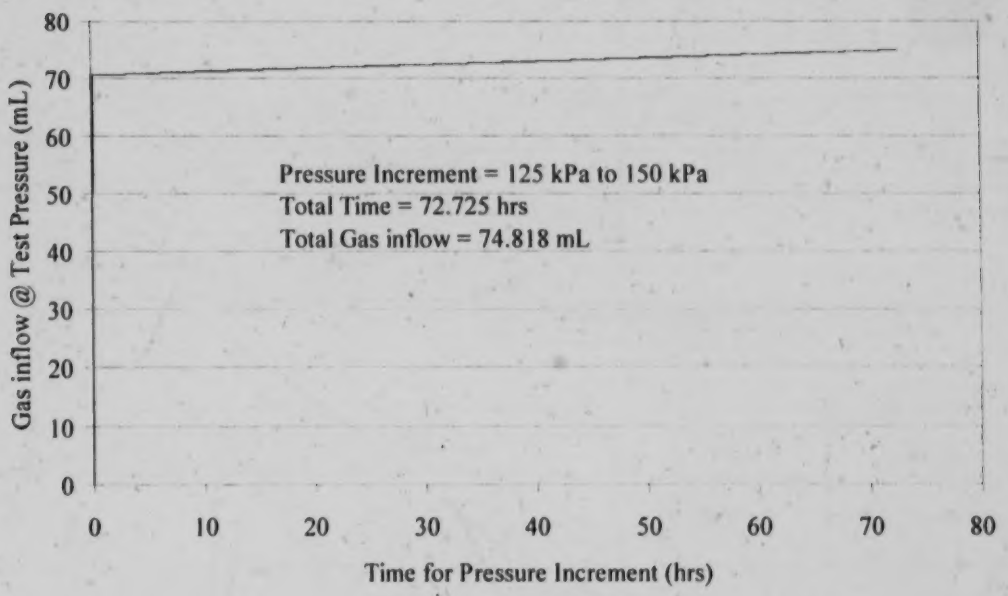

Figure D.1: Relationship Between Total Gas Inflow and Time for Pressure increment of 125kPa to 150kPa

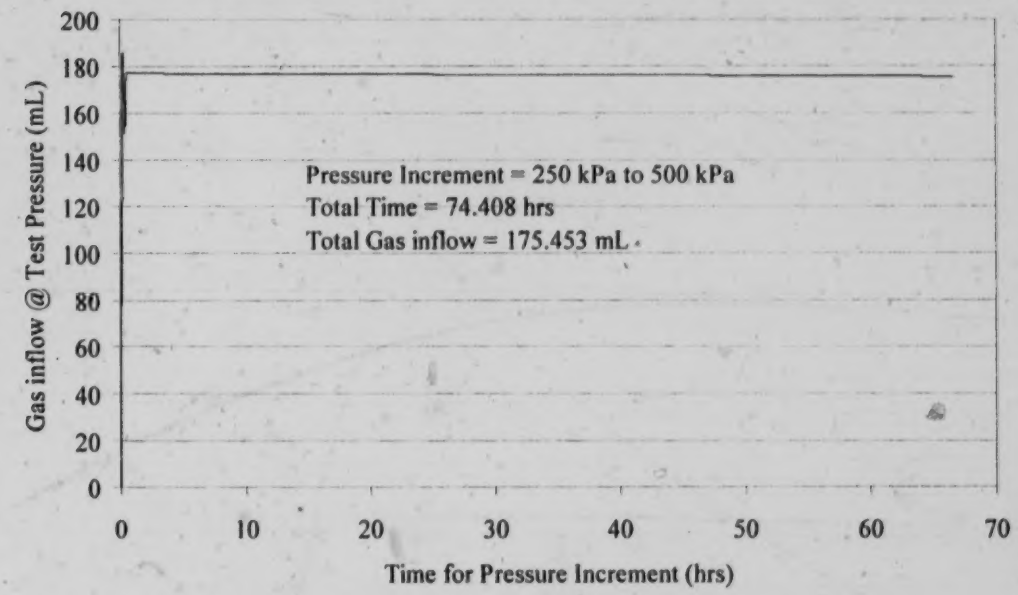

Figure D.2: Relationship Between Total Gas Inflow and Time for Pressure increment of 250kPa to 500kPa

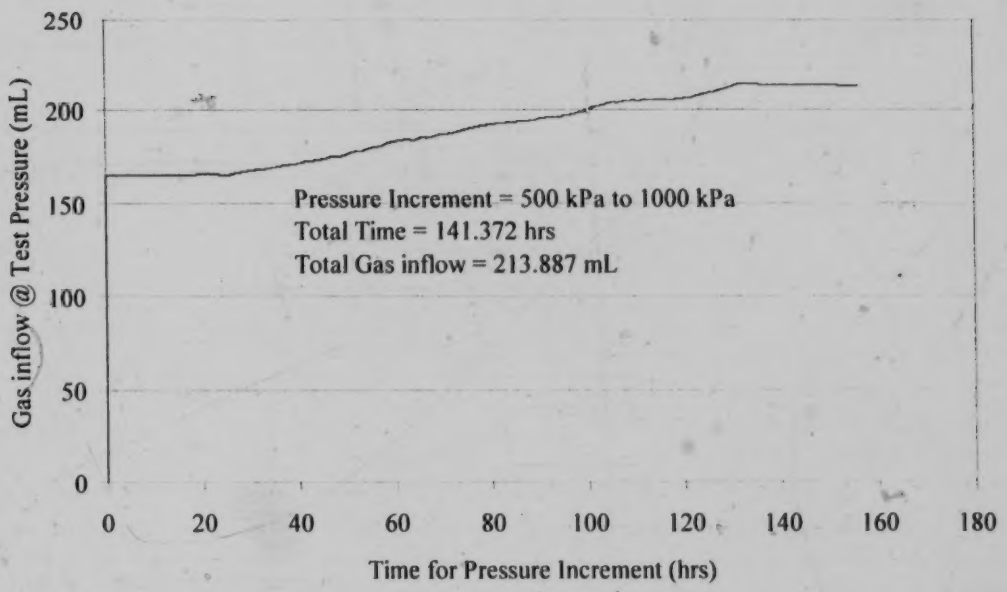

Figure D.3: Relationship Between Total Gas Inflow and Time for Pressure increment of 500kPa to 1000kPa

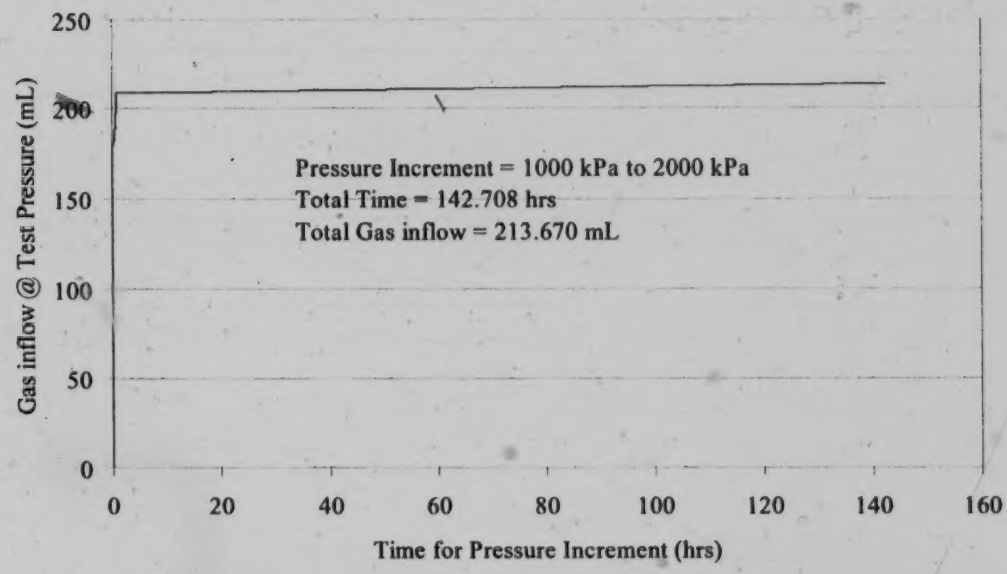

Figure D.4: Relationship Between Total Gas Inflow and Time for Pressure increment of 1000kPa to 2000kPa

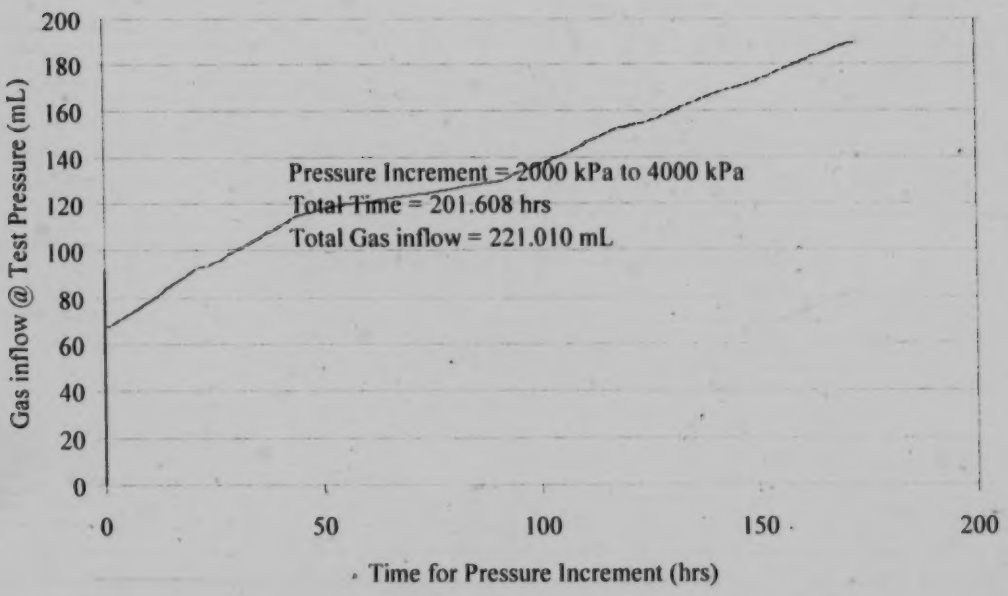

Figure D.5: Relationship Between Total Gas Inflow and Time for Pressure increment of 2000kPa to 4000kPa

APPENDIX E – Graphs between Total Gas Inflow and time for Intact Sample 2 for each pressure increment

The following pages contain Graphs Between Time and Total Gas Inflow for each Pressure range for the Intact Sample 2.

Pressures start from 150kPa and goes on to 4MPa.

The time is presented in hours while the Total Gas Inflow is in mL. The total gas Inflow includes the compressed and adsorbed gas.

Total Gas Inflow, Total time for which the pressure increment was applied and the pressure increment are written on the graph to make them easier to recognize

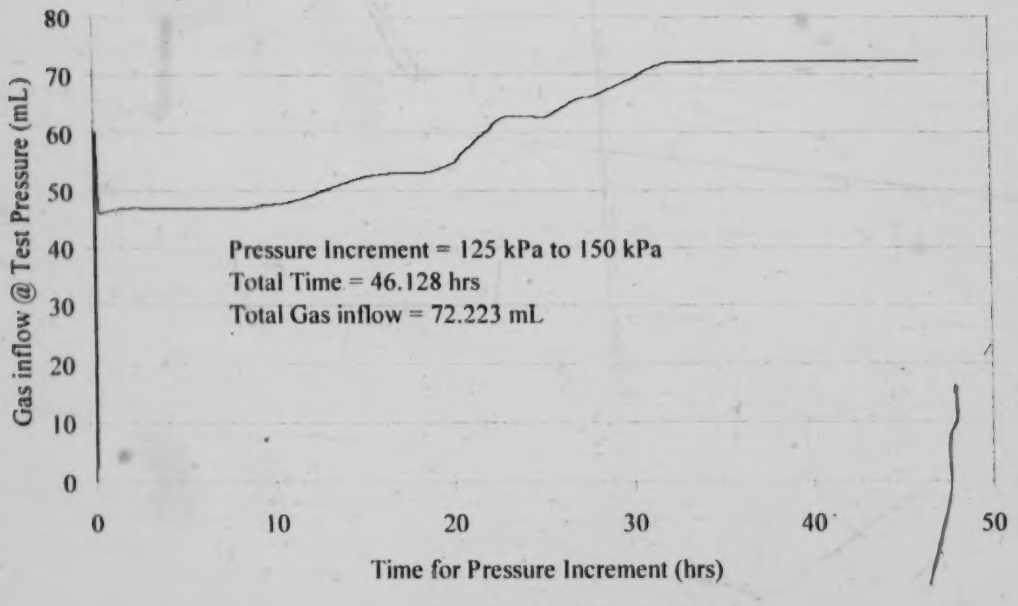

Figure E.1: Relationship Between Total Gas Inflow and Time for Pressure increment of 125kPa to 150kPa

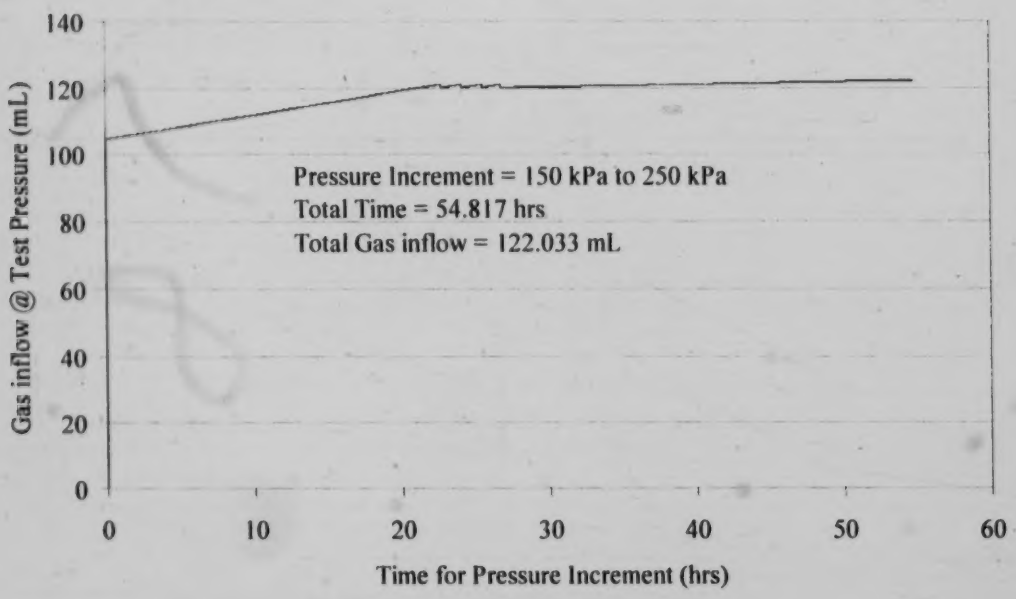

Figure E.2: Relationship Between Total Gas Inflow and Time for Pressure increment of 150kPa to 250kPa

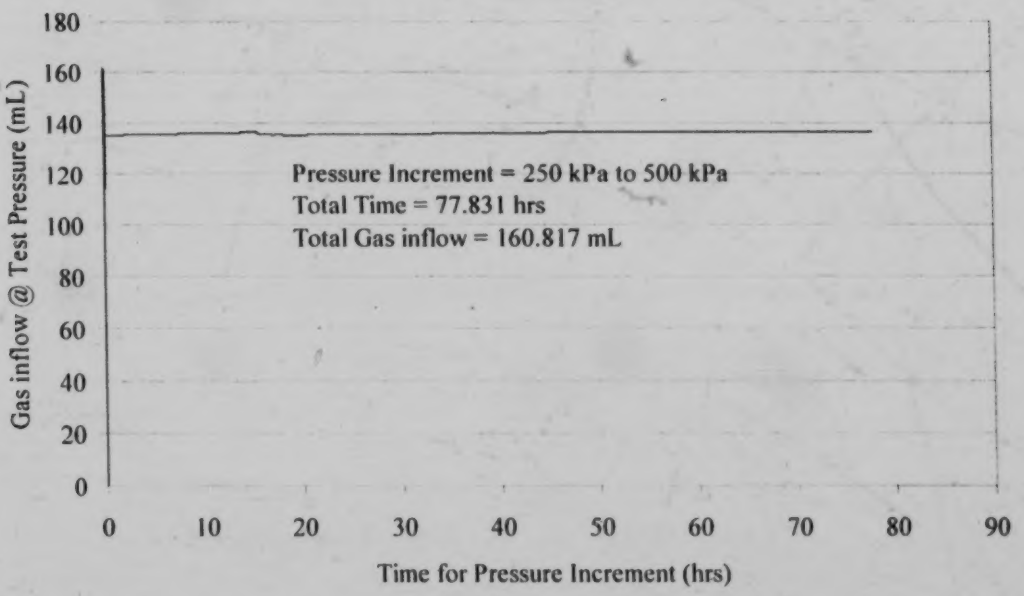

Figure E.3: Relationship Between Total Gas Inflow and Time for Pressure increment of 250kPa to 500kPa

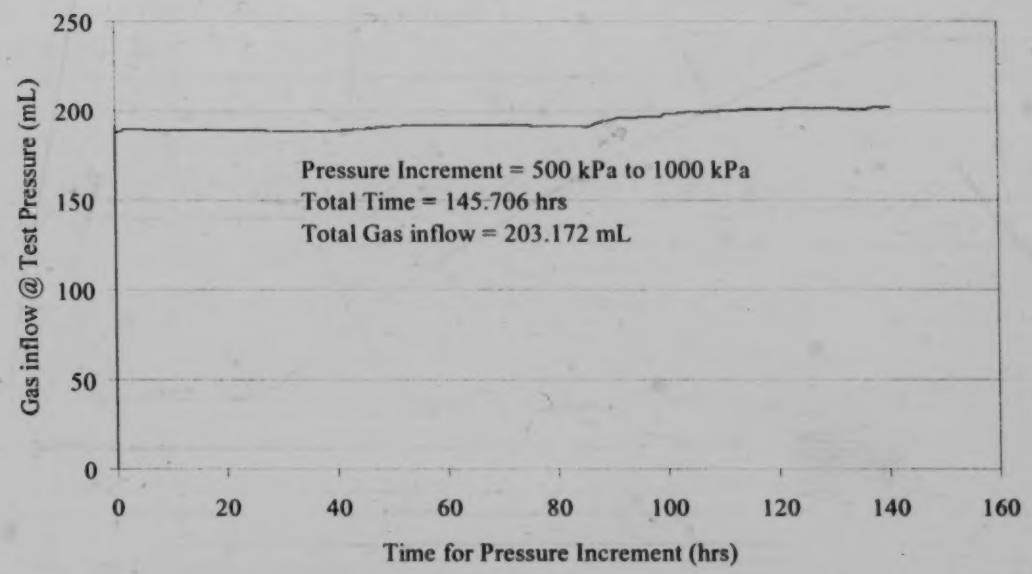

Figure E.4: Relationship Between Total Gas Inflow and Time for Pressure increment of 500kPa to 1000kPa

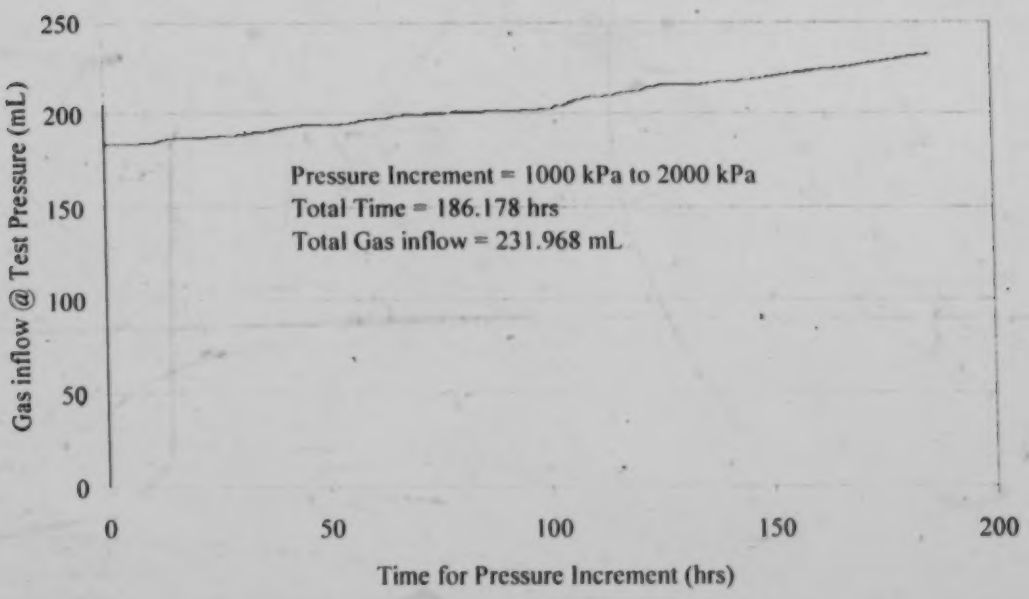

Figure E.5: Relationship Between Total Gas Inflow and Time for Pressure increment of 1000kPa to 2000kPa

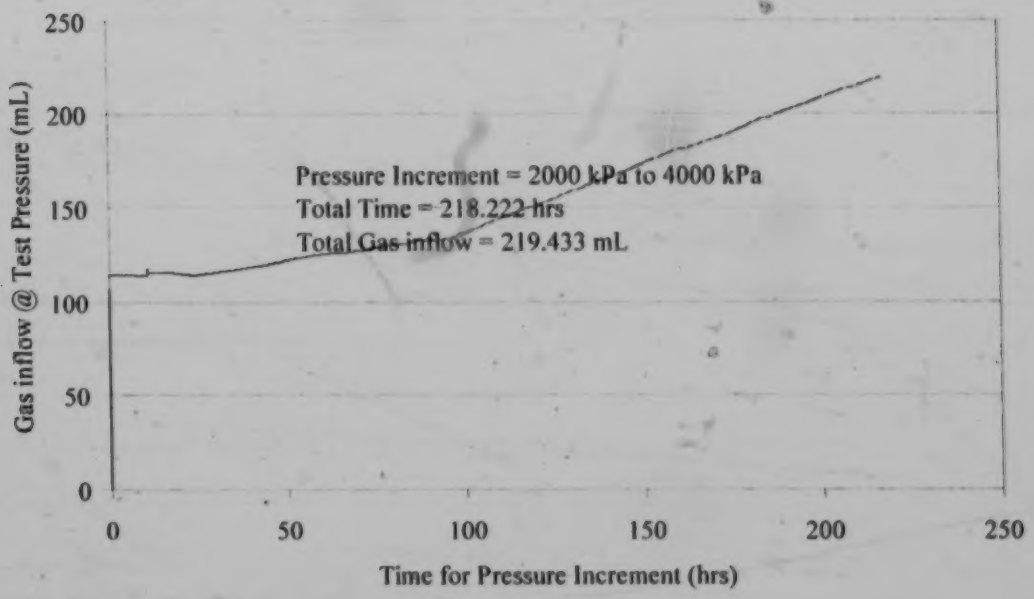

Figure E.6: Relationship Between Total Gas Inflow and Time for Pressure increment of 2000kPa to 4000kPa

APPENDIX F – Calculation of Moisture Content for Crushed Coal Sample

Moisture Content according to the ASTM D 3173-00 and ASTM D 3302-02 were tested and it was seen that there was not a big difference Between the two. Only 2.8% difference Between the two was observed which may be due to the fact that sample may be in the air for too long or there may be overlooking for some precautions.

F.1 Calculation Procedure

The total Moisture content was found using the following Calculation procedure.

$$M = [\frac{R(100 - ADL)}{100}] + ADL \qquad \text{F.1}$$

where M is Total Moisture Content, ADL is the Air Dry Loss while R is Residual Moisture

$$ADL = [\frac{L}{G}] \times 100 \qquad \text{F.2}$$

where L is the Loss in mass of the sample in Air dry sample while G is the mass of the Gross Sample

$$R = [\frac{(W - H)}{W}] \times 100 \qquad \text{F.3}$$

where W is the total mass of the sample used before heating while H is the mass of the sample after heating

Only one detail analysis will be presented here.

F.2 Sample Taken Before Testing

Table F.1 shows the mass of sample before and after the test as well as the calculations for the sample to get Residual Moisture content according to the above mentioned procedures. The detailed calculations are only being presented for the Crushed Sample 2. The calculations for the crushed sample 1 are the same.

Table F.1: Calculations for the Residual Moisture Content for Crushed sample 2

Crushed Sample 2	Tare #	Mass of Sample before Testing	Mass of Sample after Testing	Difference	Residual Moisture Content
		gm	gm	gm	%
A	1	1.1724	1.1166	0.0558	4.7595
B	2	1.4035	1.3344	0.0691	4.9234
C	3	1.4678	1.3967	0.0711	4.8440
D	4	1.0906	1.0400	0.0506	4.6396
Average Residual Moisture Content					4.7916

Table F.2 shows the data as well as the calculations for Air dry Loss carried out according to the Standard ASTM D 3302-02.

Table F.2: Calculations for the Air dry Loss

Crushed Sample 2	Tare #	Mass of Sample before Testing	Mass of Sample after Testing	Difference	Air dry Loss
		gm	gm	gm	%
A	5	2.3713	2.3179	0.0534	2.2519
B	6	1.9647	1.9214	0.0433	2.2039
C	7	1.2868	1.2602	0.0266	2.0671
D	8	2.0541	2.0001	0.0540	2.6289
Air Dry Loss					2.2880

F.3 Sample Taken after the end of Testing

Table F.3 shows the mass of sample before and after the test as well as the calculations for the sample to get Residual Moisture content according to the above mentioned standards

Table F.3: Calculations for the Residual Moisture Content

Crushed Sample 2	Tare #	Mass of Sample before Testing	Mass of Sample after Testing	Difference	Residual Moisture Content
		gm	gm	gm	%
A	9	2.2650	2.1495	0.1155	5.0995
B	10	2.6760	2.5381	0.1380	5.1551
C	11	2.2573	2.1421	0.1152	5.1057
D	12	2.1103	2.0035	0.1069	5.0633
Average Residual Moisture Content					5.1059

Table F.4 shows the data as well as the calculations for Air dry Loss carried out according to the Standard ASTM D 3302-02.

Table F.4: Calculations for the Air dry Loss

Crushed Sample 2	Tare #	Mass of Sample before Testing	Mass of Sample after Testing	Difference	Air dry Loss
		gm	gm	gm	%
A	13	1.8927	1.8509	0.0418	2.2111
B	14	1.4863	1.4522	0.0341	2.2943
C	15	1.8086	1.7709	0.0378	2.0872
D	16	1.5972	1.5608	0.0364	2.2790
Air Dry Loss					2.2179

After going through the calculation procedure for the Total Moisture Content the Moisture Content for the Crushed Sample 2 before putting it in the cell comes out to be 7.1465% while the moisture content for the sample after the testing comes out to be 7.2269% hence the difference Between the two is negligible and this can be attributed to the fact that when the sample was taken out it was left in air for a very small period of time due to negligence and this could have contributed towards the higher Residual Moisture content. Same can be said for the Crushed Sample 1 where the difference of only 0.17% is negligible.

Table F.5: Moisture Content for both Crushed samples

Sample	Moisture Content before Test (%)			Moisture Content after Test (%)		
	Residual Moisture Content	Air Dry Moisture Content	Total Moisture Content	Residual Moisture Content	Air Dry Moisture Content	Total Moisture Content
Crushed Sample 1	4.9234	2.2039	**7.0188**	5.0995	2.2111	**7.1978**
Crushed Sample 2	4.7916	2.288	**7.1465**	5.1059	2.2179	**7.2269**

APPENDIX G – Glossary of Coal Terms

Agglomerate

Collected into a ball or mass, agglomeration

Anthracite

A rank class of coals defined as having more than 86% fixed carbon and less than 14% volatile matter on a dry, mineral-matter-free basis. The rank is divided into semi anthracite, anthracite, and meta-anthracite groups on the basis of increasing fixed carbon and decreasing volatile matter.

Ash

The inorganic residue remaining after complete incineration of coal

ASTM

American Society of Testing and Materials

Bituminous coal

A rank class of coals defined by the ASTM as having less than 86% fixed carbon, and more than 14% volatile matter and more than 10,500 Btu/lb on a moist, mineral-matter-free basis. An overlap of bituminous and sub bituminous heat values from 10,500 to 11,500 Btu/lb is dependent on whether an agglomerate button with swelling characteristics is formed during volatile matter analysis. There are several divisions of bituminous coal. High-volatile C, B, and A are divided by increasing heat value. Medium and low-volatile bituminous coals are classified on the basis of increasing fixed carbon and decreasing volatile matter.

Btu

Btu is British Thermal Unit. The Btu is the amount of heat needed to raise the temperature of 1 pound of water by 1 degree Fahrenheit.

Chemical Feedstock

Raw material supplied to a machine or processing plant

Clean Coal

Low sulphur coal

Coal Ball

A concretion of mineralized plant debris, occurring in a coal seam or in adjacent rock

Coal Basin

A coal field with basinal structure

Coal

A readily combustible rock containing more than 50% by weight and more than 70% by volume of carbonaceous material, including inherent moisture, formed from compaction and in duration of variously altered plant remains similar to those in peat

Coal Field

A region in which deposits of coal occur

Coal Gas

The fuel gas produced from a high-volatile bituminous coal. Its average composition, by volume, is 50% hydrogen, 30% methane, 8% carbon monoxide, 4% other hydrocarbons, and 8% carbon dioxide, nitrogen and oxygen

Coal Measure

A succession of sedimentary rocks ("measures") ranging in thickness from a meter to a few thousand meters, and consisting mainly of clastic rocks with interstratified beds of coal

Coal Plant

A fossil plant found in association with the formation of coal beds

Coal Seam

A stratum or bed of coal

Coal Type

A classification of coal distinguished on the basis of the constituent plant materials. Refer to grade and rank

Coke

Material derived from heating bituminous coal in the absence of air and driving off the volatile constituents, so that the fixed carbon and ash are fused together.

Dry, mineral-matter-free-basis

A calculated, analytical value of a coal sample expressed as if total moisture and mineral matter had been removed

Face

Solid surface of coal being worked on

Fixed carbon

The solid residue, other than ash, remaining after the volatile matter has been liberated from coal during combustion

Fossil

Ancient remains of plants and animals

Grade

A classification of coal based on degree of purity i.e. quantity of ash left after burning. For more detail refer to rank

In-situ

Where it lies, processed underground

Lignite

Lowest rank of coal, with low heat values Between 6,300 and 8,300 Btu/lb, on a moist, mineral-matter basis

Methane

A colorless, odorless inflammable gas, the simplest paraffin hydrocarbon, formula CH4. It is the principle constituent of natural gas and is also found associated with crude oil. Reading coal gas is also helpful to understand this.

Moist, mineral-matter-free basis

A calculated number based on basic analytical data - Btu/lb, ash and sulfur - to determine a number representative of the value if mineral-matter has been removed and the natural moisture in the coal retained. Used in determining the rank of coal

Outcrop

Where coal appears on the surface of the ground

Overburden

Material of any nature, consolidated or unconsolidated, that overlies a deposit of useful materials, ores, or coal, especially those deposits that are mined from the surface

Peat

An unconsolidated deposit of semi carbonized plant remains in a water-saturated environment such as a bog, of persistently high moisture content (at least 75%). It is considered an early stage or rank in the development of coal; carbon content is about 60% and oxygen content is about 30% (moisture-free)

Rank

The classification of coals according to their degree of metamorphism or coalification (maturation) in the natural series from lignite to anthracite. Rank is defined in the United States by the American Society of Testing and Materials (ASTM) classification based on agglomeration characteristics, heat values, fixed carbon, and volatile matter content

Raw Coal

Coal that has not been cleaned or sized

Reclamation

Renewing the land where strip-mining has taken place

Recoverable resources

Oil, gas, coal, and other minerals that can be economically recovered after allowing for environmental, legal, and technological controls

Reserves

Economically recoverable minerals in-ground at present.

Resources

Coal deposits those are currently or potentially economically extractable. Resources are 14 inches or more in thickness and under less than 6,000 feet of overburden.

Seam

A large deposit or layer of coal

Subbituminous coal

A rank class of coals having a heat value content of more than 8,300 Btu/lb and less than 11,500 Btu/lb on a moist, mineral-matter-free basis. This class is divided by increasing heat value into subbituminous C, B, and A coal groups

Surface Mining

Refer to Strip-mining for details

Underground Mining

Mine reached by shaft or tunnel

Volatile matter

In coal, those products, exclusive of moisture, given off as gas and vapor determined analytically by prescribed methods

Watt - (W)

Unit of electric power; 1/745 horsepower

APPENDIX H – One Dimensional Freezing of the Sample

The results from the freezing of the sample are presented here as graphs

Figure H.1 shows the relationship Between the temperatures in the room with time. It can be seen that the temperature remained fairly constant throughout the testing time. Temperature ranged from a maximum of 7.8°C to a minimum of 4.9°C. although this is a fairly large range but this temperature do not have any significant impact on the cell temperature as the cell temperature is dependent on the circulating fluid from the bath.

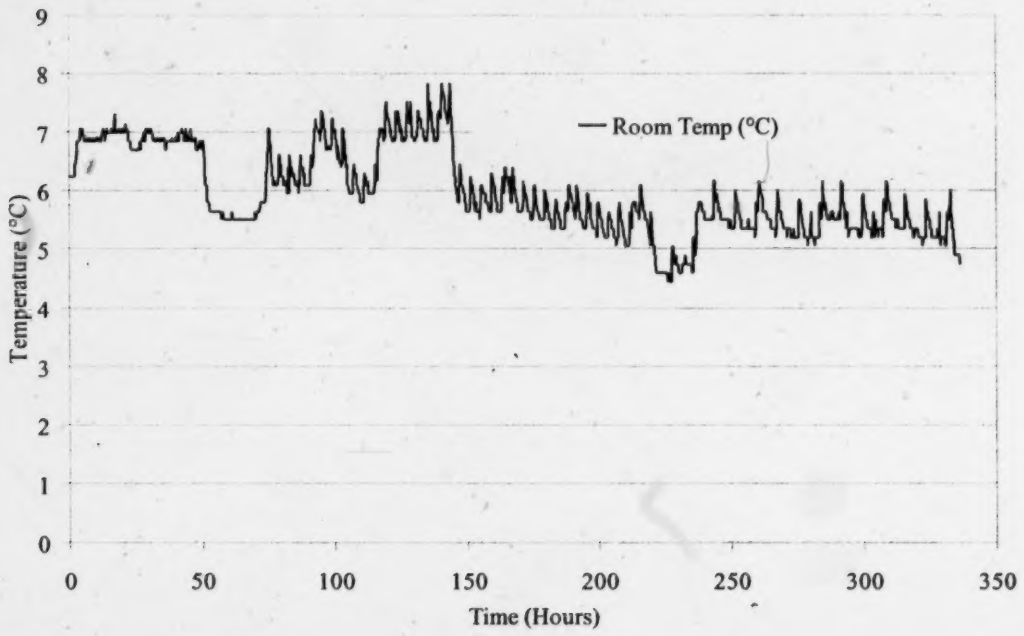

Figure H.1: Graph Between Room Temperature and Time over the length of Test

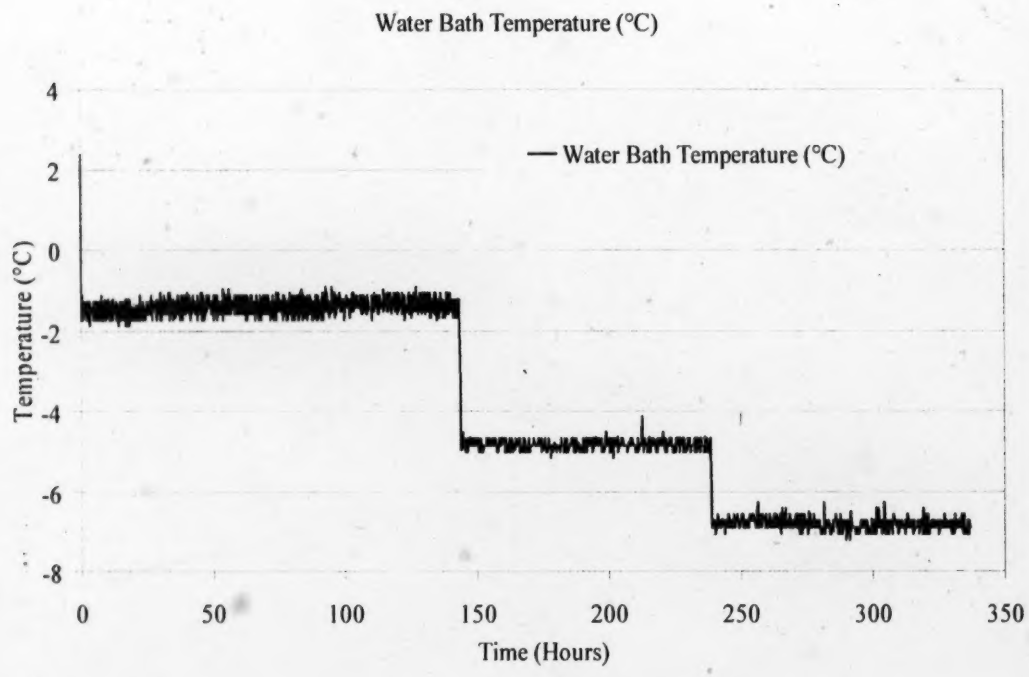

Figure H.2: Relationship Between Temperature in water bath and time

Figure H.2 shows the relationship Between time and temperature in water bath. It is obvious from the graph that for most of the time the temperature was constant. It was observed after 135 hrs that even the top of the sample has been frozen but to make sure that whole of the sample is in frozen state when taken out it was decided to drop the temperature in 2 steps. The temperature was dropped by 4°C after 140 hrs so that the final temperature is -5°C while for the second time it was dropped by 2°C to adjust the final temperature at -7°C.

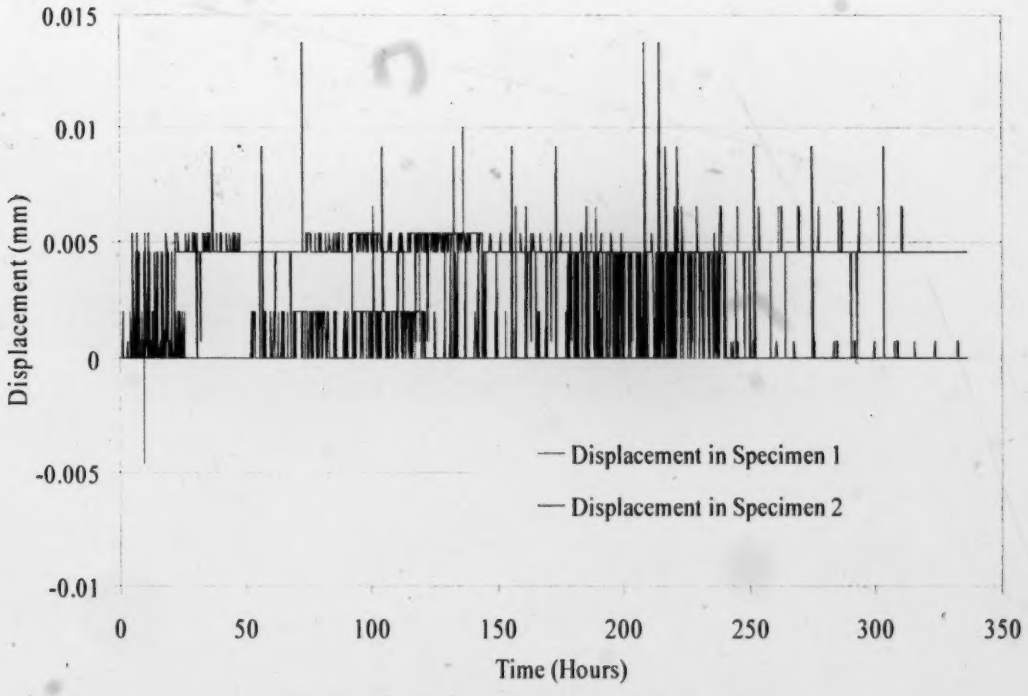

Figure H.3: Graph showing relationship Between displacement and time

Figure H.3 shows the relationship Between time and displacement in the specimens. It can be seen from the graphs that there was no visible displacement (heaving/consolidation) of the sample. This implies that the heaving and/or consolidation are not a problem for the freezing of the coal sample. Although this must be studied in detail to be generalized but it seems that for this coal heaving/consolidation s not an issue.

Figure H.4 and H.5 show the relationship Between the freezing front and time. This has been discussed earlier in the report.

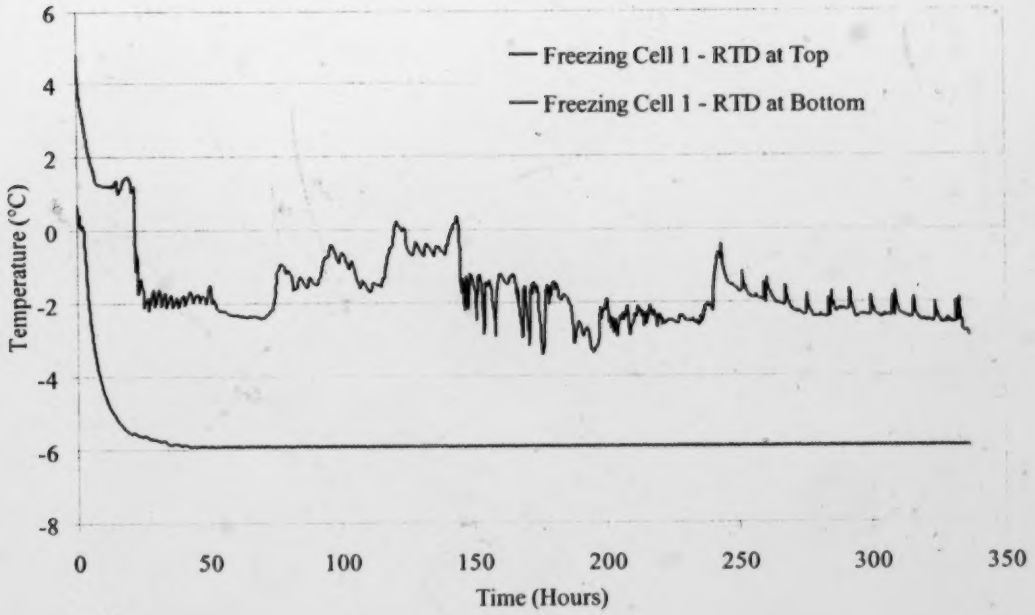

Figure H.4: Graph Between Freezing Front and time over the length of Test (Sample 1)

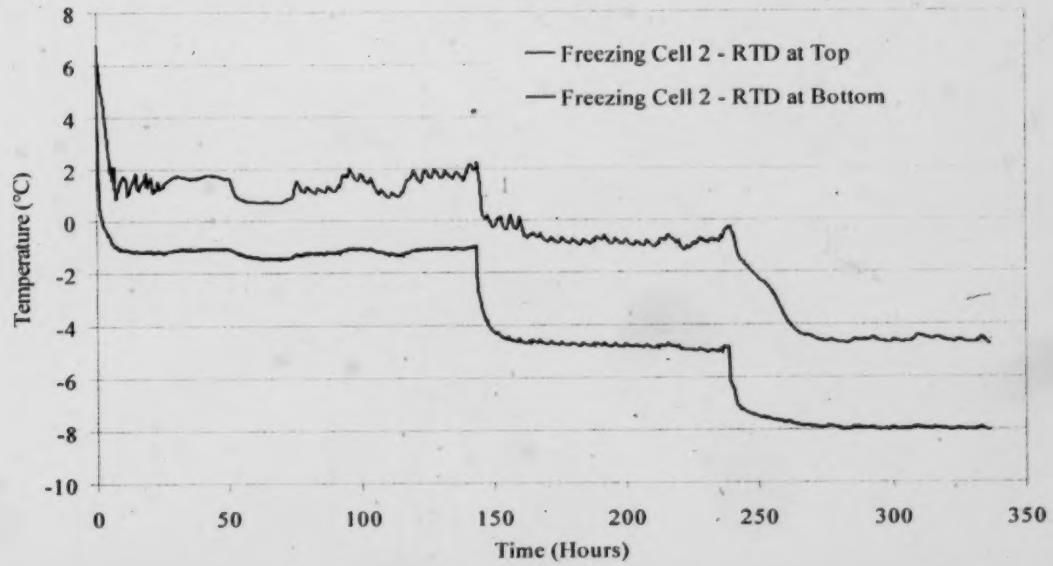

Figure H.5: Graph Between Freezing Front and Time over the length of Test (Sample 2)